



CMS-HIG-19-011

CERN-EP-2024-179
2025/02/25

Measurement of the $t\bar{t}H$ and tH production rates in the $H \rightarrow b\bar{b}$ decay channel using proton-proton collision data at $\sqrt{s} = 13$ TeV

The CMS Collaboration^{*}

Abstract

An analysis of the production of a Higgs boson (H) in association with a top quark-antiquark pair ($t\bar{t}H$) or a single top quark (tH) is presented. The Higgs boson decay into a bottom quark-antiquark pair ($H \rightarrow b\bar{b}$) is targeted, and three different final states of the top quark decays are considered, defined by the number of leptons (electrons or muons) in the event. The analysis utilises proton-proton collision data collected at the CERN LHC with the CMS experiment at $\sqrt{s} = 13$ TeV in 2016–2018, which correspond to an integrated luminosity of 138 fb^{-1} . The observed $t\bar{t}H$ production rate relative to the standard model expectation is $0.33 \pm 0.26 = 0.33 \pm 0.17\text{ (stat)} \pm 0.21\text{ (syst)}$. Additionally, the $t\bar{t}H$ production rate is determined in intervals of Higgs boson transverse momentum. An upper limit at 95% confidence level is set on the tH production rate of 14.6 times the standard model prediction, with an expectation of $19.3^{+9.2}_{-6.0}$. Finally, constraints are derived on the strength and structure of the coupling between the Higgs boson and the top quark from simultaneous extraction of the $t\bar{t}H$ and tH production rates, and the results are combined with those obtained in other Higgs boson decay channels.

Published in the Journal of High Energy Physics as doi:10.1007/JHEP02(2025)097.

1 Introduction

In the standard model (SM) of particle physics, the Higgs boson (H) couples to fermions with a Yukawa-type interaction, with a coupling strength proportional to the fermion mass. The coupling of the Higgs boson to the top quark, the heaviest known fermion, is particularly relevant both in the SM and in models of new physics beyond the SM (BSM). For example, due to its size, the top-Higgs coupling strongly affects the stability of the electroweak vacuum via virtual contributions [1] and may play a special role in the mechanism of electroweak symmetry breaking [2, 3]. Probing the coupling of the Higgs boson to the top quark is therefore instrumental in testing the SM and constraining BSM models, which may predict different coupling strengths and structures.

The associated production of a Higgs boson and a top quark-antiquark pair ($t\bar{t}H$) provides a direct probe of the top-Higgs coupling as illustrated by the Feynman diagram in Fig. 1 (left). The $t\bar{t}H$ production process has been observed by the ATLAS and CMS Collaborations by combining measurements that target different decay channels of the Higgs boson using the LHC Run-1 and part of the Run-2 datasets [4, 5]. Subsequent measurements of $t\bar{t}H$ production with the full Run-2 dataset have been performed, targeting decays of the Higgs boson into pairs of photons, W or Z bosons, tau leptons, and bottom quarks ($b\bar{b}$) [6–13]. The associated production of a single top quark and a Higgs boson (tH) occurs through two sets of diagrams, where the Higgs boson either couples to the top quark or to the W boson [14–17], as shown in Fig. 1 (centre and right). Consequently, tH production offers insights into the Higgs boson’s coupling to top quarks and vector bosons, as well as the interference of the two, allowing for the investigation of the relative sign of the two couplings. Previous searches for tH production with Run-2 data targeted Higgs boson decays to $\gamma\gamma$, WW , ZZ , $\tau\tau$, and $b\bar{b}$ [6–10, 18]. In the SM, the Higgs boson has a positive eigenvalue under combined charge-parity (CP) transformations (CP even). The combined measurement of $t\bar{t}H$ and tH production provides a probe of CP -odd admixtures in the top-Higgs coupling through interfering contributions, which would be a clear sign of physics beyond the SM. Previous constraints on the CP nature of the top-Higgs coupling have been obtained from measurements of $t\bar{t}H$ and tH production with Run-2 data targeting Higgs boson decays to $\gamma\gamma$, ZZ , WW , $\tau\tau$, and $b\bar{b}$ [7, 8, 19–21].

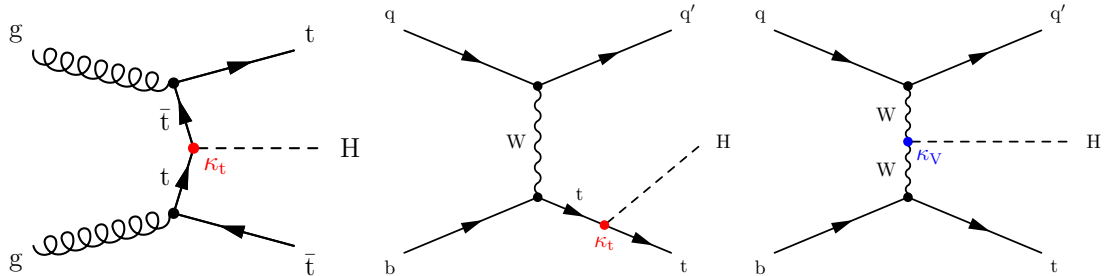


Figure 1: Representative leading order Feynman diagrams for the associated production of a Higgs boson and a top quark-antiquark pair (left) and for the associated production of a single top quark and a Higgs boson in the t channel, where the Higgs boson couples to the top quark (centre) or the W boson (right). The κ_t (red) and κ_V (blue) denote the Higgs boson coupling strength to top quarks and vector bosons, respectively.

In the SM, for a 125 GeV Higgs boson, the $H \rightarrow b\bar{b}$ decay has the largest branching fraction of 0.58 ± 0.02 [22]. Furthermore, $t\bar{t}H$ production with $H \rightarrow b\bar{b}$ decays involves Higgs boson couplings only to fermions and thus exclusively probes the Higgs Yukawa sector. The $H \rightarrow b\bar{b}$ decay channel is thus experimentally attractive, yet its measurement is challenging due to considerable SM backgrounds at the CERN LHC. The previous searches for $t\bar{t}H$ and tH production

in the $H \rightarrow b\bar{b}$ channel by the ATLAS and CMS Collaborations achieved sensitivities that correspond to observed (expected) significances of up to 1.6 (2.7) standard deviations (SD) for $t\bar{t}H$ production [11–13] and observed (expected) upper limits at 95% confidence level (CL) on SM tH production of approximately 90 (41) times the SM expectation [18]. At the time of submitting this paper, the ATLAS Collaboration reported a re-analysis of the Run-2 data with an observed (expected) significance for $t\bar{t}H$ production of 4.6 (5.4) SD [23]. Constraints on the CP nature of the top-Higgs coupling have been obtained in this channel from the combination of information from $t\bar{t}H$ and tH production by the ATLAS Collaboration [21].

This article describes the combined analysis of $t\bar{t}H$ and tH production in the $b\bar{b}$ decay channel of the Higgs boson by the CMS Collaboration. Proton-proton (pp) collision data collected during LHC Run-2 from 2016 to 2018 at a centre-of-mass energy of 13 TeV are used, corresponding to an integrated luminosity of 138 fb^{-1} . Several signal interpretations are performed. First, targeting solely the $t\bar{t}H$ signal, the $t\bar{t}H$ production rate is determined assuming the tH production rate predicted in the SM. The $t\bar{t}H$ rate is determined both inclusively and in different regions of transverse momentum p_T of the Higgs boson (p_T^H), following the simplified template cross section (STXS) approach [22]. Second, targeting the tH signal process, an upper limit on the tH production rate is determined assuming the $t\bar{t}H$ production rate predicted in the SM. Third, targeting simultaneously the $t\bar{t}H$ and tH production processes, the Higgs boson coupling to top quarks is analysed, and both the strength and the CP structure of the coupling are probed.

The analysis builds upon strategies developed in previous analyses of $t\bar{t}H$ [12, 13] and tH production [18] using 35.9 fb^{-1} of data collected in 2016. The event selection aims at identifying events in which a Higgs boson is produced in association with a $t\bar{t}$ pair or a single top quark, and decays to $b\bar{b}$. Three mutually exclusive channels are considered in the analysis, defined by the number of leptons (electrons or muons) in the $t\bar{t}$ decay modes: the fully hadronic (FH) channel, in which both W bosons decay to a $q\bar{q}$ pair, the single-lepton (SL) channel, with one W boson decaying to a charged lepton and a neutrino and the other W boson decaying to $q\bar{q}$, and the dilepton (DL) channel, with both W bosons decaying to a charged lepton and neutrino. The SL channel also includes dedicated event categories targeting tH production. No dedicated reconstruction of hadronically decaying tau leptons is performed. The experimental signature of signal events is characterised by the presence of high- p_T b quark jets (b jets) from the Higgs boson and top quark decays and, depending on the channel, jets or isolated electrons and muons, as well as missing transverse momentum arising from the presence of undetected neutrinos from the W boson or tau lepton decays. Electrons or muons from tau lepton decays can enter the selection in the SL and DL channels, while hadronically decaying tau leptons can contribute to the FH and SL channels. Dominant background contributions arise from SM events composed uniquely of jets produced through the strong interaction, referred to as quantum chromodynamics (QCD) multijet events, in the FH channel and from $t\bar{t} + \text{jets}$ production in all channels. The latter includes in particular $t\bar{t} + b\bar{b}$ production, where additional b quarks can arise from QCD radiation or loop-induced QCD processes. The $t\bar{t} + b\bar{b}$ background remains almost irreducible with respect to $t\bar{t}H$, $H \rightarrow b\bar{b}$, with both processes having four b quarks in the final state, and constitutes the critical background to the analysis.

The presence of multiple b jets in the final state and their experimental resolution complicate the event reconstruction and limit the sensitivity of the analysis using simple kinematic observables like the Higgs boson invariant mass. Therefore, the signal extraction is performed using a multivariate analysis based on artificial neural networks (ANNs) that simultaneously exploit the information from multiple experimental observables. The ANNs are used to discriminate signal from background events and, in the SL and DL channels, to categorise events into signal and background control regions. The signal rate is obtained from a combined profile likelihood

fit of distributions of the ANN score, distributions of ratios of ANN scores, or of the event yield to the data, depending on the channel and category.

Several changes in the analysis strategy have been adopted with respect to the previous analyses [12, 13, 18], including usage of the state-of-the-art $t\bar{t} + b\bar{b}$ event simulation [24, 25] in the background modelling, updates in the multivariate analysis techniques, improvements in the b tagging algorithm, and the exploitation of all three $t\bar{t}$ decay channels.

This article is structured as follows. The CMS detector is described in Section 2. In Section 3, the data samples and trigger selection are described, followed by a description of the simulated samples in Section 4. The object and event reconstruction are presented in Section 5 and the event selection in Section 6. The modelling of the critical $t\bar{t} + \text{jets}$ background is detailed in Section 7. The analysis strategy in the different channels is detailed in Section 8 and systematic uncertainties are discussed in Section 9. The statistical analysis and obtained results are presented in Section 10. Finally, a summary is provided in Section 11. Tabulated results are provided in the HEPData record for this analysis [26].

2 The CMS detector

The central feature of the CMS apparatus is a superconducting solenoid of 6 m internal diameter, providing a magnetic field of 3.8 T. Within the solenoid volume are a silicon pixel and strip tracker, a lead tungstate crystal electromagnetic calorimeter (ECAL), and a brass and scintillator hadron calorimeter, each composed of a barrel and two endcap sections. Forward calorimeters extend the pseudorapidity coverage provided by the barrel and endcap detectors. Muons are measured in gas-ionisation detectors embedded in the steel flux-return yoke outside the solenoid. A more detailed description of the CMS detector, together with a definition of the coordinate system used and the relevant kinematic variables, can be found in Refs. [27, 28].

Events of interest are selected using a two-tiered trigger system [29]. The first level (L1), composed of custom hardware processors, uses information from the calorimeters and muon detectors to select events at a rate of around 100 kHz within a fixed latency of about 4 μs [30]. The second level, known as the high-level trigger (HLT), consists of a farm of processors running a version of the full event reconstruction software optimised for fast processing, and reduces the event rate to a few kHz before data storage.

3 Data samples and trigger requirements

The analysis uses pp collision data recorded at $\sqrt{s} = 13$ TeV at the LHC during 2016–2018. Only the data-taking periods during which the CMS detector was fully operational are considered. The corresponding total integrated luminosity amounts to 138 fb^{-1} , of which 36.3, 41.5, and 59.7 fb^{-1} have been recorded in 2016, 2017, and 2018, respectively [31–33]. In this analysis, events are selected at the HLT level by different trigger requirements defined by the presence of several jets or one or two leptons and, in some cases, a large scalar sum of jet p_{T} (H_{T}) in the events, depending on the analysis channel.

Novel trigger criteria have been developed at the beginning of the LHC Run-2, targeting events in the FH channel. They require the presence of a large number of jets, large H_{T} , and one, two, or three jets tagged by the online b jet identification. To further improve the trigger efficiency, events recorded by a single-jet trigger with a high- p_{T} threshold or by a trigger with a high- H_{T} threshold are also considered. The selection criteria are detailed in Table 1. In the SL channel, events were selected by triggers requiring the presence of one muon or one electron with

p_T exceeding a given threshold. In order to compensate for the increased p_T threshold of the single-electron trigger in 2017 and 2018, a trigger requiring both an electron and large H_T was also used. The selection criteria are detailed in Table 2. In the DL channel, events were selected online by the dilepton (ee , $\mu\mu$, $e\mu$) triggers detailed in Table 3, complemented by the single-lepton triggers from Table 2 to maximise the selection efficiency. Lepton identification and isolation requirements are imposed for some of the single-lepton and dilepton triggers, and some of the dilepton triggers also impose an impact parameter requirement [34, 35]. The trigger selection efficiencies for signal events that pass the offline baseline selection criteria (see Section 6) amount to 90% in the FH and the SL channels, and to 98% in the DL channel.

Table 1: Trigger selection criteria in the fully hadronic (FH) channel. Multiple criteria, each represented by one row, are used per year and combined with a logical OR. In the case of the four-jet trigger, the minimum jet p_T is different for each jet and separated by a slash (/).

Year	Jets	b-tagged jets	Jet p_T (GeV)	H_T (GeV)
2016	≥ 6	≥ 1	>40	>450
	≥ 6	≥ 2	>30	>400
	≥ 1	—	>450	—
2017	≥ 6	≥ 1	>40	>430
	≥ 6	≥ 2	>32	>380
	≥ 4	≥ 3	$>75/60/45/40$	>300
	—	—	—	>1050
2018	≥ 6	≥ 1	>36	>450
	≥ 6	≥ 2	>32	>400
	≥ 4	≥ 3	$>75/60/45/40$	>330
	—	—	—	>1050

Table 2: Trigger selection criteria in the single-lepton (SL) channel. Multiple criteria per lepton flavour, each represented by one row, are used per year and combined with a logical OR.

Year	Flavour	Lepton p_T (GeV)	H_T (GeV)
2016	e	>27	—
	μ	>24	—
2017	e	>32	—
	e	>28	>150
	μ	>27	—
2018	e	>32	—
	e	>28	>150
	μ	>24	—

The trigger selections are also applied to the simulated events described in Section 4, and residual differences between the efficiencies in data and simulation are corrected. The size of the correction factors is approximately 0.95 in the SL channel and 0.98 in the DL channel. In the FH channel, the factors vary from approximately 0.99 in 2016 to 0.9 in 2017 and 0.95 in 2018, owing to the different trigger conditions and thresholds used in each data-taking period. The

Table 3: Trigger selection criteria in the dilepton (DL) channel. Multiple criteria per lepton flavour, each represented by one row, are used per year and combined with a logical OR.

Year	Flavour	Leading/subleading lepton p_T (GeV)	$m_{\mu\mu}$ (GeV)
2016	ee	>23/12	—
	e μ	>23 (μ)/12 (e)	—
	e μ	>23 (e)/8 (μ)	—
	$\mu\mu$	>17/8	—
2017	ee	>23/12	—
	e μ	>23 (μ)/12 (e)	—
	e μ	>23 (e)/12 (μ)	—
	e μ	>23 (e)/8 (μ)	—
	$\mu\mu$	>17/8	>3.8
2018	ee	>23/12	—
	e μ	>23 (μ)/12 (e)	—
	e μ	>23 (e)/12 (μ)	—
	e μ	>23 (e)/8 (μ)	—
	$\mu\mu$	>17/8	>3.8

efficiencies of the triggers in the FH channel and of the single-electron triggers were measured in datasets collected using single-muon triggers that present a negligible correlation with the triggers used in this analysis. The single-muon trigger efficiencies were measured using the tag-and-probe technique in a control region enriched in $Z \rightarrow \mu^+\mu^-$ events. The trigger efficiency in the DL channel was measured in a dataset collected using triggers requiring the presence of missing transverse momentum.

During the 2016 and 2017 data-taking, a gradual shift in the timing of the inputs of the ECAL L1 trigger in the region at $|\eta| > 2$, referred to as “L1 prefiring”, caused a specific trigger inefficiency [30]. For events containing an electron (a jet) with $p_T \gtrsim 50$ GeV ($\gtrsim 100$ GeV), the efficiency loss is approximately 10–20% in the region $2.5 < |\eta| < 3$. Correction factors were computed from data and applied to the efficiency evaluated from simulation.

4 Simulated samples

Several Monte Carlo (MC) event generators, interfaced with a detailed detector simulation based on GEANT4 (v. 9.4) [36], are used to model signal and background events. Separate samples corresponding to the 2016, 2017, and 2018 data-taking conditions were produced in order to match the different LHC and detector conditions and reconstruction efficiencies. Events are simulated at next-to-leading order (NLO) accuracy of QCD perturbation theory with the POWHEG (v. 2) [37–41] or MADGRAPH5_aMC@NLO (v. 2.4.2) [42] event generator, or at leading order (LO) accuracy using PYTHIA (v. 8.230) [43], depending on the process. The value of the Higgs boson mass is assumed to be 125 GeV, while the top quark mass value is set to 172.5 GeV. In all simulated samples, the proton structure is described by the parton distribution function (PDF) set NNPDF3.1 [44], except for the minor background samples matching the 2016 conditions, where the PDF set NNPDF3.0 [45] is used. Parton showering (PS) and hadronisation are simulated with PYTHIA. The parameters for the underlying event description correspond to the

CP5 tune [46] for all signal and background processes, except the minor background processes in the 2016 samples, where the CUETP8M1 [47] tune is used.

The $t\bar{t}H$ signal is simulated at NLO accuracy with POWHEG and, solely for the coupling interpretation, at LO with MADGRAPH5_aMC@NLO. The tH signal is simulated at LO with MADGRAPH5_aMC@NLO. It proceeds through t -channel production (tHq), associated tW production (tHW), and s -channel production. The contribution from s -channel tH production is negligible and is not considered in this analysis. Different flavour schemes are chosen to simulate the tHq and tHW processes. In the five-flavour scheme (5FS), bottom quarks are considered as massless sea quarks of the proton and may appear in the initial state of pp scattering processes. In the four-flavour scheme (4FS), bottom quarks are considered massive and are produced by gluon splitting at the matrix-element (ME) level [48]. The tHq process is simulated in the 4FS and the tHW process in the 5FS. This selection is made to ensure that potential interference contributions from tHW with $t\bar{t}H$ production, which are deemed negligible within the phase space considered in this analysis [49], are excluded from the simulation. In both the $t\bar{t}H$ and tH simulated samples, all relevant decay channels of the Higgs boson are considered. In the case of the Higgs boson coupling analysis, the kinematic properties of the tH events vary depending on the probed coupling strength, and the kinematic properties of both the tH and the $t\bar{t}H$ events vary depending on the probed CP structure. This is accounted for by event weights, following the approach described in Refs. [50, 51].

Major background contributions arise from $t\bar{t} + \text{jets}$ production. They are modelled with simulated events obtained from two different generators implemented in the POWHEG framework and interfaced to PYTHIA for the PS simulation. The version and configuration of the two generators are summarised in Table 4. The POWHEG generator is used to simulate the $pp \rightarrow t\bar{t}$ process at NLO accuracy in the 5FS (referred to as $t\bar{t}$ sample), while the dedicated POWHEG-BOX-RES program presented in Ref. [24] together with OPENLOOPs [52] is used to simulate the $pp \rightarrow t\bar{t} + b\bar{b}$ process at NLO accuracy in the 4FS (referred to as $t\bar{t}b\bar{b}$ sample). In the $t\bar{t}b\bar{b}$ sample, the additional b jets that do not stem from the top quark decays and that are critical for the background description are simulated at the ME level and thus expected to model more accurately the data. The choice of the renormalisation and factorisation scales (μ_R, μ_F) for the $t\bar{t}b\bar{b}$ sample follows Refs. [22, 24, 53] and is motivated by the presence of two very different relevant scales related to the $t\bar{t}$ and $b\bar{b}$ systems. Compared to Ref. [24], the values of the scales are reduced by a factor 0.5 in order to approximate the effect of missing higher-order corrections and attenuate theoretical uncertainties related to the ME-PS matching. This choice is motivated by the suggested scale options presented in Ref. [25] that were derived comparing the predictions of $t\bar{t} + b\bar{b}$ calculations to those of $t\bar{t} + b\bar{b} + 1$ jet calculations at NLO in QCD. The PDF sets have been chosen consistent with the flavour scheme, with values of the strong coupling constant α_S matching the order of the ME generation in both cases. The same PYTHIA version and underlying event tune have been used for both samples. The combination of the two samples and the details of the $t\bar{t} + \text{jets}$ background model are described in Section 7.

Minor backgrounds originate from single top quark production, the production of W and Z/γ^* bosons with additional jets (referred to as $V + \text{jets}$), $t\bar{t}$ production in association with a W , a Z boson ($t\bar{t}V$), or a photon ($t\bar{t}\gamma$), and diboson (WW , WZ , and ZZ referred to as VV) processes. The single top quark processes in the t and tW channels are simulated with POWHEG [54–56]. The s -channel single top quark processes, as well as the $V + \text{jets}$, $t\bar{t}V$, and $t\bar{t}\gamma$ processes are simulated with MADGRAPH5_aMC@NLO. For all of them, except for the s -channel single top quark sample, the matching of ME to PS jets is performed using the FxFx [57] prescription. Diboson production is simulated using the PYTHIA event generator. Contributions from rare top quark processes, including $4t$, tWZ , and $3t$ production, are below 1% of the total background

Table 4: Generator version and configuration of the $t\bar{t}$ and $t\bar{t}b\bar{b}$ samples. The parameters m_t and m_b denote the top quark and bottom quark mass, respectively, $m_{T,t}$, $m_{T,b}$, and $m_{T,g}$ the transverse mass of the top quark, the bottom quark, and additional gluons, respectively, and h_{damp} the parton shower matching scale.

	$t\bar{t}$ sample	$t\bar{t}b\bar{b}$ sample
POWHEG version	POWHEG v2	POWHEG-BOX-RES
PYTHIA version	8.230	8.230
Flavour scheme	5	4
PDF set	NNPDF3.1	NNPDF3.1
m_t	172.5 GeV	172.5 GeV
m_b	0	4.75 GeV
μ_R	$\sqrt{\frac{1}{2} \left(m_{T,t}^2 + m_{T,\bar{t}}^2 \right)}$	$\frac{1}{2} \sqrt[4]{m_{T,t} m_{T,\bar{t}} m_{T,b} m_{T,\bar{b}}}$
μ_F	μ_R	$\frac{1}{4} \left[m_{T,t} + m_{T,\bar{t}} + m_{T,b} + m_{T,\bar{b}} + m_{T,g} \right]$
h_{damp}	$1.379 m_t$	$1.379 m_t$
Tune	CP5	CP5

and under 2% of the signal in the most signal-enriched regions, and are therefore neglected.

In the FH channel, the dominant background originates from QCD multijet production. Simulated QCD multijet events, generated with MADGRAPH5_aMC@NLO at LO accuracy using the MLM [58] prescription for the ME-PS matching, are employed solely for additional validation of observables and procedures. For the actual analysis, its validation and optimisation, the QCD background contribution is estimated from data as described in Section 8.

For comparison with the observed distributions, the event yields in the simulated samples are normalised to the integrated luminosity of the corresponding data sample, according to their predicted cross sections. The SM $t\bar{t}H$ cross section of 507^{+35}_{-50} fb is taken from calculations including QCD and electroweak corrections at NLO [22]. The SM cross section for tH production is computed in the 5FS at NLO accuracy in QCD [22], which results in $74.3^{+5.6}_{-11.3}$ fb for tHq and $15.2^{+1.2}_{-1.4}$ fb for tHW production. The DR2 scheme [49] is employed in the calculation of tHW production to remove overlapping contributions between tHW and $t\bar{t}H$ processes. In this scheme, the squared double resonant term is removed from the squared amplitude of the tHW process, while the interference term between double- and single-resonant contributions is kept. Higgs boson branching fractions are obtained from calculations with at least NLO accuracy [22]. The calculated $t\bar{t}H$ and tH cross sections and Higgs boson branching fractions are rescaled assuming a Higgs boson mass of 125.38 GeV, corresponding to the latest measurement by the CMS Collaboration [59]. The $t\bar{t}$ cross section of 832 pb corresponds to the next-to-next-to-leading order (NNLO) calculation with resummation to next-to-next-to-leading logarithmic (NNLL) accuracy [60–66]. The cross sections of the other background processes are taken at NNLO ($V + \text{jets}$), approximate NNLO (single top quark tW -channel [67]), and NLO (single top quark t - and s -channels [68, 69], $t\bar{t}V$ [70], and diboson [71]) accuracy.

Effects from additional pp interactions in the same or nearby bunch crossings (pileup) are modelled by adding simulated minimum bias events to all simulated events. The pileup multiplicity distribution in simulation is reweighted to reflect the luminosity profile of the observed pp

collisions [72]. Further correction factors described in Section 5 are applied to the simulation where necessary to improve the description of the data.

5 Object and event reconstruction

Events are reconstructed offline based on a particle-flow (PF) technique [73], which aims to reconstruct and identify each individual particle produced in pp collisions by optimally combining information from the various elements of the CMS detector.

The primary vertex is taken to be the vertex corresponding to the hardest scattering in the event, evaluated using tracking information alone, as described in Section 9.4.1 of Ref. [74].

The reconstruction of muons relies on a combination of measurements in the tracker and in the muon detectors [75]. The muons are identified based on the quality of the combined track fit and on the number of hits in the different tracking detectors, with an efficiency of about 95%. Electrons are reconstructed by combining the momentum measurement in the tracker with the energy measurement of the corresponding cluster in the ECAL and with the energy sum of all bremsstrahlung photons, obtained from the ECAL, spatially compatible with originating from the electron track [35, 76]. The electrons are identified using criteria on the cluster shape in the ECAL, the track quality, and the compatibility between the tracker and ECAL measurements, corresponding to an identification efficiency of approximately 80%, including the isolation requirements described below. Both muons and electrons are required to lie within the acceptance of the tracker, covering the region up to $|\eta| = 2.4$. Electrons reconstructed in the transition region $1.44 < |\eta| < 1.56$ between the barrel and the endcap calorimeters are discarded. Isolation requirements are imposed on the leptons based on the scalar p_T sum of all PF objects in a cone of radius $\Delta R = 0.3$ (0.4) around the track direction of the electron (muon), where $\Delta R = \sqrt{\Delta\eta^2 + \Delta\phi^2}$. The isolation is corrected by removing contributions from pileup. Residual differences between the lepton reconstruction, identification, and isolation efficiencies in data and simulation are corrected, based on efficiency measurements in high-purity data samples of Z boson decays [35, 75].

Hadronic jets are reconstructed by clustering PF candidates using the anti- k_T algorithm [77, 78] with a distance parameter of 0.4, omitting charged particles matched to pileup vertices. The jet energy is corrected for the neutral-hadron contribution expected from pileup interactions [79]. Further energy corrections depending on the jet p_T and η are applied, which are derived in simulation such that the average measured energy of the jets becomes identical to that of the particle-level jets. Residual differences between the jet energy scale in data and in simulation are measured using the momentum balance in dijet, $\gamma + \text{jets}$, $Z + \text{jets}$, and multijet events, and appropriate corrections are made. The jet energy resolution amounts typically to 15–20% at 30 GeV and 10% at 100 GeV [80]. Jets overlapping with an electron or muon passing the criteria described above within a cone of $\Delta R = 0.4$ are discarded. Further selection criteria are applied to each jet to remove jets potentially dominated by instrumental effects or reconstruction failures as well as jets arising from pileup interactions [72, 81]. Only jets within the tracker acceptance of $|\eta| < 2.4$ and with $p_T > 30$ GeV are considered in the analysis. In addition, jets with $p_T > 40$ GeV and $2.4 < |\eta| < 4.7$ (forward jets) are selected in the SL channel for the event reconstruction under the hypothesis of tHq production, which is characterised by the presence of jets with large $|\eta|$ values.

The b jets are identified using b tagging techniques [82]. This analysis benefits from the DEEP-JET [83, 84] tagger, featuring an increase of the b tagging efficiency by 5–10% with respect to the tagger used in the previous analyses [12, 13, 18] for the same mistag rate. Jets are considered

as b tagged if they fulfil a requirement on the DEEPJET score that corresponds to a b tagging efficiency of about 75–80% and 1.5–2% (15–17%) mistag rate for light-flavour (c quark) jets. Specifically for the estimation of the QCD multijet background, a second requirement on the DEEPJET output is utilised, which corresponds to approximately 90% b tagging efficiency at a 10% (43–47%) light-flavour (c quark) mistagging rate, referred to as “loose” b tag. The DEEPJET discriminant, and thus b tagging efficiencies and mistag rates, in the simulation is corrected to match the one measured in data [82]. The DEEPJET discriminant value is further used in the analysis as one of the input variables for the ANN discriminants described in Section 8.

The missing transverse momentum vector \vec{p}_T^{miss} is computed as the negative vector sum of the transverse momenta of all the PF candidates in an event, and its magnitude is denoted as p_T^{miss} [85]. The \vec{p}_T^{miss} is recomputed to account for corrections to the energy scale of the reconstructed jets in the event.

6 Event selection

The first step of the event classification, referred to as baseline selection, defines the events assigned to the DL, SL, and FH channels, and is summarised in Table 5 and described in the following.

Table 5: Baseline selection criteria in the fully hadronic (FH), single-lepton (SL), and dilepton (DL) channels based on the observables defined in the text. Leptons and jets are ranked in p_T . The * indicates that the requirement is only applied to the same-flavour DL channels. Where the criteria differ per year of data taking, they are quoted as three values, corresponding to 2016/2017/2018, respectively.

	FH channel	SL channel	DL channel
Number of leptons	0	1	2
Sign and flavour of leptons	—	e^\pm, μ^\pm	$e^+e^-, \mu^\pm e^\mp, \mu^+ \mu^-$
p_T of leading electron (GeV)	—	>29/30/30	>25
p_T of leading muon (GeV)	—	>26/29/26	>25
p_T of additional leptons (GeV)	<15	<15	>15
$ \eta $ of leptons	<2.4	<2.4	<2.4
$m_{\ell\ell}$ (GeV)	—	—	>20 (and <76 or >106)*
Number of jets	≥ 7	≥ 5	≥ 3
p_T of jets (GeV)	>30	>30	>30
p_T of 6 th jet (GeV)	>40	—	—
$ \eta $ of jets	<2.4	<2.4	<2.4
Number of b-tagged jets	≥ 2	≥ 4	≥ 3
m_{qq} (GeV)	>30 and <250	—	—
H_T (GeV)	>500	—	—
p_T^{miss} (GeV)	—	>20	>40*

Events with exactly two opposite-sign leptons (electrons or muons) with p_T of at least 25 (15) GeV for the (sub)leading p_T lepton and at least three b-tagged jets are assigned to the DL channel. The offline and online flavour content of the event must be consistent, meaning, e.g. that $\mu\mu$ events are required to be recorded by single-muon or dimuon triggers. The invariant

mass of the selected lepton pair, $m_{\ell\ell}$, is required to be larger than 20 GeV to suppress events from heavy-flavour resonance decays and low-mass Drell–Yan processes. In order to reject $Z + \text{jets}$ events, same-flavour events with $76 < m_{\ell\ell} < 106$ GeV are discarded.

The baseline selection for the SL channel requires the presence of exactly one electron or muon, consistent with the trigger that accepted the event. The lepton p_T requirement is chosen based on the trigger thresholds, and therefore depends on the data-taking year. Muons must have $p_T > 26$ (29) GeV for data recorded in 2016 and 2018 (2017), while the p_T thresholds for electrons are 29 (30) GeV in 2016 (2017 and 2018). Furthermore, no additional leptons with $p_T > 15$ GeV must be present in the event. Only events with at least five jets, of which at least four are b tagged, are considered. A minimum p_T^{miss} of 40 and 20 GeV is required in the DL channels with same-flavour leptons and in the SL channel, respectively, to further suppress minor background contributions from $V + \text{jets}$ and QCD multijet production.

All remaining events with no leptons passing the selection criteria in the DL and SL channels and with at least seven jets, of which at least two are b tagged, are assigned to the FH channel. In order to match the online trigger selection, events with $H_T < 500$ GeV or less than six jets with $p_T > 40$ GeV are discarded. The invariant mass m_{qq} of the pair of non-b-tagged jets for which m_{qq} is closest to the nominal W boson mass is required to lie between 30 and 250 GeV. To estimate the dominant QCD multijet background from control samples in data in this channel, events are further split into a signal region (SR) and several control and validation regions (CRs and VRs, respectively) according to the value of m_{qq} , as described in Section 8.

The aforementioned criteria have been optimised for a high $t\bar{t}H$ signal selection efficiency, while still retaining a sufficiently high tH signal acceptance. The minimum number of jets required in each channel is lower than the one expected for $t\bar{t}H$ production at LO in order to recover events with jets falling outside of the object acceptance and to increase the efficiency for tH signal events.

Figure 2 shows the jet multiplicity distribution for the FH, SL, and DL channels after the baseline selection and prior to the final fit to data. The expected signal and background contributions are estimated using the simulations for the various processes introduced in Section 4. Good agreement between data and simulation is observed in the SL and DL channels within the uncertainties. In the FH channel, where the dominant background contribution stems from QCD multijet production, a significant trend in data is observed towards higher jet multiplicity; the poor modelling of the QCD multijet background by the simulation is expected and the reason it is estimated directly from data.

To maximise the analysis sensitivity, two likelihood ratios are computed in each event and provided as input to the final ANN discriminants described in Section 8. First, a b tagging likelihood ratio (BLR) is computed that is designed to discriminate between events compatible with the presence of four and two b jets. The likelihoods are evaluated under either the hypothesis that four jets or that two jets in the event originate from b quarks, based on the expected b tagging discriminant probability densities from simulation, summing over all possible permutations of quark-jet associations. The BLR is defined as the ratio of the four-b-jets likelihood to the sum of the four- and the two-b-jets likelihoods. Second, a likelihood ratio comparing the $t\bar{t}H$, $H \rightarrow b\bar{b}$ signal and the $t\bar{t} + b\bar{b}$ background hypotheses is computed based on an ME method (MEM) [86] that utilises the full kinematic properties of the event, as documented in Refs. [13, 87].

Furthermore, in the SL channel boosted decision trees (BDTs), referred to as reconstruction BDTs, are used to assign the jets in an event to partons under the hypothesis of the event being

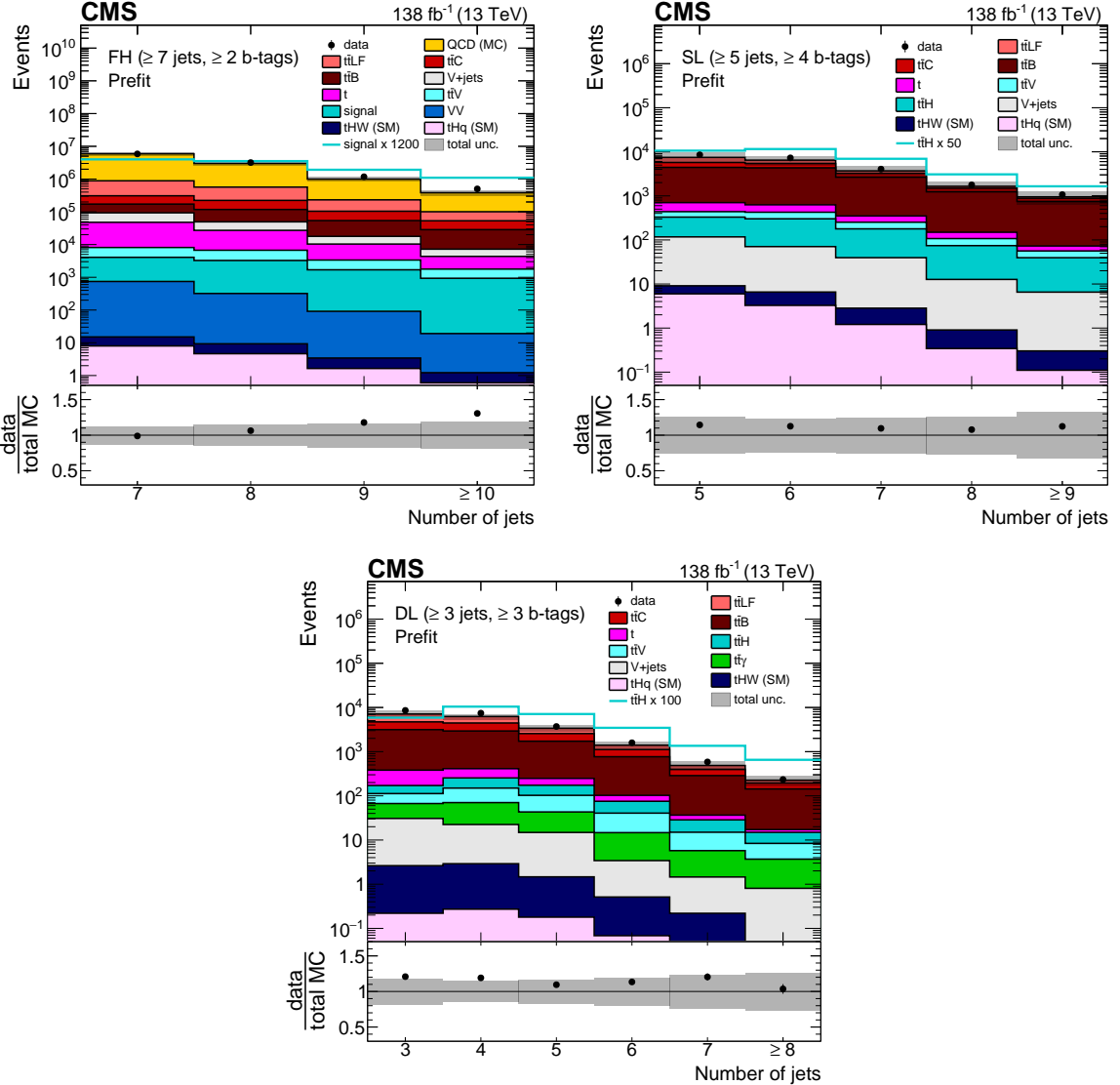


Figure 2: Jet multiplicity distribution in the FH (upper left), SL (upper right), and DL (lower) channels, after the baseline selection and prior to the fit to the data. Here, the QCD multijet background prediction is taken from simulation. The different $t\bar{t}$ + jets background contributions ($t\bar{t}LF$, $t\bar{t}B$, and $t\bar{t}C$) are discussed in Section 7. The expected $t\bar{t}H$ signal contribution, scaled as indicated in the legend for better visibility, is also overlaid (line). The uncertainty band represents the total (statistical and systematic) uncertainty. The last bin in each distribution includes the overflow events.

either a $t\bar{t}H$, tHq , tHW , or $t\bar{t}$ event. The BDTs take as input observables such as the invariant mass and p_T of the reconstructed particles, the b tagging discriminant value of jets, as well as angular distances between reconstructed particles. They are trained separately for each hypothesis, such that the most probable jet assignment under the given hypothesis yields the largest BDT output value. In case of the tHq hypothesis, the forward jets are also taken into account in the event reconstruction as candidates for the light-flavour quarks, which typically have large $|\eta|$ values in tHq events. The procedure achieves reconstruction efficiencies of approximately 43%, 60%, 52%, and 66% for $t\bar{t}H$, tHq , tHW , or $t\bar{t}$ events, respectively. The lower efficiency for $t\bar{t}H$ events compared to $t\bar{t}$ events is caused by the greater combinatorial challenge due to the presence of two additional b jets for $t\bar{t}H$ events. The output values of the reconstruction BDTs as well as several observables that are obtained based on the chosen jet assignments are among the input variables to the ANNs used for the signal extraction in this channel.

The further event categorisation within each channel and the strategy adopted to extract the signal are described in Section 8.

7 The $t\bar{t} + \text{jets}$ background model

After the baseline selection, contributions from $t\bar{t} + \text{jets}$ production constitute more than 95% of the total expected background events in the leptonic channels. Particularly critical among these are $t\bar{t}$ events with additional b jet production, since their final state is identical to that of the $t\bar{t}H$ signal events, the cross section is approximately 10–20 times larger than that of the signal in the phase space considered, and the events are difficult to model theoretically due to the multiparton final state with two very different mass scales.

Several dedicated measurements [88–90], as well as the observations in previous versions of this analysis [12] and the observations in the control regions studied in this analysis (see Section 8), show that the $t\bar{t} + b$ jets contribution present in data is larger than predicted by the simulation, by a factor of typically 1.2–1.4, depending on the MC event generator. In Ref. [88], also normalised differential $t\bar{t} + bb$ cross-section measurements in the one-lepton channel are presented for various observables. For events with ≥ 6 jets and ≥ 4 b-tagged jets, the shapes of the distributions observed in data in Ref. [88] mostly agree to those predicted with the $t\bar{t}bb$ sample described in Section 4 within the uncertainties. Larger discrepancies, in particular in the jet and b-tagged jets multiplicity distributions, are observed in Ref. [88] for events with 3 b-tagged jets, which are not considered in the analysis presented in this paper. The results in Ref. [88] were, however, obtained in a slightly different phase space, selecting for example jets with $p_T > 25 \text{ GeV}$, and unfolded to the particle level, such that a direct comparison with the distributions presented here is not possible.

The $t\bar{t} + \text{jets}$ background is modelled using a combination of the $t\bar{t}$ and $t\bar{t}bb$ samples described in Section 4. The simulated $t\bar{t} + \text{jets}$ events are separated into three mutually exclusive processes, based on the flavour of the additional jets at the particle level that do not originate from the top quark decays. The jet flavour is defined using the ghost-matching procedure described in Ref. [91], and the particle level jets need to fulfil the acceptance requirements of $p_T > 20 \text{ GeV}$ and $|\eta| < 2.4$. The three processes are defined as: $t\bar{t}B$, comprising events with at least one additional jet generated within the acceptance that contains one or more b hadrons; $t\bar{t}C$, for which events have at least one additional jet containing c hadrons within the acceptance and no additional jets containing b hadrons; or else $t\bar{t} + \text{light-flavour jets}$ ($t\bar{t}LF$), which corresponds to events that do not belong to any of the above processes. The $t\bar{t}B$ events are further separated into two mutually exclusive processes. The subset of events with exactly two additional b hadrons that are close enough in direction to be inside a single jet is denoted as $t\bar{t} + 2b$. This

separation is important because the processes are subject to different systematic uncertainties arising from the modelling of collinear gluon splitting. The remaining subset of events is denoted as $t\bar{t} + b(\bar{b})$.

The $t\bar{t}B$ background events, which represent the most critical background component, are taken from the $t\bar{t}bb$ sample. Here, the additional b jets are modelled by the ME calculation and are subject, in particular, to the renormalisation and factorisation scale uncertainties. The $t\bar{t}C$ and $t\bar{t}LF$ events, which do not include additional b jets within the acceptance but can still pass the event selection (e.g. due to mistagging), are taken from the $t\bar{t}$ sample. Prior to the fit to data, the fractional contributions of the $t\bar{t}B$, $t\bar{t}C$, and $t\bar{t}LF$ events are chosen according to the $t\bar{t}$ sample in the inclusive phase space and the total yield of the $t\bar{t} + \text{jets}$ events is scaled to the NNLO+NNLL $t\bar{t}$ cross section of 832 pb. The final yields of the $t\bar{t}B$ and $t\bar{t}C$ contributions are free parameters in the fit to data, providing flexibility to adjust the predicted $t\bar{t}B$ yield to the one observed in data through dedicated CRs. The impact of potential mismodelling of the $t\bar{t}B$ background on the extracted signal was studied using pseudo-experiments and found to be well covered by the systematic uncertainties, as described in Section 9.

The modelling of the $t\bar{t}B$ background has been validated in data in various observables and relevant phase space regions. Only observables for which also the correlation to other observables is well-modelled were used further in the analysis, as described in Section 8. For example, the shape of the predicted jet multiplicity distributions in the SL and DL channels, shown in Fig. 2 after the baseline selection and prior to the fit to data, agrees well with the one observed in data. The overall normalisation difference is attributed to the underprediction of the $t\bar{t}B$ component in the simulation. Further example distributions are shown in Figs. 3 and 4 for events in signal-enriched regions of high jet and b -tagged jet multiplicity: the average $\Delta\eta$ and the minimum ΔR between any two b -tagged jets, which are sensitive to the $t\bar{t}B$ modelling details; the MEM discriminant output, which is one of the most powerful single variables used in the analysis to separate the $t\bar{t}H$ signal from the $t\bar{t}B$ background; and the p_T of the Higgs boson candidate identified either using the aforementioned reconstruction BDT or as the pair of b -tagged jets closest in ΔR , which is relevant specifically for the STXS measurement. Prior to the fit to data, the shapes of the data distributions are well described by the simulation. Differences in the normalisation are attributed to the expected under-prediction of the $t\bar{t}B$ yield. With the postfit background model obtained from the final fit to data described in Section 10, the predicted distributions agree well with the ones observed in data. The effect of the fit on these observables mostly changes the relative normalisation of each component, reduces the corresponding uncertainties, and slightly modifies the shapes of the distributions within the associated systematic uncertainties.

8 Analysis strategy and classification

In each analysis channel, the selected events are divided into categories depending on the jet and b -tagged jet multiplicity. In each category, dedicated ANNs are trained and optimised to separate specific signal or background processes. The ANN output is used, in the SL and DL channels, to categorise further the events and, in all channels, to construct the final discriminating observables. The events are categorised independently for the 2016, 2017, and 2018 data-taking periods.

The signal is extracted in a simultaneous binned profile likelihood fit to the data of the expected signal and background distributions of the discriminating observable or of the event yield, depending on the channel and category [92]. The fit is performed across all categories and channels. The systematic uncertainties discussed in Section 9 are taken into account using

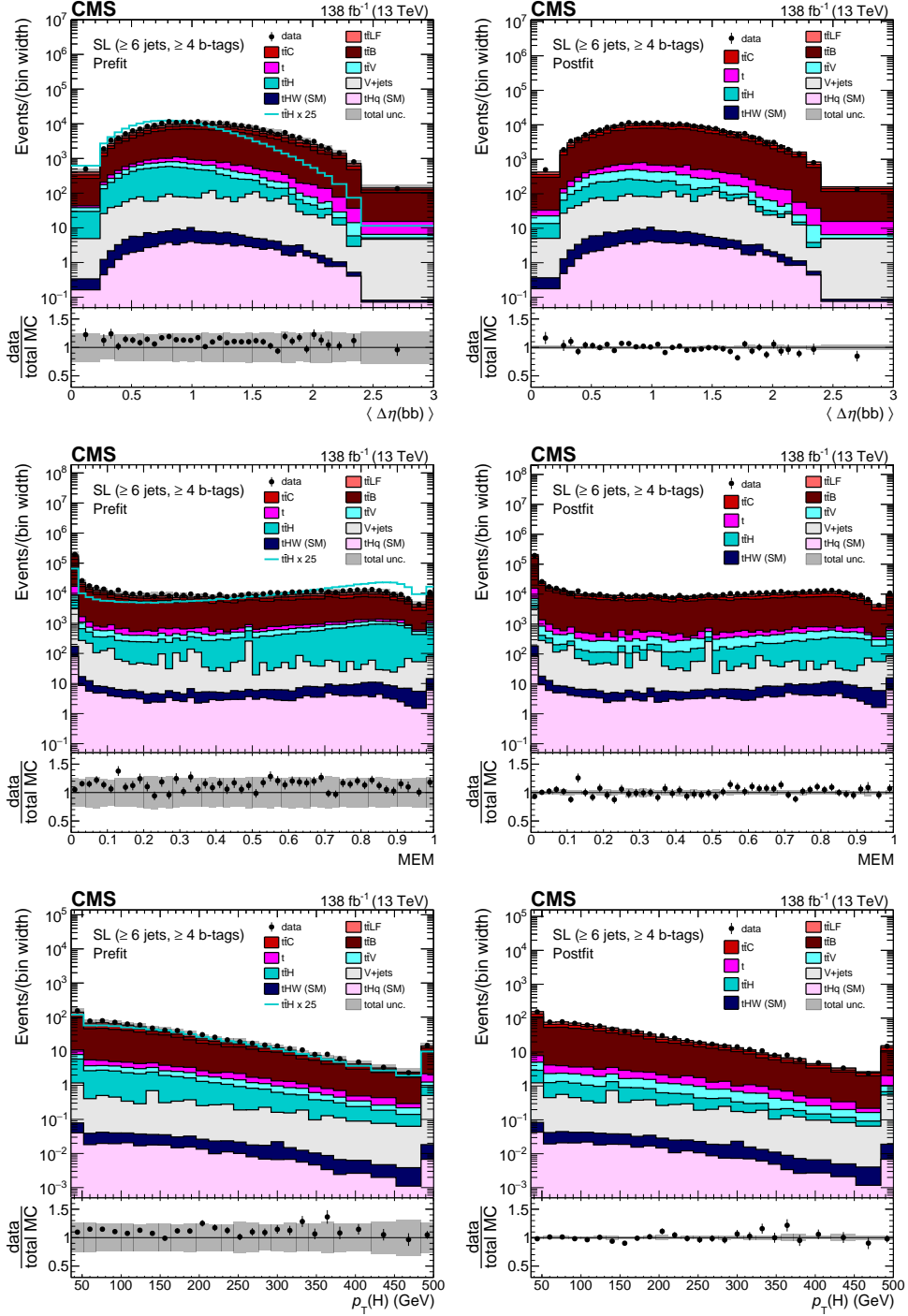


Figure 3: Average $\Delta\eta$ between any two b-tagged jets (upper), MEM discriminant output (middle), and p_T of the Higgs boson candidate identified with the reconstruction BDT for the $t\bar{t}H$ hypothesis (lower) for events passing the baseline selection requirements and additionally ≥ 6 jets in the SL channel prefit (left) and with the postfit background model (right) obtained from the fit to data described in Section 10. In the prefit case, the $t\bar{t}H$ signal contribution, scaled by a factor 25 for better visibility, is also overlayed (line). The uncertainty band represents the total (statistical and systematic) uncertainty. Where applicable, the last bin in each distribution includes the overflow events.

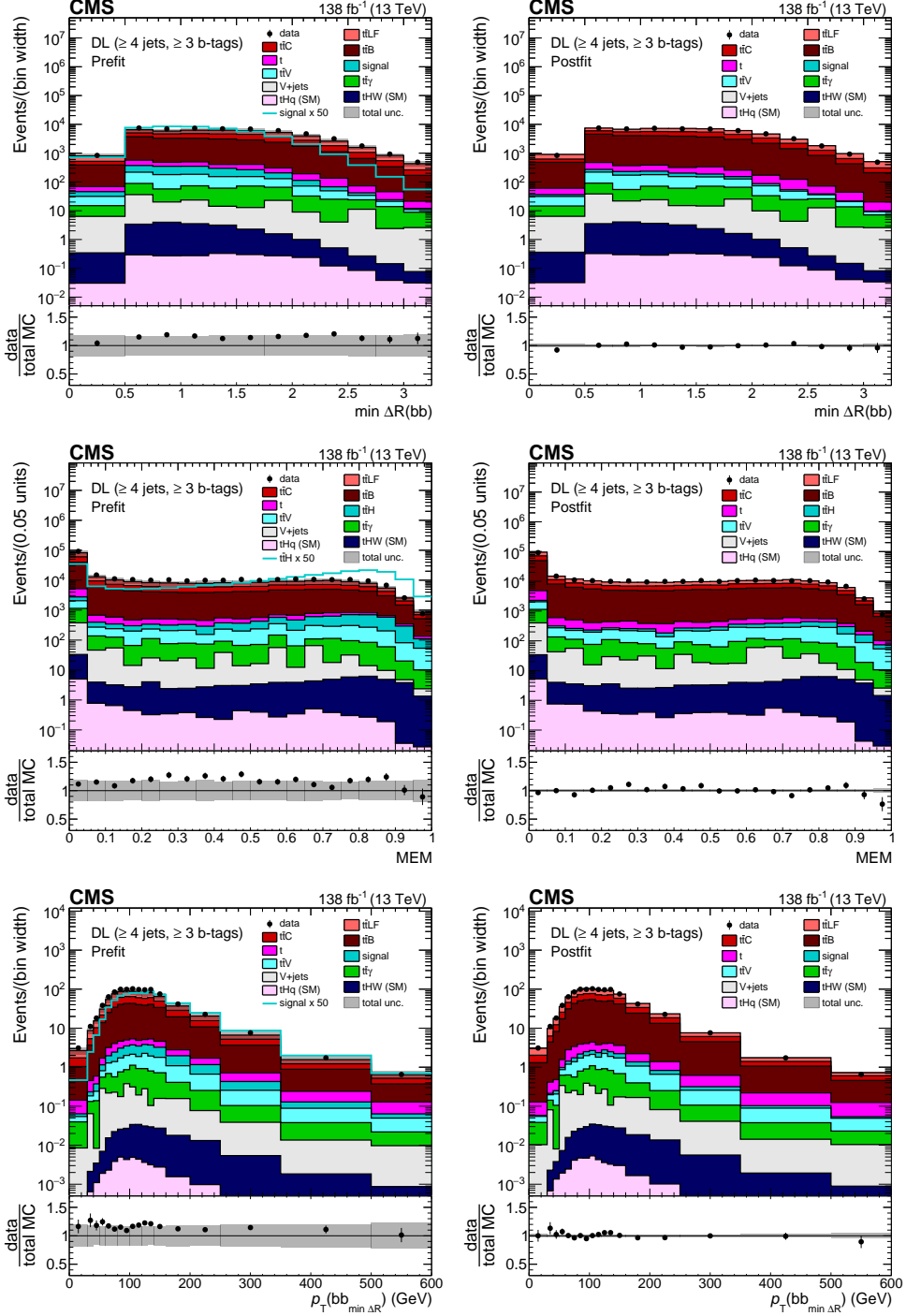


Figure 4: Minimum ΔR between any two b-tagged jets (upper), MEM discriminant output (middle), and p_T of the Higgs boson candidate identified as the pair of b-tagged jets closest in ΔR (lower) for events passing the baseline selection requirements and additionally ≥ 4 jets in the DL channel prefit (left) and with the postfit background model (right) obtained from the fit to data described in Section 10. In the prefit case, the $t\bar{t}H$ signal contribution, scaled by a factor 50 for better visibility, is also overlayed (line). The uncertainty band represents the total (statistical and systematic) uncertainty. Where applicable, the last bin in each distribution includes the overflow events.

nuisance parameters with appropriate constraints [92, 93], and are correlated among the processes, categories, channels, and data-taking periods, as described in Section 9. The different background composition in the categories helps to constrain the uncertainties and, thus, to increase the overall sensitivity. The signal distributions include contributions from all SM Higgs boson decays to take into account contamination by other decay channels than $H \rightarrow b\bar{b}$. The other decay channels contribute approximately 7% of the signal events, dominated by $H \rightarrow \tau\tau$ and $H \rightarrow WW$ decays.

The categorisation of the signal events differs depending on the interpretation. As a first step, the signal categories are optimised for the inclusive $t\bar{t}H$ and tH production rate measurements, as well as for the coupling and CP measurement. For the STXS measurement, the $t\bar{t}H$ signal categories in the different channels are split further into five subcategories (STXS categories) that target different ranges of p_T^H (with lower boundaries at 0, 60, 120, 200, and 300 GeV). Independent signal templates are constructed per particle-level Higgs boson p_T bin and fitted simultaneously. In each subcategory, the contributions from all p_T bins are considered, thereby taking into account migration of events across bins due to reconstruction and resolution effects.

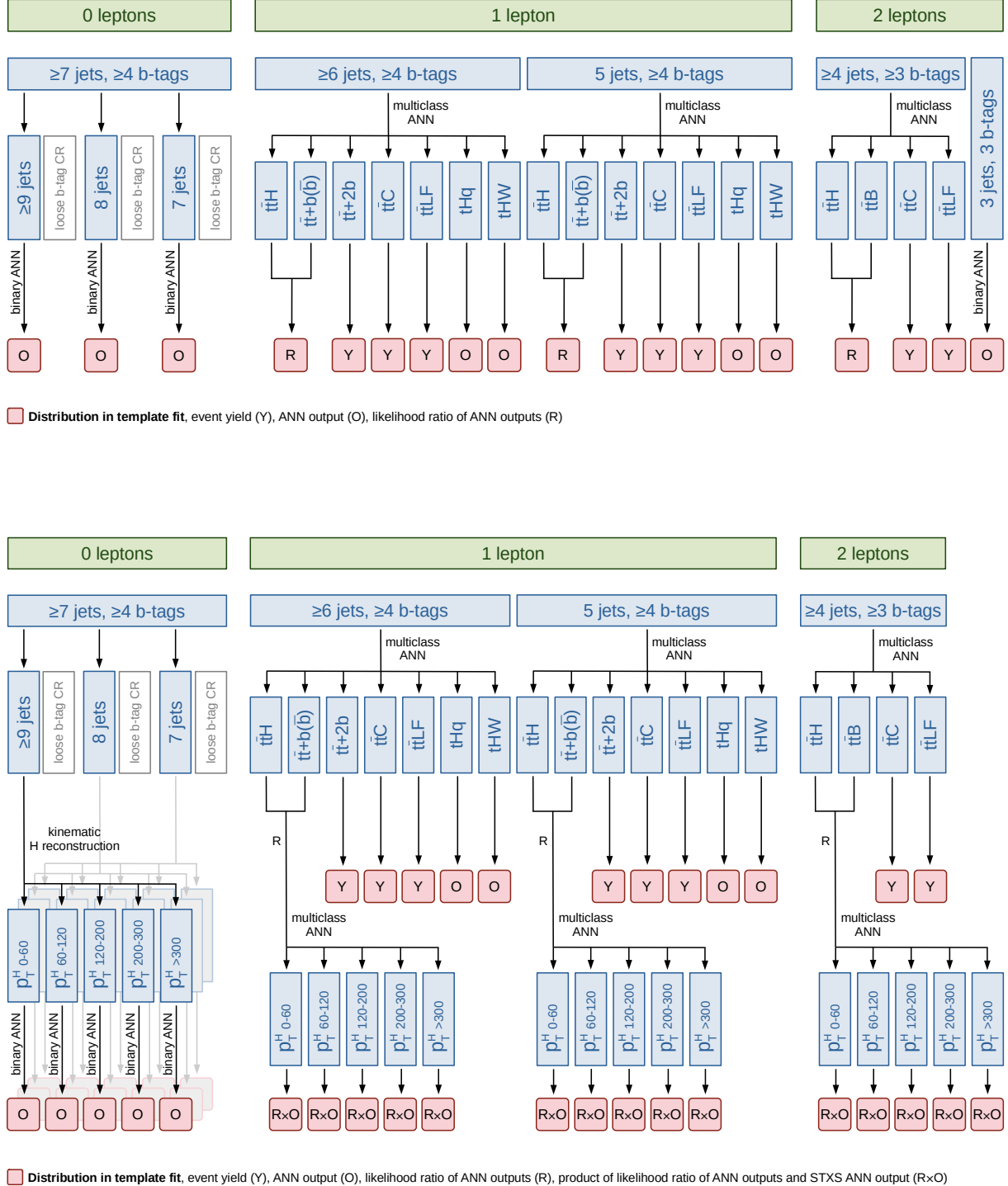
The analysis strategy is illustrated in Fig. 5 and detailed in the following. It has been optimised separately in each channel, based on both the quality of the background modelling and the expected sensitivity to an SM signal evaluated with simulated events and, in the case of the FH channel, data for the QCD multijet background determination. Common aspects of the ANNs are described in Section 8.1, followed by a description of the analysis strategy in the FH channel in Section 8.2, and in the SL and DL channels in Section 8.3.

8.1 Neural network architecture and training

In all analysis channels, dedicated ANNs are utilised for event categorisation or classification, as detailed further below. The ANNs are implemented in KERAS [94] as feed-forward neural networks. The architecture consists of three or four hidden layers with between 100 to 2048 nodes, depending on the channel and category. The activation function used in the nodes of the hidden layers are the “ReLU” function in the FH channel and the “LeakyReLU” function in the SL and DL channels [95]. The hyperparameters have been optimised using a “Tree Parzen Estimator” [96, 97], which uses information from past trials when testing the next set of hyperparameters. The cost function that is minimised during the training is the “categorical cross entropy” in case of multiclassification ANNs, and the “squared hinge” function or the “binary cross entropy” in case of binary classification ANNs [95]. Potential overtraining is minimised using dropout and L2 regularisation or dropout and simultaneously L1 and L2 regularisation, depending on the channel [98]. The ANNs have been found to provide the best analysis sensitivity compared to other types of ANNs or BDTs, evaluated using simulated data.

In each category, one single ANN is trained that is valid for all three data-taking periods. Simulated data and, in case of the FH channel, data of all three periods, weighted to reflect the different integrated luminosities, are used in the training, thereby reducing statistical fluctuations in the trained ANN parameter values. When evaluating the ANNs to obtain the final discriminant distributions in simulation and data, separate distributions are constructed per data-taking period in order to better control systematic uncertainties specific to the different periods, such as components of the jet energy scale and the b tagging uncertainties discussed in Section 9. It has been validated that the sensitivity of the analysis does not degrade compared to the case of training ANNs separately for each data-taking period or when using information about the year of data taking as an input feature to the ANN.

Depending on the category, between 0.5 and 1.5 million events are used for the training pro-



■ Distribution in template fit, event yield (Y), ANN output (O), likelihood ratio of ANN outputs (R), product of likelihood ratio of ANN outputs and STXS ANN output (RxO)

Figure 5: Illustration of the analysis strategy for the inclusive $t\bar{t}H$ and tH production rate, coupling, and CP measurements (upper), and for the $t\bar{t}H$ STXS measurement (lower). Details of the ANNs and the definition of the likelihood ratio are given in the text. The procedure is applied separately for the three years of data taking.

cedure, with at least 16 000 events for the $t\bar{t}B$ class in all cases. These events are further split into three independent subsamples used for the actual training (60%), for the optimisation of the hyperparameters (20%), and for validating the performance of the ANNs (20%). Additional weights are applied such that the effective number of events per class is the same in order to avoid that the ANN classification decision is biased by the relative frequency of the different processes or, in case of the STXS classification, the p_T^H bins. The training is terminated once either the performance obtained with the validation sample does not improve after 50 full passes over the training data (“epoch”) or the relative difference between the performance on the training and validation samples diverges (“early stopping”). The aforementioned events are used exclusively for training, optimisation, and validation, and another statistically independent set of events is used for the final analysis of the data to avoid biases due to potential overtraining.

The input variables of the ANNs are listed in Table 6. The variables have been chosen out of a larger set of possible variables as the ones that are most important for the performance of the ANNs, based on several ranking procedures including a Taylor expansion of the ANN output as a function of the input variables [99] and a “data Shapley” metric [100].

8.2 Fully hadronic channel

In the FH channel, events are categorised depending on the jet and b-tagged jet multiplicity, as well as the invariant mass of the pair of non-b-tagged jets closest to the nominal W boson mass, m_{qq} . Three categories, referred to as SRs, with (7 jets, ≥ 4 b tags), (8 jets, ≥ 4 b tags), and (≥ 9 jets, ≥ 4 b tags) are used for the signal extraction and enter the final fit. The events in the SR are in addition required to fulfil $60 < m_{qq} < 100$ GeV for events with 7 or 8 jets, and $72 < m_{qq} < 90$ GeV for events with ≥ 9 jets, where the different m_{qq} ranges reflect the dependency of the signal efficiency of the m_{qq} criterion on the jet multiplicity. Dedicated binary classification ANNs are trained in each SR to separate the $t\bar{t}H$ signal from the background, and the ANN classifier output distribution is used as the final discriminating observable.

For each SR, two mutually exclusive CRs with looser b tagging requirements, referred to as “evaluation regions” (ERs) and “training regions” (TRs), are defined, which are used to estimate the QCD multijet background and to train the ANNs, respectively. Events in the ERs (TRs) are required to contain at least four jets fulfilling the loose b tag requirement, out of which exactly three (two) are also b tagged. Otherwise, events in the ERs and TRs must pass the same selection criteria as events in the SRs. For each SR, ER, and TR, further mutually exclusive regions, referred to as “validation regions” (VR-SR, VR-ER, VR-TR), are defined by inverting the criterion on m_{qq} . The VRs are signal depleted, with an expected $t\bar{t}H$ contribution below 0.6%, and used to test the background estimation and ANN training procedures described in the following. The categorisation scheme is summarised in Table 7.

The dominant background contribution (approximately 72–80%) in the SR originates from QCD multijet production. The contribution is determined from the data to avoid effects from inaccurate modelling and insufficient number of events in the relevant phase space regions of the QCD simulation. The procedure is as follows: the ANNs are trained using the events from the TRs, which are estimated to originate from QCD multijet production more than 80% of the time, followed by $t\bar{t}LF$ events, as background together with simulated $t\bar{t}H$ events, where only Higgs boson decays to $b\bar{b}$ are considered. Differences of the expected distributions of the other, non-QCD backgrounds between the prefit and the postfit configurations are negligible for the procedure, given their small size compared to the QCD background in the TRs. The shape of the discriminant distribution is then determined from the events in the ERs by evaluating the

Table 6: Observables used as input variables to the primary ANNs (\times) and STXS ANNs (\circ) per channel. Categories are labelled as “<(min.) number jets>-<min. number b-tagged jets>”, e.g. the FH (≥ 9 jets, ≥ 4 b tags) category is labelled as “9-4”. The \dagger indicates that the observable is constructed using information from the BDT-based event reconstruction.

Observable	FH	SL		DL			
	9-4	8-4	7-4	6-4	5-4	4-3	3-3
MEM	matrix element method discriminant	\times	\times	\times	\times, \circ	\times, \circ	\times, \circ
BLR	b tagging likelihood ratio discriminant					\times, \circ	
$\ln\left(\frac{\text{BLR}}{1-\text{BLR}}\right)$	transformed b tagging likelihood ratio discriminant		\times	\times			
$p_T(j^2)$	p_T of second leading jet, ranked in p_T					\times, \circ	
$p_T(j^3)$	p_T of third leading jet, ranked in p_T						\times, \circ
$p_T(j^7)$	p_T of seventh leading jet, ranked in p_T	\times					
$p_T(b^i)$	p_T of i^{th} , $i=1-4$, leading b-tagged jet, ranked in p_T					\times, \circ	
$\eta(j^i)$	η of i^{th} , $i=1-2$, leading jet, ranked in b tag. discr. value	\times	\times	\times			
$\langle d_b(j) \rangle$	average b tagging discriminant value of all jets			\times	\times		
$\langle d_b(b) \rangle$	average b tagging discriminant value of all b-tagged jets		\times	\times			
$d_b^3(j)$	third highest b tagging discriminant value of all jets			\times	\times		
$\text{Var}(d_b(j))$	variance of b tagging discriminant values of all jets			\times	\times		
$\langle \Delta R(bb) \rangle$	average of ΔR between two b-tagged jets			\circ	\circ	\times, \circ	
$\langle \Delta R(jj) \rangle$	average of ΔR between two jets	\times	\times				
$\min \Delta R(jj)$	minimum of ΔR between two jets		\times	\times			\times, \circ
$\max \Delta R(jj)$	maximum of ΔR between two jets	\times	\times	\times			
$\langle \Delta\eta(bb) \rangle$	average of $\Delta\eta$ between two b-tagged jets			\times	\times		
$\langle \Delta\eta(jj) \rangle$	average of $\Delta\eta$ between two jets	\times	\times	\times	\times		
$\langle m(b) \rangle$	average invariant mass of all b-tagged jets			\times, \circ	\times, \circ		
$\langle m(j) \rangle$	average invariant mass of all jets			\times	\times		
$m(bb_{\min \Delta R})$	invariant mass of pair of b-tagged jets closest in ΔR			\times	\times	\times, \circ	
$m(jb_{\min \Delta R})$	invariant mass of pair of jet and b-tagged jet closest in ΔR					\times, \circ	
$m(jj_{125\text{GeV}})$	invariant mass of pair of jets with mass closest to 125 GeV	\times			\circ	\circ	
$m(bb_{\max m})$	maximum invariant mass of pairs of b-tagged jets	\times	\times			\times, \circ	\times, \circ
$m(jbb_{\max p_T})$	inv. mass of jet and pair of b-tagged jets with highest p_T					\times, \circ	
$\langle p_T(j) \rangle$	average p_T of all jets			\times, \circ	\times, \circ		
$\langle p_T(b) \rangle$	average p_T of all b-tagged jets			\times, \circ	\times, \circ		
$p_T(bb_{\min \Delta R})$	p_T of pair of b-tagged jets closest in ΔR			\times, \circ	\times, \circ	\times, \circ	\times, \circ
$p_T(jj_{\min \Delta R})$	p_T of pair of jets closest in ΔR						\times, \circ
$p_T(jb_{\min \Delta R})$	p_T of pair of jet and b-tagged jet closest in ΔR						\times, \circ
$H_T(j)$	scalar sum of p_T of all jets			\times	\times	\times, \circ	
$H_T(b)$	scalar sum of p_T of all b-tagged jets			\times	\times	\times, \circ	
$N(j)$	number of jets			\times			
$N(b^{\text{loose}})$	number of jets with loose b tag					\times, \circ	
$d_b(b_t^{\text{tHW}})^{\dagger}$	b tagging discr. value of b jet from t quark from tHW reco.			\times	\times		
$p_T(H^i)^{\dagger}$	p_T of Higgs boson from $t\bar{t}H$, tHq , tHW reconstruction			\circ	\circ		
$\ln(\min b_H^{\text{tHQ}})^{\dagger}$	log. of min. p_T of b jets from Higgs boson from tHq reco.			\circ	\circ		
$ \eta(q^{\text{tHQ}}) ^{\dagger}$	$ \eta $ of light-quark jet from tHq reconstruction			\times	\times		
$\Delta R(bb_H^i)^{\dagger}$	ΔR of b jets from Higgs boson from $t\bar{t}H$, tHq , tHW reco.			\circ	\circ		
$m(H^i)^{\dagger}$	inv. mass of Higgs boson from $t\bar{t}H$ reconstruction			\circ	\circ		
$m(t_{\text{lep}}^{\text{t}\bar{t}H})^{\dagger}$	inv. mass of leptonically decaying t quark from $t\bar{t}H$ reco.			\times, \circ	\times, \circ		
$\text{BDT}^{i\dagger}$	reconstruction BDT output for tHq , $t\bar{t}H$, $t\bar{t}$ hypotheses			\times	\times		
A, S	event aplanarity and sphericity [101]	\times	\times	\times			
H_i^{FW}	$i^{\text{th}}, i=0-5$, Fox-Wolfram moment [102]	\times	\times	\times			
$H_i^{\text{FW}} / H_0^{\text{FW}}$	ratio of Fox-Wolfram moments, $i=1-4$	\times	\times	\times			

Table 7: Categorisation scheme in the FH channel, applied independently in each jet-multiplicity category. The m_{qq} selection criteria refer to events with 7 or 8 (≥ 9) jets.

$60(72) < m_{\text{qq}} < 100(90) \text{ GeV}$		$30 < m_{\text{qq}} < 60(72) \text{ GeV}$ or $100(90) < m_{\text{qq}} < 250 \text{ GeV}$
2 b tags	<i>training region (TR)</i>	<i>validation region (VR-TR)</i>
≥ 4 loose b tags	QCD events for ANN training	input variable validation
3 b tags	<i>evaluation region (ER)</i>	<i>validation region (VR-ER)</i>
≥ 4 loose b tags	discriminant shape for QCD	discriminant shape for QCD
≥ 4 b tags	<i>signal region (SR)</i> analysis region	<i>validation region (VR-SR)</i> comparison of QCD shape with data

ANN output from these events, and then subtracting the remaining contributions from non-QCD backgrounds (mainly $t\bar{t} + \text{jets}$) using simulation. The yield of the QCD events is left as free parameter in the final fit, independently in each SR. The subtracted non-QCD background contribution amounts to 20–29% in the ERs, depending on the category. The subtraction is performed in-situ in the final fit, and the full set of systematic uncertainties, discussed in Section 9, in the non-QCD backgrounds is taken into account in the procedure.

Due to differing heavy-flavour compositions, the kinematic properties of b-tagged and untagged jets vary across the TR, ER, and SR. To align the kinematic properties of loosely b-tagged jets with those of b-tagged jets, event weights are applied to events in the TR and ER. These weights are calculated using per-jet correction factors (TF_L).

In the ER, the TF_L correction factor for the leading loosely b-tagged jet that is not also b tagged is used as the event weight. In the TR, TF_L correction factors for the two leading loosely b-tagged jets that are not also b tagged are multiplied to determine the event weight. The TF_L corrections are derived from jets in events that pass the baseline selection, excluding the first two jets, based on the jet p_T , η , and the minimum distance between the jet and the first two b-tagged jets, following the procedure in Ref. [13]. The jet ranking is based on the b tagging discriminant value.

Once the event weights are applied, the ANN output distribution shape in the ER is expected to accurately represent the QCD multijet background shape in the SR. This is confirmed by applying the same procedure to events in the VR-ER and comparing the predicted shape to the observed one in the VR-SR. The method is further validated by dividing the ER into two regions based on b tagging discriminant values and applying the procedure analogously.

The ANNs are constructed to separate $t\bar{t}\text{H}$ events from QCD multijet background events. Taking into account explicit separation against $t\bar{t} + \text{jets}$ events has been found to not improve the results further. The ANNs utilise input variables related to the kinematic properties of individual objects and event shape information, as well as the MEM discriminant output, as listed in Table 6. It has been verified that the distributions of the chosen variables agree between each SR, ER, and TR after application of the TF_L correction, using the data in the VR and simulated $t\bar{t}\text{H}$ events. For example, variables that are directly correlated with the b tagging discriminant value do not fulfil this criterion and are not used as input. The observed distributions of the chosen input variables have been further verified to be well modelled based on a χ^2 criterion, with corresponding p -values well above 5%.

For the STXS measurement, a Higgs boson candidate is reconstructed from that pair of jets, out of the four jets with the highest b tagging discriminant value, whose invariant dijet mass is most compatible with that of a 125 GeV Higgs boson, based on a χ^2 criterion taking into account the experimental resolution of the jet p_T . Depending on the p_T of the reconstructed Higgs boson candidate, the SR events are categorised further and assigned to one of the five p_T^H ranges, resulting in 38–57% correct assignments for $t\bar{t}H$ events, as presented in Fig. 6. Thus, there are in total 15 STXS categories in the FH channel for each of the three data-taking periods. In each category, the ANN output distribution is used as final discriminant in the fit to extract the STXS.

8.3 Single-lepton and dilepton channels

In the channels with leptons, events are separated based on the jet and b-tagged jet multiplicity. In the SL channel, two categories with (≥ 6 jets, ≥ 4 b tags) and (5 jets, ≥ 4 b tags) are considered, and in the DL channel two categories with (≥ 4 jets, ≥ 3 b tags) and (3 jets, 3 b tags) are used.

In each of the two SL categories and in the (≥ 4 jets, ≥ 3 b tags) DL category, events are further categorised based on the output of multiclassification ANNs, which are designed to separate between different signal and background processes. The values obtained in the output nodes of the ANNs are normalised to unity using a “soft-max” function [103], and, as a result, the output values $O(i)$ can be interpreted as probabilities describing the likelihood of the event being of a certain process i . Events are assigned to a category corresponding to the most probable process according to this ANN multiclassification. In the SL channel, the three signal processes $t\bar{t}H$, tHq , and tHW , and the four $t\bar{t}$ + jets background processes $t\bar{t}LF$, $t\bar{t}C$, $t\bar{t} + 2b$, and $t\bar{t} + b(\bar{b})$ are considered in the ANN multiclassification. The dedicated class for $t\bar{t} + 2b$ events out of the $t\bar{t}B$ background is designed in order to constrain the uncertainty related to collinear gluon splitting. In the DL channel, the $t\bar{t}H$ signal process and the three $t\bar{t}$ + jets background processes $t\bar{t}LF$, $t\bar{t}C$, and $t\bar{t}B$ are considered in the ANN multiclassification. No dedicated classes for tHq , tHW , or $t\bar{t} + 2b$ events are included in the DL channel, motivated by the reduced statistical precision due to the lower tH and $t\bar{t}$ + jets event rate in this channel.

The output values of the ANNs are subsequently used to compute the final discriminant observables. In the SL channel, for events in the $t\bar{t}H$ and $t\bar{t} + b(\bar{b})$ process categories, a likelihood ratio discriminant is computed from the ANN output values O as

$$R_{SL} = \frac{O(t\bar{t}H)}{O(t\bar{t}H) + O(t\bar{t} + b(\bar{b})) + O(t\bar{t} + 2b)}, \quad (1)$$

and used as the discriminating observable. This allows exploiting more information from the ANN multiclassification: e.g., for an event that is categorised as $t\bar{t}H$, not only the output value of the $t\bar{t}H$ node is used but also the output values of the $t\bar{t} + b(\bar{b})$ and $t\bar{t} + 2b$ nodes, which provides further information about the likelihood of the categorisation. With the likelihood ratio discriminant, an improvement of the expected sensitivity by 18% is achieved compared to fitting directly the ANN output values $O(t\bar{t}H)$ and $O(t\bar{t} + b(\bar{b}))$. In the tHq and tHW process categories, the $O(tHq)$ and $O(tHW)$ distributions are used as the final discriminating observables, respectively. The binning of the discriminant distributions has been chosen to optimise the sensitivity, while at the same time avoiding artificial constraints of the uncertainties that can arise if their parametrisation is not flexible enough to describe all shape variations of the distributions. The main purpose of the remaining process categories $t\bar{t}LF$, $t\bar{t}C$, and $t\bar{t} + 2b$ is to constrain the normalisation of the corresponding background processes; therefore, in these categories only the event yield is considered instead of the full distribution. Similarly, in the

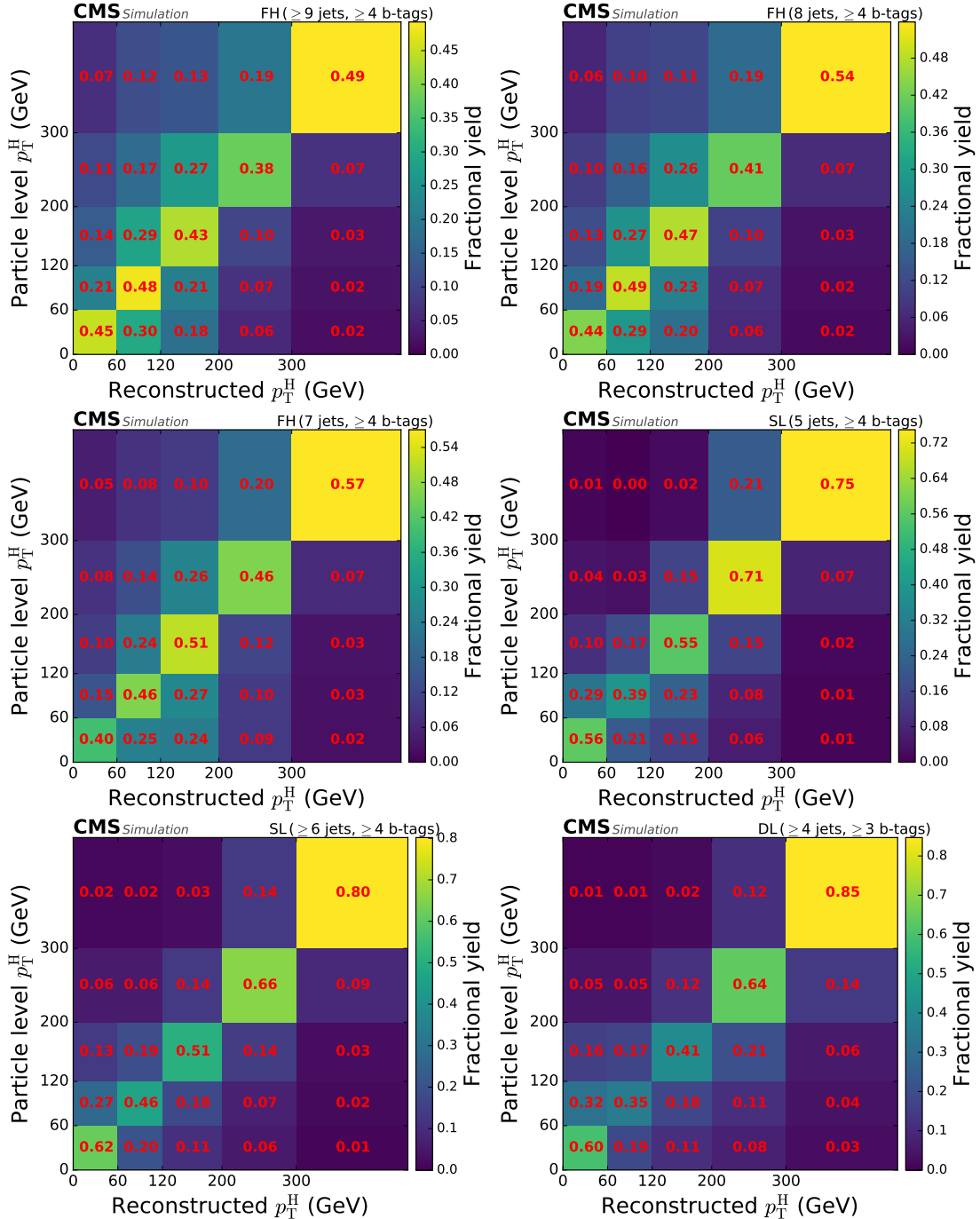


Figure 6: Categorisation efficiency of the $t\bar{t}H$ signal events in the STXS analysis in the different categories of the FH channel (upper row, middle row left), the SL channel (middle row right, lower row left), and the DL channel (lower row right).

DL (≥ 4 jets, ≥ 3 b tags) category, a likelihood ratio discriminant is computed from the events in the $t\bar{t}H$ and $t\bar{t}B$ process categories as

$$R_{\text{DL}} = \frac{O(t\bar{t}H)}{O(t\bar{t}H) + O(t\bar{t}B)}, \quad (2)$$

and used as the discriminating observable, while for the $t\bar{t}LF$ and $t\bar{t}C$ process categories, the event yield is used.

In the DL (3 jets, 3 b tags) category, a binary classification ANN is designed to separate the $t\bar{t}H$ signal from the inclusive $t\bar{t}$ + jets background, and the ANN classifier output distribution is used as final discriminating observable.

In total, this leads to 12 categories in the SL channel and four categories in the DL channel per data-taking period, as shown Fig. 5.

As for the FH channel, the ANN input variables are related to the kinematic properties of individual objects, the event shape, as well as the MEM discriminant outputs, and in addition the jet b tagging and the BLR discriminants, as listed in Table 6. In the SL channel, variables constructed using information from the BDT-based event reconstruction are also used (marked with a dagger symbol (\dagger) in Table 6). The input variables and their correlations have been verified to be well described in data, based on a goodness-of-fit test that takes into account the full uncertainty model, i.e. including statistical and systematic uncertainties, using the “saturated model” method [92, 104]. For each variable and each pair of variables under scrutiny, the one- and two-dimensional distributions, respectively, have been fitted to the data in the analysis categories, confirming they are well modelled with p -values greater than 5%. The effect of the signal contribution on the validation procedure has been found to be negligible, given the limited sensitivity to the signal of each of the input variables alone.

The ANNs are trained using simulated $t\bar{t}H$, tH , and $t\bar{t}$ + jets events. Only events with Higgs boson decays to $b\bar{b}$ are considered, and the $t\bar{t}$ system is required to have one or two leptons in the final state for the SL and the DL channels, respectively. For the tH events, only those with leptonic decays of the top quark are considered. The achieved classification accuracy ranges from 35–65% for $t\bar{t}H$ events to 40–70% for tH events, as well as 30–40% and 60–70% for $t\bar{t}B$ and $t\bar{t}LF$ events, respectively, depending on the channel.

For the STXS measurement, the most signal-like events are categorised further, targeting the five regions in p_T^H . Specifically, these are the events in the $t\bar{t}H$ and $t\bar{t} + b(\bar{b})$ process categories of the SL (≥ 6 jets, ≥ 4 b tags) and (5 jets, ≥ 4 b tags) categories, and the $t\bar{t}H$ and $t\bar{t}B$ process categories of the DL (≥ 4 jets, ≥ 3 b tags) category. The STXS categorisation is performed by additional multiclassification ANNs (STXS ANNs) designed to classify $t\bar{t}H$ events by p_T^H . Each event is assigned to the p_T^H bin with the highest probability according to the STXS ANN multiclassification; the STXS ANN output value in that node, multiplied by the observable value of the inclusive $t\bar{t}H$ measurement, i.e. the likelihood ratio value, is used as final discriminating observable. Events that are categorised with high certainty by the STXS ANN thus contribute with a higher weight to the final discriminating observable. This approach has been found to achieve superior sensitivity compared to other classification approaches studied, including approaches based on a kinematic reconstruction of p_T^H . Thus, in total, there are ten STXS categories in the SL channel, corresponding to the five Higgs boson p_T ranges in each of the jet multiplicity categories, and five STXS categories in the DL channel. The categorisation of all other events remains the same as for the inclusive $t\bar{t}H$ measurement, with the exception of the events in the DL (3 jets, 3 b tags) category, which are not used since they do not improve the

sensitivity in the STXS analysis.

A dedicated STXS ANN is trained in each of the (≥ 6 jets, ≥ 4 b tags) and (5 jets, ≥ 4 b tags) categories of the SL channel and in the (≥ 4 jets, ≥ 3 b tags) category of the DL channel, using the input variables listed in Table 6. For the training, only simulated $t\bar{t}H$ events are used, and from these only those where both b quarks are within the experimental acceptance defined by the event selection described in Section 6. The achieved categorisation efficiency is presented in Fig. 6.

9 Systematic uncertainties

Several sources of systematic uncertainties are considered in the analysis. The uncertainties are taken into account via nuisance parameters in the final profile likelihood fit described in Section 10 and alter either the rate or both the rate and the discriminant shape of the signal or background processes [92]. The effects from the same source are treated as fully correlated among the different categories. In general, and unless stated otherwise hereafter, theoretical uncertainties are treated as fully correlated among the different data-taking periods, while experimental uncertainties are treated as uncorrelated for the data recorded in 2016, 2017, and 2018. The latter is justified since the experimental uncertainties are mainly of statistical origin related to the limited size of the data and simulation samples used in auxiliary measurements, which are independent between the data-taking periods.

The theoretical uncertainties in the cross sections used to predict the rates of the signal and background processes, which arise primarily from the factorisation and renormalisation scale choices and the PDFs, are propagated to the yield estimates. The cross section uncertainties are each separated into their scale (renorm./fact. scales) and PDF components, and are correlated where appropriate among processes. In addition, the normalisation of the $t\bar{t}B$ and $t\bar{t}C$ background processes is left unconstrained in the final fit. To take into account additional uncertainties in the modelling of collinear gluon splitting, an additional 100% log-normal constrained rate uncertainty is assigned to the $t\bar{t} + 2b$ component relative to the normalisation of the overall $t\bar{t}B$ process. Since the shapes of the relevant distributions are different for the $t\bar{t} + 2b$ component and the overall $t\bar{t}B$ background, this leads effectively to a rate and shape variation of the $t\bar{t}B$ distributions. The prior size of 100% has been chosen conservatively to give the fit the freedom to adjust the distributions to the data, and it is constrained in the fit.

Uncertainties arising from missing higher-order terms in the POWHEG $t\bar{t}bb\bar{b}$ and $t\bar{t}$ simulations at ME level are evaluated by independent variations of the renormalisation and factorisation scales by factors of two up and down with respect to the nominal values, and two independent nuisance parameters are assigned in the fit (μ_R/μ_F scale). In addition, the uncertainties are treated as independent among the signal, the $t\bar{t}B$, and the other $t\bar{t}$ processes. The uncertainty arising from the PDF set is determined from the PDF variations provided with the NNPDF set [45], correlating processes for which the same FS and order in α_S are used in the PDF set. The corresponding uncertainty in the PYTHIA PS is determined by varying the parameters controlling the amount of initial- and final-state radiation independently by factors of two up and down [105] (PS scale ISR/FSR), separately for signal, $t\bar{t}B$, $t\bar{t}C$, and $t\bar{t}LF$. These variations are applied using event weights obtained directly from the generators. Uncertainties related to the ME-PS matching scheme and the underlying event tune are evaluated by comparing the reference $t\bar{t}bb\bar{b}$ and $t\bar{t}$ simulation with samples with varied parton-shower matching scale ($hdamp$ parameter) and varied tune parameters, respectively. The event count in these additional samples was small and induced changes to the discriminant distributions comparable in size to the statistical fluctuations of the additional samples and compatible with a pure rate variation. For

this reason, the uncertainties have been estimated as the changes in the rates of the different $t\bar{t} + \text{jets}$ subprocesses independently for each category. The derived rate variations amount typically to 5–10% and the uncertainties are treated as uncorrelated among the $t\bar{t} + \text{jets}$ subprocesses. This approach has been verified with an independent estimation of the variations obtained from the same additional samples and applying the same analysis selection, except for using events with fewer b-tagged jets, thus reducing the statistical fluctuations. In this cross-check, the effect of the selection with fewer b-tagged jets is accounted for via event weights that act as transfer factors, that depend on the p_T , η , and flavour of the jets in the event and encode the probability to observe jets originating from b quarks among the non-b-tagged jets. The impact of the mismodelling of the top quark p_T spectrum in the $t\bar{t}$ simulation [106] has been found to be negligible.

The flexibility of the background model and its robustness against potential mismodelling of the $t\bar{t}B$ component have been confirmed using pseudo-experiments. A large number of pseudo-experiments have been sampled, both from the nominal and from alternative $t\bar{t}B$ predictions, and fitted using the nominal background model, taking into account the systematic uncertainties. The fits have also been performed including only the theoretical $t\bar{t} + \text{jets}$ modelling uncertainties. Several alternative $t\bar{t}B$ predictions have been used to sample the pseudo-data, including scaling the $t\bar{t}B$ component by a factor of 1.2 in order to verify the ability of the background model to compensate for the expected larger rate, or using the $t\bar{t}B$ component of the POWHEG $t\bar{t}$ sample, which is not otherwise used in the analysis, or combinations thereof. The average fitted signal strength deviated from the injected value by at most 3% in case the $t\bar{t}B$ background was sampled from the nominal model, and by at most 6% when it was sampled from the $t\bar{t}$ sample, which is well within the systematic uncertainty of the measurement, and the average fitted $t\bar{t}B$ normalisation corresponded to the applied scale of the $t\bar{t}B$ background.

For the STXS measurement, the $t\bar{t} + \text{jets}$ background uncertainty model is extended to provide further flexibility towards potential effects that depend on the reconstructed p_T^H . The extension is a conservative choice, intentionally made because the STXS measurement is inherently sensitive to effects that depend on p_T^H . The $t\bar{t}B$ normalisation parameter, as well as the nuisance parameters associated with the uncertainties due to the modelling of collinear gluon splitting, the ISR and FSR PS scale, and the ME-PS matching scheme are partially decorrelated between each of the five STXS categories and the other categories. The decorrelation is implemented by assigning, per uncertainty, one parameter that acts on all categories and five additional parameters that act each on one of the STXS categories. This effectively allows an overall variation in all categories simultaneously and additional independent variations per STXS category.

Furthermore, the renormalisation and factorisation scale uncertainty model of the $t\bar{t}H$ signal process is extended, following Refs. [107, 108]. The extended model comprises an uncertainty component in the inclusive cross section prediction as before, as well as uncertainties in the migration and acceptance effects of signal events between the STXS bins. The uncertainties are constructed by studying the effect of all combinations of factorisation and renormalisation scale variations across each p_T^H boundary on the total cross section above this boundary. The largest effect is taken as the absolute uncertainty, which is propagated by increasing the process normalisation in the STXS bins above the p_T^H boundary, and decreasing the process normalisation in the bin directly below the boundary under consideration of potential double-counting effects. The migration uncertainties are implemented as rate uncertainties per STXS bin and amount to 5–10% per parameter. Acceptance effects within each STXS bin are taken into account by varying the renormalisation and factorisation scales, taking into account a normalisation factor to ensure that the variations do not change the overall $t\bar{t}H$ cross section. The

resulting shape variation is typically 1–3% and as large as up to 7% depending on the classifier bin. In addition, for the simulated $t\bar{t}H$ signal events, the renormalisation and factorisation scale variations (μ_R/μ_F scale) are performed simultaneously, and, as well as the parton-shower uncertainties (PS scale ISR/FSR), are treated as uncorrelated for events with p_T^H below and above 300 GeV.

The integrated luminosities for the 2016, 2017, and 2018 data-taking years have 1.2–2.5% individual uncertainties [31–33], which are partially correlated to account for common sources of uncertainty in the luminosity measurement. They amount to an overall uncertainty of 1.6% for the 2016–2018 period. The trigger efficiency uncertainty in the FH channel is determined from the bin-by-bin uncertainties in the ratio of efficiency in data relative to simulation, and are 1–2% on average, with some being as large as 9%. The efficiencies of the single-electron and dilepton triggers are measured in data using reference triggers based on single-muon and p_T^{miss} requirements, respectively, that are uncorrelated with those used in the analysis; the uncertainties range up to 8%, dominated by statistical fluctuations in the data samples used in the auxiliary measurement. Uncertainties in the electron and muon reconstruction, identification, and isolation efficiency corrections are found to be small, typically at the 1% level. The uncertainty in the L1 trigger prefire correction is determined from the uncertainty in the prefire probability estimate and amounts to approximately 0.5%.

Effects of the uncertainty in the distribution of the number of pileup interactions are evaluated by varying the total inelastic cross section used to predict the number of pileup interactions in the simulated events by $\pm 4.6\%$ from its nominal value [72].

The uncertainty related to the jet energy scale (resolution) is determined by varying the energy scale (resolution) correction of all jets in the signal and background predictions by one standard deviation. The jet energy scale uncertainty is divided into 11 independent sources, which include uncertainties owing to the extrapolation between samples of different jet-flavour composition and the presence of pileup collisions in the derivation of the corrections, and which are treated as fully uncorrelated in the fit. While most of the sources are dominated by statistical fluctuations in auxiliary measurements and are treated as uncorrelated among the data-taking periods, some sources are related to theoretical predictions in the MC simulation used, e.g. to extrapolate between samples of different jet-flavour composition, and are thus treated as correlated among the data-taking periods [80].

The b tagging discriminant corrections receive uncertainties due to the contamination of background processes in the data samples used in the correction factor measurements, the jet energy scale uncertainty, and the statistical uncertainty in the correction factor evaluation [82]. The impact of the statistical uncertainty is parameterised as the sum of two contributions: one term with linear dependence on the b tagging discriminant value, allowing an overall tilt of the discriminant distribution, and another term with quadratic dependence, allowing an overall shift of the discriminant distribution. Each source of b tagging uncertainty is considered separately per jet flavour. The uncertainty related to the background contamination is treated as correlated among the data-taking periods of 2017 and 2018, and as uncorrelated with 2016 to allow for effects due to the upgraded pixel detector [28]. The statistical component is treated as uncorrelated among the data-taking periods.

Many uncertainties that are related to the MC simulation of the QCD multijet background in the FH channel are avoided by estimating this contribution from data. Small uncertainties remain in the TF_L correction applied to the loosely b-tagged jets, which is estimated by applying an additional η -dependent correction to TF_L to account for small effects of missing higher-order iterations in the correction procedure. The total QCD background normalisation in each

category is left unconstrained in the final fit.

The impact of statistical fluctuations in the signal and background prediction due to the limited sample size is accounted for using the Barlow–Beeston lite approach [109].

The described sources of uncertainty are summarised in Table 8 and their impact on the final result is discussed in Section 10.

10 Statistical analysis and results

The production rates of the $t\bar{t}H$ and tH signal processes are determined in a simultaneous binned profile likelihood fit to the final discriminant distributions in all channels, categories, and data-taking periods, using the techniques detailed in Ref. [92]. The rates of the $t\bar{t}B$, $t\bar{t}C$, as well as the QCD multijet background, are separately left unconstrained in the fit. Several signal interpretations are performed and described below.

10.1 The $t\bar{t}H$ production rate

First, the $t\bar{t}H$ production rate is measured. For this interpretation, the tH contribution is assumed to conform to the SM expectation and is treated as background.

The event yields observed in data in the different analysis channels and categories, together with the signal and background yields after the fit to data, are listed in Table 9. The observed yields in each bin of the final discriminant distributions in all channels and categories entering the fit are shown in Fig. 7, together with the fitted signal and background yields. The best fit values of the inclusive $t\bar{t}H$ production rate relative to the SM expectation, denoted as the signal strength modifier $\mu_{t\bar{t}H}$, are presented in Fig. 8. Results are shown for fits performed simultaneously in all channels and years using either one signal-strength modifier per channel or per year and correlating the uncertainties, or using one overall signal-strength modifier. For the overall signal-strength modifier, a best fit value of $\mu_{t\bar{t}H} = 0.33 \pm 0.26 = 0.33^{+0.17}_{-0.16} (\text{stat})^{+0.20}_{-0.21} (\text{syst})$ is obtained, with an expected uncertainty of $\pm 0.17 (\text{stat})^{+0.23}_{-0.19} (\text{syst})$. The observed signal has a significance compared to the background-only hypothesis corresponding to 1.3 SD, with an expectation of 4.1 SD. The goodness-of-fit is quantified using a p -value that takes into account the postfit uncertainty model [92, 104] and amounts to $p = 0.88$, indicating good description of the data by the fit model.

The postfit values and uncertainties of the $t\bar{t}B$ and $t\bar{t}C$ background normalisation parameters obtained in the combined fit of all channels are $1.19^{+0.13}_{-0.12}$ and $1.07^{+0.20}_{-0.19}$, respectively. These values are consistent with the results of dedicated inclusive $t\bar{t}bb$ and $t\bar{t}cc\bar{c}$ cross section measurements in similar phase space regions, which are at the level of 6–20% relative precision depending on the exact phase space and the size of the analysed dataset [88–90, 110], and are consistent with the known underprediction of the $t\bar{t}bb$ cross section by the simulation. The anticorrelation between the $t\bar{t}H$ signal strength and the $t\bar{t}B$ background normalisation is 48% and is visible in Fig. 9.

The best fit values and the impacts of the 20 nuisance parameters ranked highest in impact are presented in Fig. 10. The impact of each nuisance parameter is evaluated as the difference of the nominal best fit value of μ and the best fit value obtained when fixing the nuisance parameter under scrutiny to its best fit value plus/minus its postfit uncertainty. The nuisance parameters with the highest impact are related to the $t\bar{t}B$ background modelling, followed by the QCD multijet background normalisation and, to a lesser extent, the jet energy scale, the uncertainty in the signal cross section ($\sigma_{t\bar{t}H}$), and the statistical uncertainty in the signal and background

Table 8: Systematic uncertainties considered in the analysis. “Type” refers to rate (R) or rate and shape (S) altering uncertainties. “Correlation” indicates whether the uncertainty is treated as correlated, partially correlated (as detailed in the text), or uncorrelated across the years 2016–18. Uncertainties for $t\bar{t} + \text{jets}$ events marked with a $^+$ are treated as partially correlated between each of the STXS categories and the other categories in the STXS analysis.

Source	Type	Correlation	Remarks
Renorm./fact. scales	R	correlated	Scale uncertainty of (N)NLO prediction, independent for $t\bar{t}H$, tHq , tHW , $t\bar{t}$, t , $V + \text{jets}$, VV
PDF+ α_S (gg)	R	correlated	PDF uncertainty for gg initiated processes, independent for $t\bar{t}H$, tHq , tHW , and others
PDF+ α_S ($q\bar{q}$)	R	correlated	PDF uncertainty for $q\bar{q}$ initiated processes ($t\bar{t}W, W, Z$) except tHq
PDF+ α_S (qg)	R	correlated	PDF uncertainty for qg initiated processes (single t) except tHW
Collinear gluon splitting $^+$	S	correlated	Additional 100% rate uncertainty on $t\bar{t} + 2b$ component of $t\bar{t}B$ background
μ_R scale	S	correlated	Renormalisation scale uncertainty of the ME generator, independent for $t\bar{t}H$, tHq , tHW , $t\bar{t}B$ ($t\bar{t}bb$ sample), other $t\bar{t}$ ($t\bar{t}$ sample)
μ_F scale	S	correlated	Factorisation scale uncertainty of the ME generator, independent for $t\bar{t}H$, tHq , tHW , $t\bar{t}B$ ($t\bar{t}bb$ sample), other $t\bar{t}$ ($t\bar{t}$ sample) and $t\bar{t}H$
PDF shape	S	correlated	From NNPDF variations, independent for tHq , tHW , $t\bar{t}B$ ($t\bar{t}bb$ sample), other $t\bar{t}$ ($t\bar{t}$ sample) and $t\bar{t}H$
PS scale ISR $^+$	S	correlated	Initial state radiation uncertainty of the PS (PYTHIA), independent for $t\bar{t}H$, $t\bar{t}B$, $t\bar{t}C$, $t\bar{t}LF$
PS scale FSR $^+$	S	correlated	Final state radiation uncertainty of the PS (PYTHIA), independent for $t\bar{t}H$, $t\bar{t}B$, $t\bar{t}C$, $t\bar{t}LF$
ME-PS matching ($t\bar{t}$) $^+$	R	correlated	NLO ME-PS matching (for $t\bar{t} + \text{jets}$ events), independent for $t\bar{t}B$, $t\bar{t}C$, $t\bar{t}LF$
Underlying event ($t\bar{t}$)	R	correlated	Underlying event (for all $t\bar{t} + \text{jets}$ events)
STXS migration	R	correlated	Signal, only in STXS measurement
STXS acceptance	S	correlated	Signal, only in STXS measurement
Integrated luminosity	R	partially	Signal and all backgrounds
Lepton ID/Iso (2 sources)	S	uncorrelated	Signal and all backgrounds
Trigger efficiency (4 sources)	S	uncorrelated	Signal and all backgrounds
L1 prefiring correction	S	uncorrelated	Signal and all backgrounds
Pileup	S	correlated	Signal and all backgrounds
Jet energy scale (11 sources)	S	partially	Signal, $t\bar{t} + \text{jets}$ and single t
Jet energy resolution	S	uncorrelated	Signal, $t\bar{t} + \text{jets}$ and single t
b tag bkg. contam. (2 sources)	S	partially	Signal and all backgrounds
b tag bkg. contam. stat. (4 sources)	S	uncorrelated	Signal and all backgrounds
b tag charm (2 sources)	S	partially	Signal and all backgrounds
TF _L correction	S	uncorrelated	QCD multijet background estimate
Size of the MC samples	S	uncorrelated	Statistical uncertainty of signal and background prediction due to limited sample size

Table 9: Event yields observed in data and expected for the $t\bar{t}H$ signal and total background after the fit to data in the different analysis categories for all data-taking periods together. The uncertainties denote the total uncertainty of the fit model. Contributions from $t\bar{t} + \text{jets}$ and tH background processes are also listed individually.

Categories	$t\bar{t}\text{LF}$	$t\bar{t}\text{C}$	$t\bar{t}\text{B}$	tH	Total bkg.	$t\bar{t}H$	Data
FH ≥ 4 b tags							
7 jets	2980	2790	8100	2	69950 ± 300	134 ± 99	70070
8 jets	3510	3970	11850	2	78960 ± 360	190 ± 140	79179
≥ 9 jets	2460	3850	13200	0.98	60950 ± 410	180 ± 140	61193
SL 5 jets, ≥ 4 b tags							
$t\bar{t}\text{LF}$	996	494	667	0.689	2254 ± 88	7 ± 5	2235
$t\bar{t}\text{C}$	377	374	564	0.80	1408 ± 56	6 ± 5	1449
$t\bar{t} + 2b$	161	196	984	0.885	1406 ± 44	9 ± 7	1396
tHq	102	83	536	3	790 ± 26	10 ± 8	846
tHW	64	100	446	1	697 ± 29	7 ± 5	665
$t\bar{t}H/t\bar{t} + b(\bar{b})$	125	139	1555	3	1930 ± 63	35 ± 26	1965
SL ≥ 6 jets, ≥ 4 b tags							
$t\bar{t}\text{LF}$	1020	820	1133	1	3100 ± 120	14 ± 11	3074
$t\bar{t}\text{C}$	347	562	1078	0.71	2108 ± 78	13 ± 10	2114
$t\bar{t} + 2b$	161	252	1680	0.97	2188 ± 75	17 ± 13	2284
tHq	146	201	1471	3	1946 ± 55	25 ± 19	1992
tHW	65	82	952	3	1244 ± 39	16 ± 13	1217
$t\bar{t}H/t\bar{t} + b(\bar{b})$	101	197	3020	3	3460 ± 110	74 ± 56	3507
DL 3 jets, 3 b tags							
	2500	1700	3980	3	8510 ± 160	20 ± 16	8594
DL ≥ 4 jets, ≥ 3 b tags							
$t\bar{t}\text{LF}$	1760	1090	1017	0.816	4045 ± 79	9 ± 6	4050
$t\bar{t}\text{C}$	970	1100	1325	0.995	3534 ± 74	13 ± 10	3586
$t\bar{t}H/t\bar{t}\text{B}$	538	890	4270	4	5980 ± 120	57 ± 41	5931

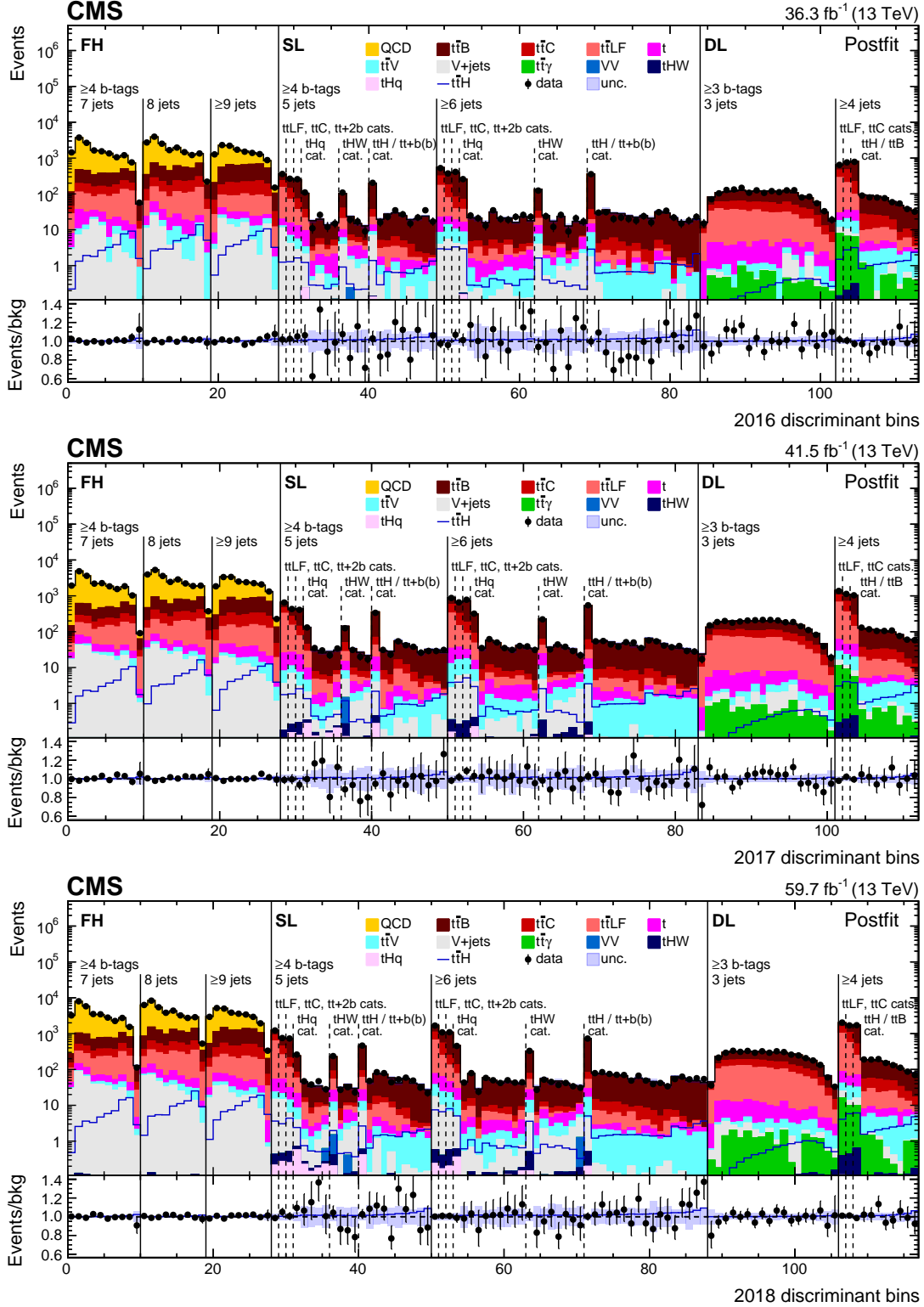


Figure 7: Observed (points) and postfit expected (filled histograms) yields in each discriminant (category yield, ANN score, or ratio of ANN scores) bin for the 2016 (upper), 2017 (middle), and 2018 (lower) data-taking periods. The uncertainty bands include the total uncertainty of the fit model. The lower pads show the ratio of the data to the background (points) and of the postfit expected signal+background to the background-only contribution (line).

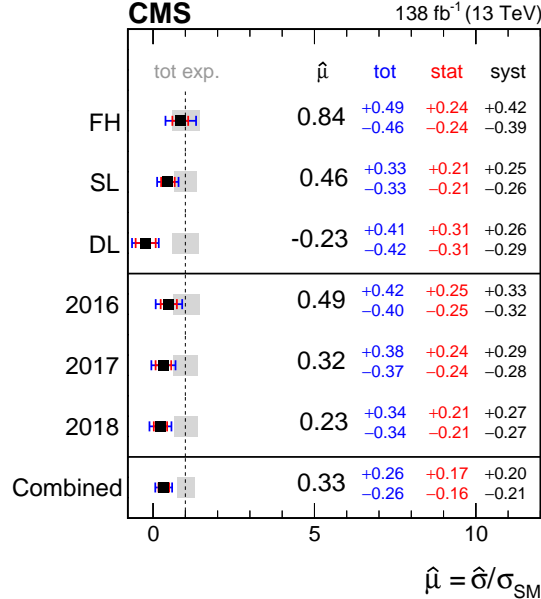


Figure 8: Best fit results $\hat{\mu}$ of the $t\bar{t}H$ signal-strength modifier $\mu_{t\bar{t}H}$ in each channel (upper three rows), in each year (middle three rows), and in the combination of all channels and years (lower row). Uncertainties are correlated between the channels and years.

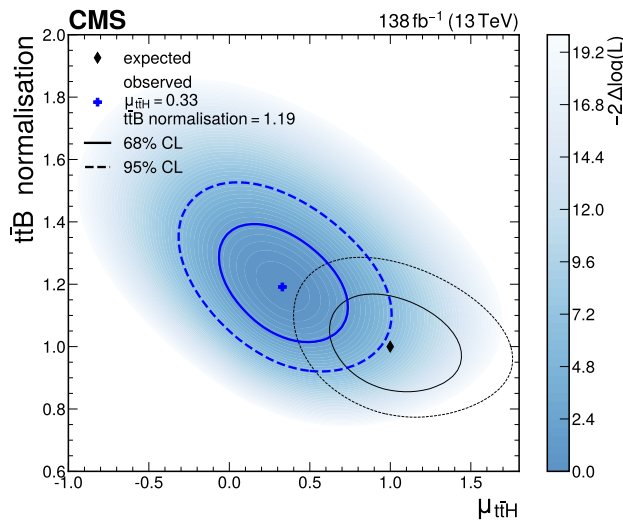


Figure 9: Observed likelihood-ratio test statistic (blue shading) as a function of the $t\bar{t}H$ signal-strength modifier $\mu_{t\bar{t}H}$ and the $t\bar{t}B$ background normalisation, together with the observed (blue) and SM expected (black) best fit points (cross and diamond markers) as well as the 68% (solid lines) and 95% (dashed lines) CL regions. The $t\bar{t}C$ background normalisation and all other nuisance parameters are profiled such that the likelihood attains its minimum at each point in the plane.

prediction due to the number of simulated events (MC stat.). The three highest ranked nuisance parameters of the jet energy scale uncertainty are related to the p_T dependence of the jet energy scale and resolution of the forward jets (1) as well as to the uncertainty in the response obtained from the in-situ calibration of the absolute jet energy scale (2, 3).

The best fit values of the nuisance parameters are within 1 SD of the prior uncertainty for more than 93% of the total number of nuisance parameters. As expected, significant shifts from the nominal value are observed for nuisance parameters related to the $t\bar{t}B$ background modelling, such as the $t\bar{t}B$ normalisation and the gluon-splitting uncertainty, since the a-priori knowledge does not reflect the data distributions. Furthermore, the values of the nuisance parameters related to the μ_R scale uncertainty of the $t\bar{t}$ sample used to model the $t\bar{t}LF$ and $t\bar{t}C$ processes as well as the uncertainty in the PS modelling (PS scale FSR) of the $t\bar{t}LF$ process are shifted by +1 SD and -1 SD, respectively; the nuisance parameters are not shown in Fig. 10 since their impact is lower than those of the shown parameters. Consequently, the fit constrains these nuisance parameters relative to their prior values. Several other nuisance parameters, in particular those related to jet energy scale and b tagging uncertainties, are constrained. This is attributed to the following: events are selected according to different, large multiplicities of jets and b-tagged jets, thus increasing the sensitivity of the analysis to changes of the jet energy scale and b tagging efficiency, for example by their effect on the event yield per analysis category; and in several cases the prior uncertainties are large. No large constraints are observed in the measurement of the remaining nuisance parameters.

The contributions of the statistical and various groups of systematic uncertainties to the uncertainty in $\mu_{t\bar{t}H}$ are listed in Table 10. The statistical uncertainty is evaluated by fixing all nuisance parameters to their postfit values and repeating the fit. The contribution by a group of systematic uncertainties is evaluated by repeating the fit fixing only the nuisance parameters related to the uncertainty under scrutiny to their postfit values, and subtracting the uncertainty obtained in quadrature from the total uncertainty of the fit in which no parameters are fixed. The uncertainties obtained in the fit to data agree with the expectation from simulation. The total uncertainty of the full fit on the signal strength (± 0.26) is different from the quadratic sum of the listed contributions because of correlations between the nuisance parameters. The statistical uncertainty also includes components from the background normalisations. The total contribution from the systematic uncertainties ($+0.20/-0.21$) is larger than from the statistical uncertainties ($+0.17/-0.16$), which include the uncertainties due to the freely-floating background normalisations, albeit at a similar level. The theoretical uncertainties amount to ± 0.16 and are dominated by the uncertainties of the $t\bar{t} + \text{jets}$ background modelling. Experimental uncertainties amount to ± 0.10 , dominated by the jet energy scale and resolution as well as b tagging related uncertainties. Systematic uncertainties due to the size of the various simulated samples used to model the background and signal templates are at the same order and amount to $+0.13/-0.12$.

The single-channel best fit results for $\mu_{t\bar{t}H}$ are compatible with the combined result at a level corresponding to a p -value of 0.28 (1.1 SD), and the p -value compatibility of the combined result with the SM expectation of $\mu_{t\bar{t}H} = 1$ is 0.02 (2.4 SD). The result obtained in the combination of the leptonic channels with the 2016 data only is compatible to the central value of the earlier result in Ref. [12] obtained from a similar dataset at a p value of 0.41 (0.8 SD). For the p -value computation, the postfit uncertainty model was taken into account in each case. The result was extensively validated through several methods, including fitting different observables like MEM and H_T , testing the stability of the background model with various combinations of categories, decorrelating uncertainties between different $t\bar{t}B$ components (such as those with one or two b jets within acceptance), and using background predictions derived from data. The

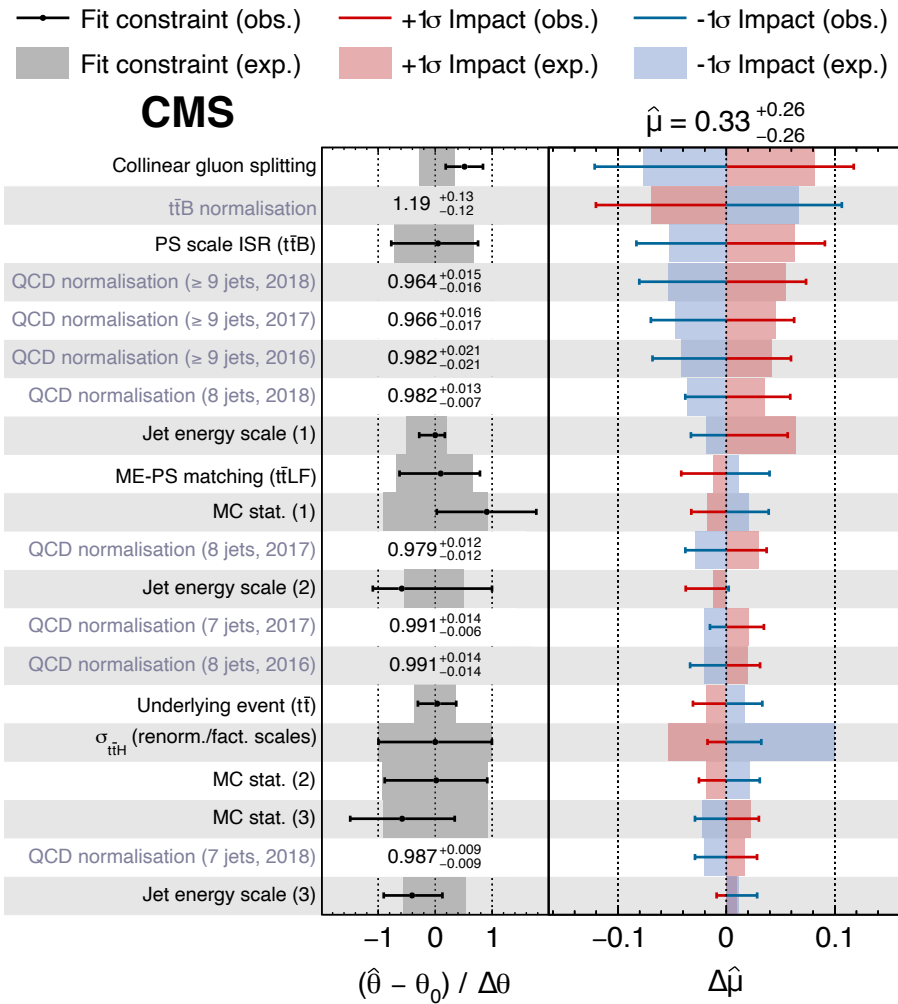


Figure 10: Postfit values of the nuisance parameters (black markers), shown as the difference of their best fit values, $\hat{\theta}$, and prefit values, θ_0 , relative to the prefit uncertainties $\Delta\theta$. The impact $\Delta\hat{\mu}$ of the nuisance parameters on the signal strength $\mu_{t\bar{t}H}$ is computed as the difference of the nominal best fit value of μ and the best fit value obtained when fixing the nuisance parameter under scrutiny to its best fit value $\hat{\theta}$ plus/minus its postfit uncertainty (coloured areas). The nuisance parameters are ordered by their impact, and only the 20 highest ranked parameters are shown.

Table 10: Contributions of different sources of uncertainty to the result for the fit to the data (observed) and to the expectation from simulation (expected). The quoted uncertainties $\Delta\mu_{t\bar{t}H}$ in $\mu_{t\bar{t}H}$ are obtained by fixing the listed sources of uncertainties to their postfit values in the fit and subtracting the obtained result in quadrature from the result of the full fit. The statistical uncertainty is evaluated by fixing all nuisance parameters to their postfit values and repeating the fit. The quadratic sum of the contributions is different from the total uncertainty because of correlations between the nuisance parameters.

Uncertainty source	$\Delta\mu_{t\bar{t}H}$ (observed)	$\Delta\mu_{t\bar{t}H}$ (expected)
Total experimental	+0.10 / -0.10	+0.11 / -0.10
jet energy scale and resolution	+0.08 / -0.07	+0.09 / -0.09
b tagging	+0.07 / -0.06	+0.06 / -0.02
integrated luminosity	+0.02 / -0.02	+0.01 / -0.01
Total theory	+0.16 / -0.16	+0.18 / -0.14
t̄ + jets background	+0.15 / -0.16	+0.12 / -0.11
signal modelling	+0.06 / -0.01	+0.13 / -0.06
Size of the simulated event samples	+0.13 / -0.12	+0.10 / -0.10
Total systematic	+0.20 / -0.21	+0.23 / -0.19
Statistical	+0.17 / -0.16	+0.17 / -0.17
background normalisation	+0.13 / -0.13	+0.13 / -0.13
t̄B and t̄C normalisation	+0.12 / -0.12	+0.12 / -0.12
QCD normalisation	+0.01 / -0.01	+0.01 / -0.01
Total	+0.26 / -0.26	+0.28 / -0.25

performed cross checks confirm the observed result, albeit at a lower precision. The value is very close to the result reported by the ATLAS Collaboration in Ref. [11], but lower than the one reported in Ref. [23]. The latter includes several changes with respect to Ref. [11], most notably, an updated treatment of the $t\bar{t} + \text{jets}$ background with a revised $t\bar{t}bb$ simulation and corresponding systematic uncertainty model.

The observed yields in each bin of the final discriminant distributions of the STXS measurement in the signal regions of the SL and DL channels, which drive the signal sensitivity, are shown in Fig. 11, together with the fitted signal and background yields. The results of the STXS measurement are presented in Fig. 12, which shows the best fit values of the $t\bar{t}H$ signal-strength modifier per region of p_T^H and their correlations, obtained in the combination of all channels and years. The goodness-of-fit p -value is 0.89, indicating good description of the data by the fit model. The highest expected sensitivity is reached in the medium- p_T^H range between 120 and 300 GeV.

The measured best fit values are compatible with the central result of the inclusive $t\bar{t}H$ production rate measurement, corresponding to an overall p -value of 0.67 (0.4 SD). This p -value takes into account the correlations between the p_T bins shown in Fig. 12. The post fit values of the $t\bar{t}B$ normalisation parameters are compatible with the value obtained in the inclusive result. As an additional compatibility test, a combined fit of the STXS signal templates with a single parameter of interest was performed, resulting in a best fit value that agrees within 3% to that of the inclusive result with uncertainties that are larger by 20%. The larger uncertainty is expected and an effect of the additional p_T^H dependent uncertainties of the $t\bar{t}B$ background model in the STXS fit described in Section 9.

The compatibility with the SM expectation has a p -value of 0.21 (1.3 SD). No significant trend in p_T^H compared to the SM expectation is observed. The largest deviation from the SM expectation is observed for $p_T > 300$ GeV with a local significance of approximately 2 SD.

10.2 The tH production rate

Second, the tH signal process is targeted. Here, the $t\bar{t}H$ contribution is assumed to conform to the SM expectation ($\mu_{t\bar{t}H} = 1$) and is treated as background. An upper limit at 95% CL on the tH production rate relative to the SM expectation, denoted as the signal strength modifier μ_{tH} , of 14.6 is obtained, with an expectation of $19.3^{+9.2}_{-6.0}$. The limits per channel and year and in their combination are shown in Fig. 13. The expected limit for 2017 is slightly lower than the one for 2018 despite the higher luminosity of the 2018 dataset, driven by a slightly larger selection efficiency for $t\bar{t}H$ and $t\bar{t} + \text{jets}$ background processes in 2018. The systematic uncertainties with the highest impact are related to the $t\bar{t}B$ background modelling, the jet energy scale, and the uncertainty in the tH signal cross section. When fixing $\mu_{t\bar{t}H}$ to the measured value of 0.33, an upper limit on μ_{tH} of 16.1 is obtained.

Furthermore, a simultaneous fit of the $t\bar{t}H$ and tH signal strength modifiers is performed. The observed and expected values of the likelihood-ratio test statistic are shown in Fig. 14, with best fit values of $(\mu_{t\bar{t}H}, \mu_{tH})$ of $(0.35, -3.83)$. The correlation between the $t\bar{t}H$ and tH signal strength modifiers is of moderate size (-15%), which demonstrates the discrimination between the two signal processes achieved in this analysis.

10.3 Coupling measurement

Third, the Higgs boson coupling is analysed in different models, where both $t\bar{t}H$ and tH are treated as signal. Variations in the kinematic properties of the signal events are taken into

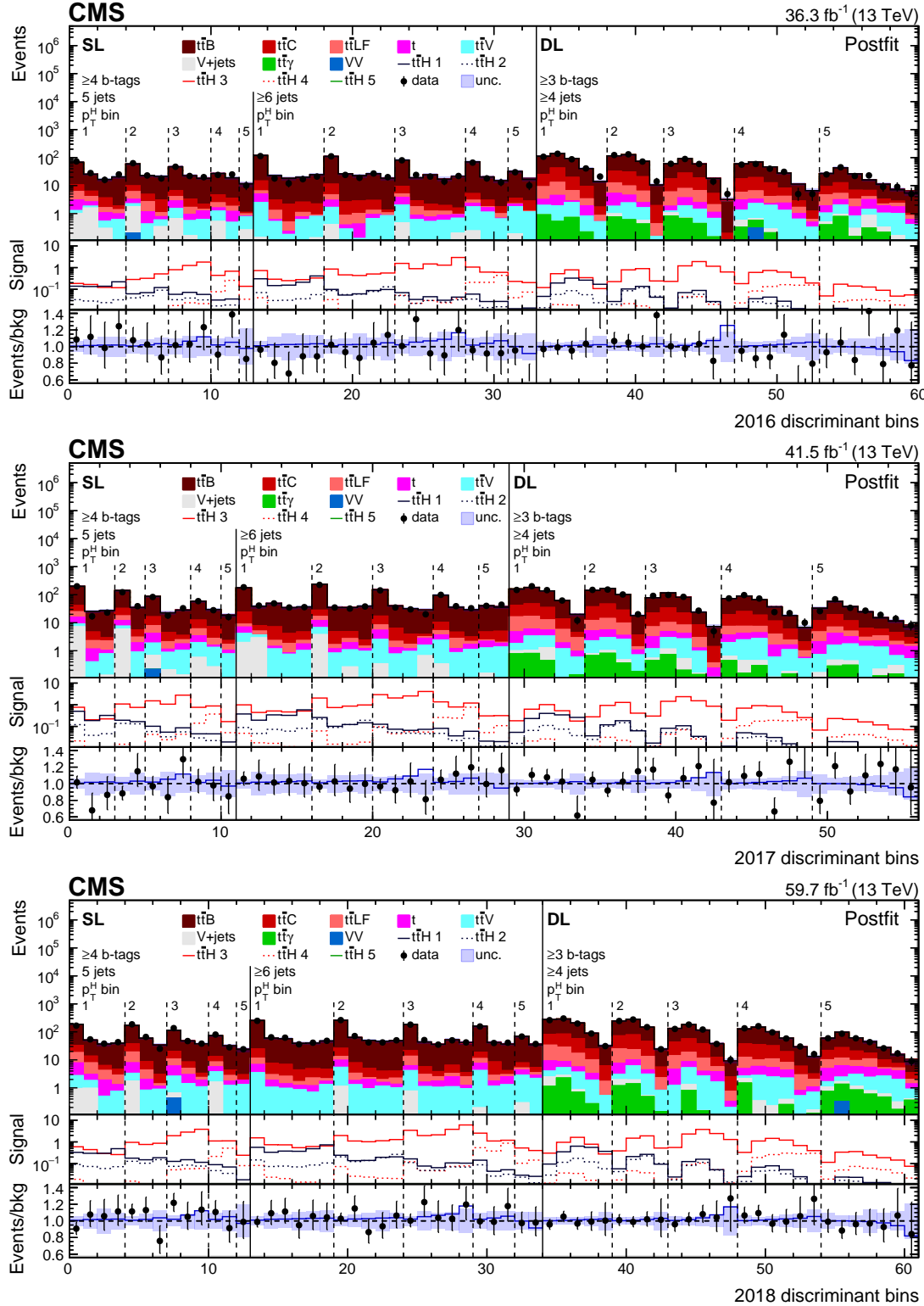


Figure 11: Observed (points) and postfit expected (filled histograms) yields in each STXS analysis discriminant bin in the signal regions of the SL and DL channels for the 2016 (upper), 2017 (middle), and 2018 (lower) data-taking periods. The vertical dashed lines separate the STXS categories (labelled 1 to 5). The fitted signal distributions (lines labelled $t\bar{t}H$ 1 to 5) in each p_T^H bin are shown in the middle pads. The lower pads show the ratio of the data to the background (points) and of the postfit expected total signal+background to the background-only contribution (line). The uncertainty bands include the total uncertainty of the fit model.

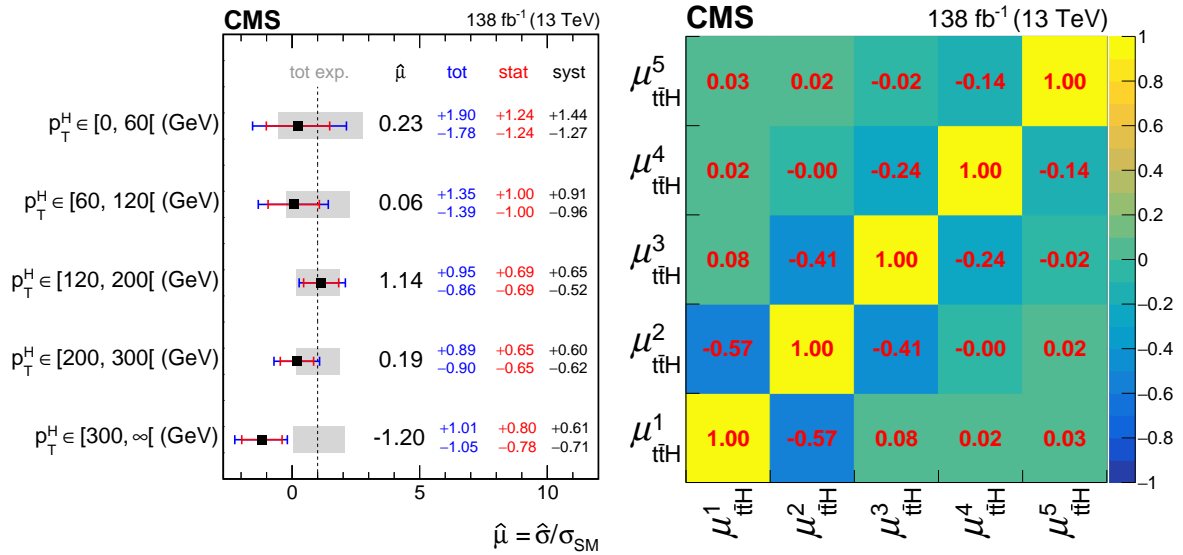


Figure 12: Best fit results $\hat{\mu}$ of the $t\bar{t}H$ signal-strength modifiers $\mu_{t\bar{t}H}$ in the different p_T^H bins (left) and their correlations (right) of the STXS measurement.

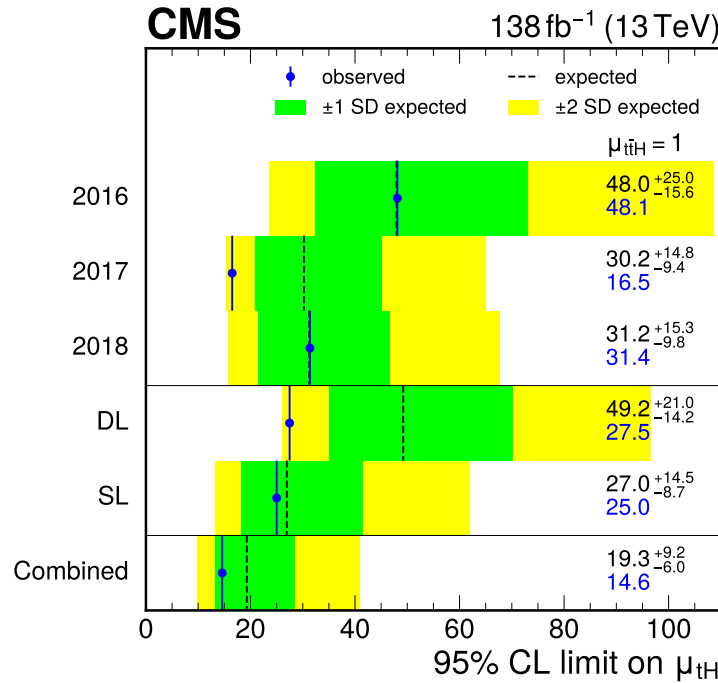


Figure 13: Observed (solid vertical line) and expected (dashed vertical line) upper 95% CL limit on the tH signal strength modifier μ_{tH} for different channels and years, where the uncertainties are uncorrelated between the channels and years, and in their combination. The green (yellow) areas indicate the one (two) standard deviation confidence intervals on the expected limit.

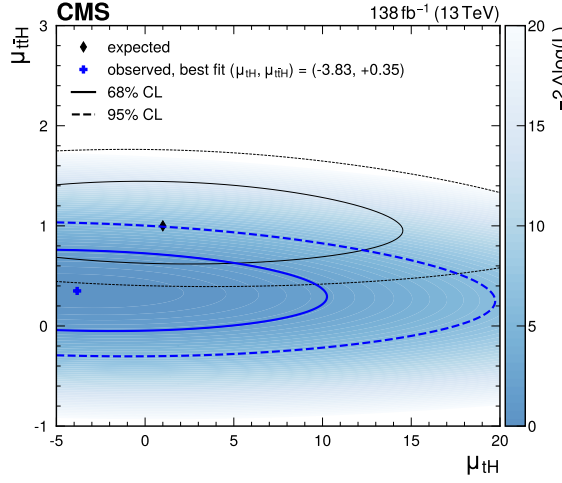


Figure 14: Observed likelihood-ratio test statistic (blue shading) as a function of the $t\bar{t}H$ and tH signal strength modifiers $\mu_{t\bar{t}H}$ and μ_{tH} , together with the observed (blue) and SM expected (black) best fit points (cross and diamond markers) as well as the 68% (solid lines) and 95% (dashed lines) CL regions.

account via event weights in the simulated samples, as described in Section 4.

Assuming SM Higgs boson coupling structure, the coupling strength of the Higgs boson to top quarks and to vector bosons is allowed to vary. This is parameterised in terms of the coupling strength modifiers κ_t and κ_V , which denote the coupling strengths relative to the SM expectation following Ref. [111]. While the $t\bar{t}H$ production rate is proportional to κ_t^2 , for tH production interference occurs between processes in which the Higgs boson couples to the top quark or to the W boson, as shown in Fig. 1. As such, the tH production cross section $\sigma_{tHq/tHW}$ is sensitive to the relative sign of κ_t and κ_V :

$$\begin{aligned}\sigma_{tHq} &= \left(2.63\kappa_t^2 + 3.58\kappa_V^2 - 5.21\kappa_t\kappa_V\right)\sigma_{tHq}^{SM}, \\ \sigma_{tHW} &= \left(2.91\kappa_t^2 + 2.31\kappa_V^2 - 4.22\kappa_t\kappa_V\right)\sigma_{tHW}^{SM}.\end{aligned}\quad (3)$$

The observed and expected values of the likelihood ratio test statistic for different values of κ_t and κ_V are shown in Fig. 15. Best fit values of (κ_t, κ_V) of $(+0.59, +1.40)$ are observed, compatible with the SM expectation at the level of 2.4 SD. Assuming $\kappa_V = 1$, a best fit value of $\kappa_t = +0.54$ is obtained with the 68% CL region ranging from -0.55 to -0.24 and $+0.20$ to $+0.72$.

Furthermore, the CP structure of the top-Higgs coupling is probed for potential non-SM contributions. For this, the amplitude of the top-Higgs interaction is parameterised as in Ref. [112] as

$$\mathcal{A}(Htt) = -\frac{m_t}{v}\bar{\psi}_t \left(\kappa_t + i\tilde{\kappa}_t\gamma_5\right) \psi_t, \quad (4)$$

where ψ_t and $\bar{\psi}_t$ are a Dirac spinor and its adjoint, respectively, m_t is the top quark mass, κ_t and $\tilde{\kappa}_t$ denote the coupling strength modifiers to a purely CP -even and a purely CP -odd component, respectively, and v is the vacuum expectation value of the Higgs field. In the SM, $\kappa_t = 1$ and $\tilde{\kappa}_t = 0$. The same interference model as in Eq. (3) is taken into account for the CP -even top-Higgs coupling.

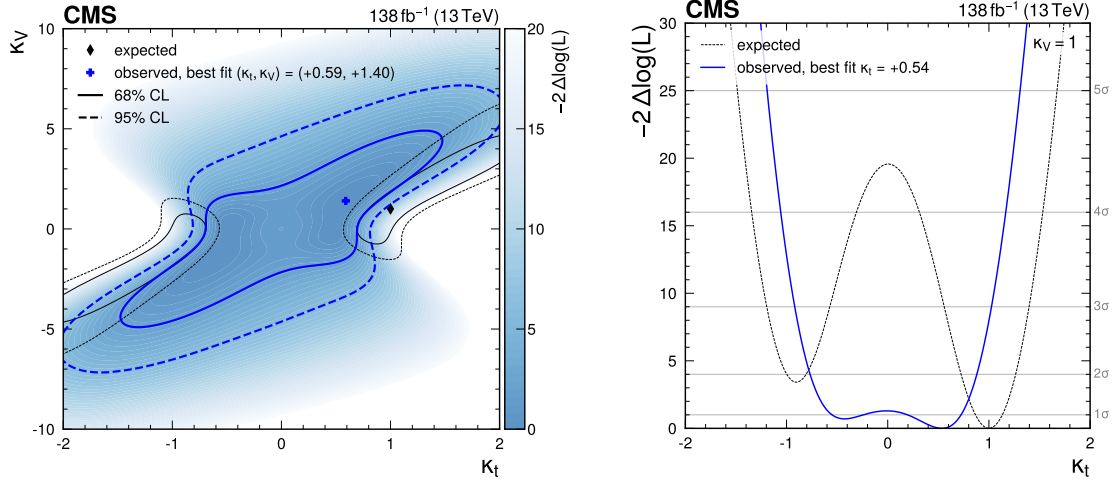


Figure 15: Observed likelihood ratio test statistic (blue shading) as a function of κ_t and κ_V , together with the observed (blue) and SM expected (black) best fit points (cross and diamond markers) as well as the 68% (solid lines) and 95% (dashed lines) CL regions (left). The observed (solid blue line) and expected (dotted black line) values of the likelihood ratio for $\kappa_V = 1$ are also shown (right).

Figure 16 shows the observed and expected values of the likelihood ratio test statistic as a function of κ_t and $\tilde{\kappa}_t$, where κ_V is fixed to the SM value of 1. Best fit values of $(\kappa_t, \tilde{\kappa}_t)$ of $(+0.53, 0.00)$ are observed, compatible with the SM expectation at the level of 2SD. The results are also expressed in terms of the CP -odd fraction [112]

$$f_{CP} = \frac{\tilde{\kappa}_t^2}{\tilde{\kappa}_t^2 + \kappa_t^2} \text{sign}(\tilde{\kappa}_t / \kappa_t) \quad (5)$$

as well as the CP mixing angle [113]

$$\cos \alpha = \frac{\kappa_t}{\sqrt{\tilde{\kappa}_t^2 + \kappa_t^2}} \quad (6)$$

shown in Fig. 17. The reduction in observed sensitivity relative to the expectation is a consequence of the best fit value of κ_t being smaller than 1, which leads to a shallower likelihood contour along a circle in $(\kappa_t, \tilde{\kappa}_t)$ space.

10.4 Combination of coupling measurement with results in other channels

The results for κ_t and $\tilde{\kappa}_t$ are combined with the results of $t\bar{t}H$ measurements by the CMS Collaboration in the $H \rightarrow \gamma\gamma$ [8] and $H \rightarrow ZZ$ [19], and the $H \rightarrow WW$ and $H \rightarrow \tau\tau$ [20] decay channels. Potential overlap of events selected in the different analyses is considered negligible, due to the lepton and b-tagged jets selection requirements, as well as the used multivariate classifiers. Systematic uncertainties are correlated between the decay channels following the scheme described in Ref. [20], where also a combination of the results in the aforementioned non- $b\bar{b}$ channels is presented. In particular, theoretical uncertainties on the rates of signal and background processes estimated from simulation as well as uncertainties in the acceptance due to missing higher orders are treated as correlated; uncertainties in the background rates determined from dedicated control regions in data are taken as uncorrelated; and uncertainties in the luminosity estimate and the pileup modelling are correlated. Several of the components

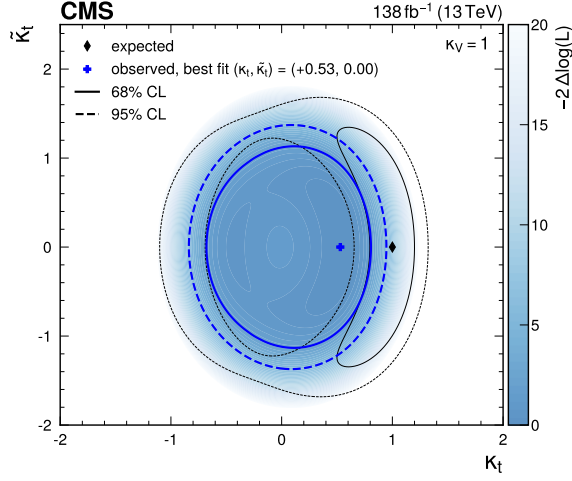


Figure 16: Observed likelihood ratio test statistic (blue shading) as a function of κ_t and $\tilde{\kappa}_t$, where $\kappa_V = 1$, together with the observed (blue) and SM expected (black) best fit points (cross and diamond markers) as well as the 68% (solid lines) and 95% (region between dashed lines) CL regions.

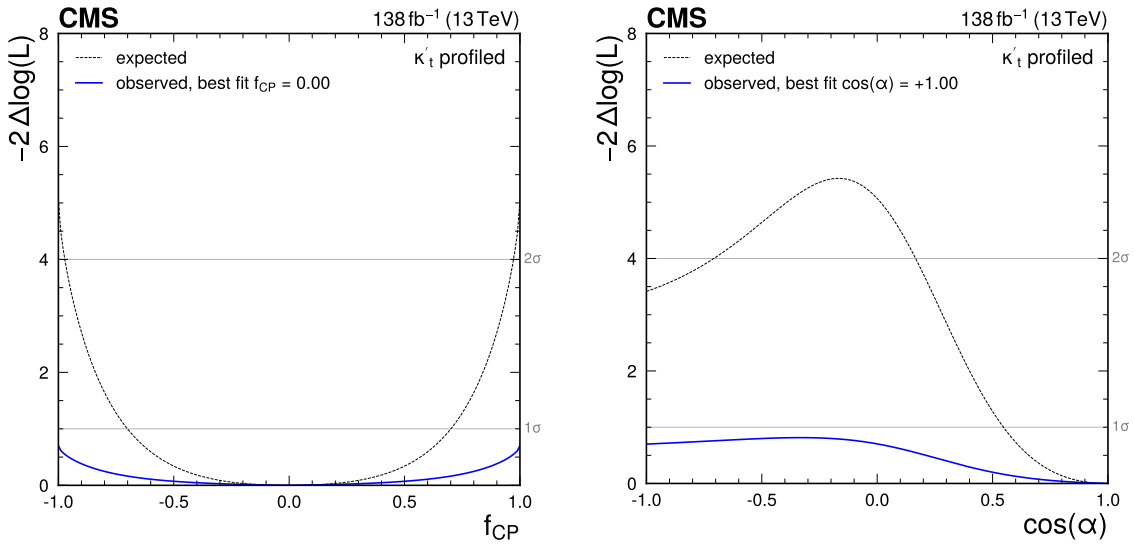


Figure 17: Observed (solid blue line) and expected (dotted black line) likelihood ratio test statistic as a function of f_{CP} (left) and $\cos \alpha$ (right), where κ_V is 1 and $\kappa'_t = \sqrt{\tilde{\kappa}_t^2 + \kappa_t^2}$, the overall modifier of the top-Higgs coupling strength, is profiled.

of the experimental uncertainties related to the b tagging and the jet energy scale are common between the channels and are correlated, while the other components as well as all other experimental uncertainties are analysis specific and therefore treated as uncorrelated.

The result of the combination is presented in Fig. 18, which shows the values of the likelihood ratio test statistic as a function of κ_t and $\tilde{\kappa}_t$ for the individual channels and the combination, which yields best fit values of $(\kappa_t, \tilde{\kappa}_t)$ of $(0.82, -0.65)$. The change of sign of $\tilde{\kappa}_t$ for the result in the $H \rightarrow WW$ and $H \rightarrow \tau\tau$ channels compared to Ref. [20] is not meaningful but reflects the degeneracy of the likelihood with respect to $\tilde{\kappa}_t$. The sensitivity of the combined result is driven by the non- $b\bar{b}$ channels, but the addition of the $H \rightarrow b\bar{b}$ channel leads to a slight improvement in sensitivity, visible in the reduction of the 68% and 95% CL confidence regions compared to the combination in Ref. [20].

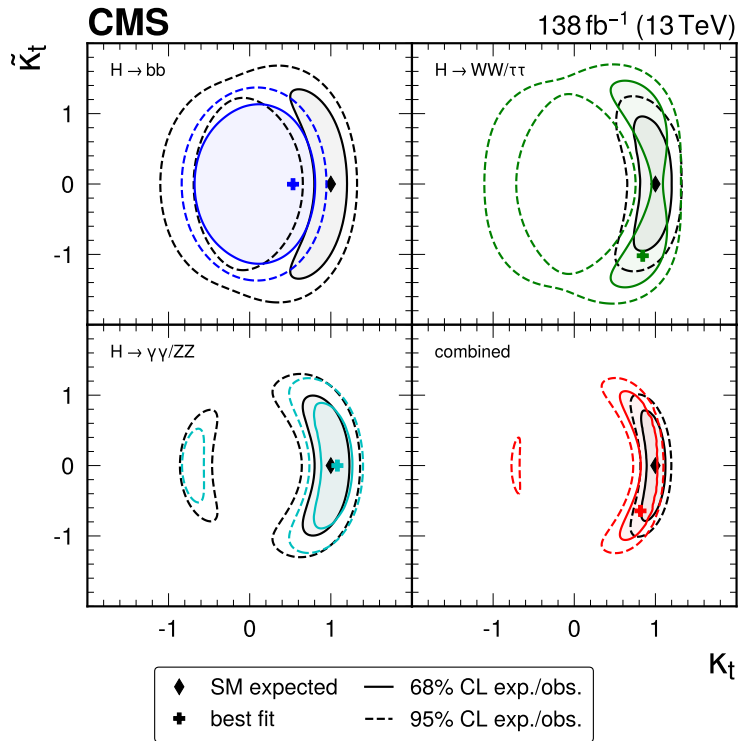


Figure 18: Observed 68% (solid lines) and 95% (dashed lines) CL regions of the likelihood ratio test statistic as a function of κ_t and $\tilde{\kappa}_t$, where $\kappa_V = 1$, and best fit values (crosses), for the $H \rightarrow b\bar{b}$ decay channel (blue), the $H \rightarrow \gamma\gamma$ and $H \rightarrow ZZ$ channels (cyan), the $H \rightarrow WW$ and $H \rightarrow \tau\tau$ channels (green), and for the combination of all channels (red). The SM expected CL regions (black lines) and best fit values (black diamonds) are superimposed.

Figure 19 shows the corresponding results for f_{CP} and $\cos \alpha$. They are constrained to $|f_{CP}| < 0.85$ and $\cos \alpha > 0.39$ at 95% CL. While the sensitivity to parameter values close to the SM expectation remains essentially unchanged, consistent with Fig. 18, the addition of the $H \rightarrow b\bar{b}$ channel leads to a substantial improvement in the expected sensitivity to non-SM scenarios with values of $|f_{CP}|$ close to 1 and $\cos \alpha$ around 0, corresponding to large values of $|\tilde{\kappa}_t|$ or small values of $|\kappa_t|$. The significance of the observed exclusion is reduced, also with respect to the previous combination in Ref. [20]. This is driven by the low observed $t\bar{t}H$ signal strength in the $H \rightarrow b\bar{b}$ channel compared to the other channels. Given that the sensitivity of the presented analysis to the $t\bar{t}H$ signal strength is at a similar level as in the other channels, the overall

top-Higgs coupling strength in the combination is reduced, leading in turn to the reduced significance of the observed exclusion in f_{CP} and $\cos \alpha$.

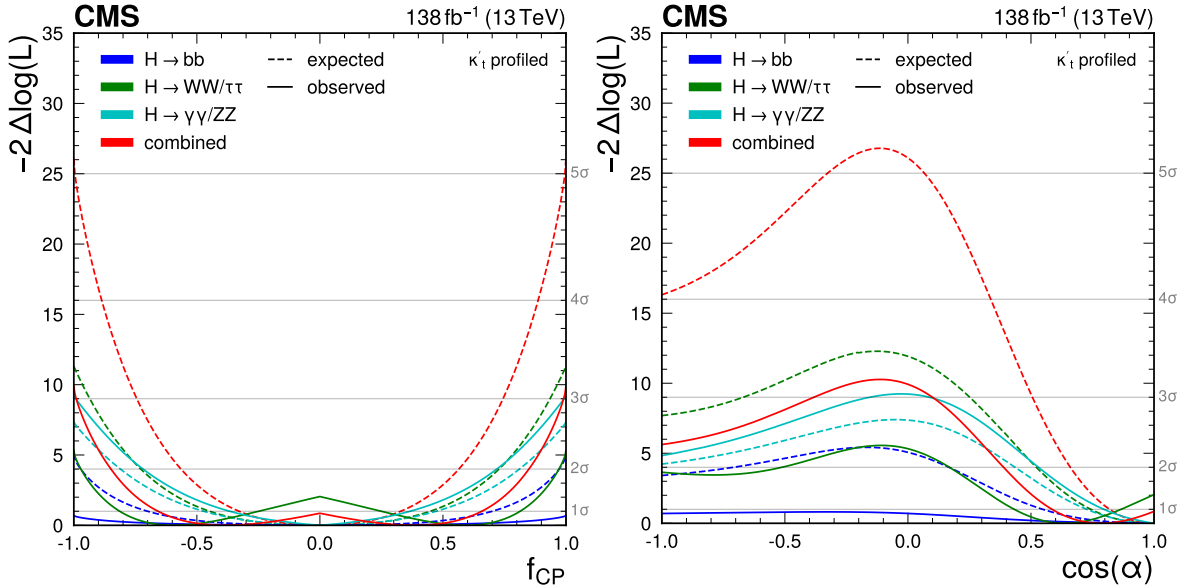


Figure 19: Observed (solid lines) and expected (dotted lines) likelihood ratio test statistic as a function of f_{CP} (left) and $\cos \alpha$ (right), where κ_V is 1 and $\kappa'_t = \sqrt{\tilde{\kappa}_t^2 + \kappa_t^2}$, the overall modifier of the top-Higgs coupling strength, is profiled, for the $H \rightarrow b\bar{b}$ decay channel (blue), the $H \rightarrow \gamma\gamma$ and $H \rightarrow ZZ$ channels (cyan), the $H \rightarrow WW$ and $H \rightarrow \tau\tau$ channels (green), and for the combination of all channels (red).

11 Summary

A combined analysis of the associated production of a Higgs boson (H) with a top quark-antiquark pair ($t\bar{t}H$) or a single top quark (tH) with the Higgs boson decaying into a bottom quark-antiquark pair has been presented. The analysis has been performed using proton-proton collision data recorded with the CMS detector at a centre-of-mass energy of 13 TeV, corresponding to an integrated luminosity of 138 fb^{-1} . Candidate events are selected in mutually exclusive categories according to the lepton and jet multiplicity, targeting three different final states of the top quark decays. Neural network discriminants are used to further categorise the events according to the most probable process, targeting the signal and different topologies of the dominant $t\bar{t} + \text{jets}$ background, as well as to separate the signal from the background. Compared to previous CMS results in this channel, which were obtained with an approximately four times smaller dataset, several refinements of the analysis strategy as well as modelling of the $t\bar{t} + \text{jets}$ background based on state-of-the-art $t\bar{t} + b\bar{b}$ simulations have been adopted. Furthermore, an extended set of interpretations is performed, including the first analysis within the simplified template cross section (STXS) framework and the first analysis of the CP structure of the top-Higgs coupling in this channel by the CMS Collaboration.

A best fit value of the $t\bar{t}H$ production cross section relative to the standard model (SM) expectation of $0.33 \pm 0.26 = 0.33 \pm 0.17(\text{stat}) \pm 0.21(\text{syst})$ is obtained. The observed rate of the dominant background from $t\bar{t} + b\bar{b}$ production is larger than predicted, in agreement with dedicated measurements of the process [88], and the results motivate further studies of $t\bar{t} + b\bar{b}$ production. The analysis is additionally performed within the STXS framework in five in-

ervals of Higgs boson p_T , probing potential p_T dependent deviations from the SM expectation. An observed (expected) upper limit on the $t\bar{t}H$ production cross section relative to the SM expectation of 14.6 (19.3) at 95% confidence level (CL) is derived. Information on the Higgs boson coupling strength is furthermore inferred from a simultaneous fit of the $t\bar{t}H$ and tH production rates, probing either the coupling strength of the Higgs boson to top quarks and to heavy vector bosons, or possible CP -odd admixtures in the coupling between the Higgs boson and top quarks. The results on the CP nature of the coupling are combined with those from measurements in other Higgs boson decay channels, constraining the CP -odd fraction f_{CP} to $|f_{CP}| < 0.85$ and the CP mixing angle $\cos \alpha$ to $\cos \alpha > 0.39$ at 95% CL.

Acknowledgments

We congratulate our colleagues in the CERN accelerator departments for the excellent performance of the LHC and thank the technical and administrative staffs at CERN and at other CMS institutes for their contributions to the success of the CMS effort. In addition, we gratefully acknowledge the computing centres and personnel of the Worldwide LHC Computing Grid and other centres for delivering so effectively the computing infrastructure essential to our analyses. Finally, we acknowledge the enduring support for the construction and operation of the LHC, the CMS detector, and the supporting computing infrastructure provided by the following funding agencies: SC (Armenia), BMBWF and FWF (Austria); FNRS and FWO (Belgium); CNPq, CAPES, FAPERJ, FAPERGS, and FAPESP (Brazil); MES and BNSF (Bulgaria); CERN; CAS, MoST, and NSFC (China); MINCIENCIAS (Colombia); MSES and CSF (Croatia); RIF (Cyprus); SENESCYT (Ecuador); ERC PRG, RVTT3 and MoER TK202 (Estonia); Academy of Finland, MEC, and HIP (Finland); CEA and CNRS/IN2P3 (France); SRNSF (Georgia); BMBF, DFG, and HGF (Germany); GSRI (Greece); NKFIH (Hungary); DAE and DST (India); IPM (Iran); SFI (Ireland); INFN (Italy); MSIP and NRF (Republic of Korea); MES (Latvia); LMELT (Lithuania); MOE and UM (Malaysia); BUAP, CINVESTAV, CONACYT, LNS, SEP, and UASLP-FAI (Mexico); MOS (Montenegro); MBIE (New Zealand); PAEC (Pakistan); MES and NSC (Poland); FCT (Portugal); MESTD (Serbia); MCIN/AEI and PCTI (Spain); MOSTR (Sri Lanka); Swiss Funding Agencies (Switzerland); MST (Taipei); MHESI and NSTDA (Thailand); TUBITAK and TENMAK (Turkey); NASU (Ukraine); STFC (United Kingdom); DOE and NSF (USA).

Individuals have received support from the Marie-Curie programme and the European Research Council and Horizon 2020 Grant, contract Nos. 675440, 724704, 752730, 758316, 765710, 824093, 101115353, 101002207, and COST Action CA16108 (European Union); the Leventis Foundation; the Alfred P. Sloan Foundation; the Alexander von Humboldt Foundation; the Science Committee, project no. 22rl-037 (Armenia); the Belgian Federal Science Policy Office; the Fonds pour la Formation à la Recherche dans l’Industrie et dans l’Agriculture (FRIA-Belgium); the F.R.S.-FNRS and FWO (Belgium) under the “Excellence of Science – EOS” – be.h project n. 30820817; the Beijing Municipal Science & Technology Commission, No. Z191100007219010 and Fundamental Research Funds for the Central Universities (China); the Ministry of Education, Youth and Sports (MEYS) of the Czech Republic; the Shota Rustaveli National Science Foundation, grant FR-22-985 (Georgia); the Deutsche Forschungsgemeinschaft (DFG), among others, under Germany’s Excellence Strategy – EXC 2121 “Quantum Universe” – 390833306, and under project number 400140256 - GRK2497; the Hellenic Foundation for Research and Innovation (HFRI), Project Number 2288 (Greece); the Hungarian Academy of Sciences, the New National Excellence Program - ÚNKP, the NKFIH research grants K 131991, K 133046, K 138136, K 143460, K 143477, K 146913, K 146914, K 147048, 2020-2.2.1-ED-2021-00181, and TKP2021-NKTA-64 (Hungary); the Council of Science and Industrial Research, India; ICSC –

National Research Centre for High Performance Computing, Big Data and Quantum Computing and FAIR – Future Artificial Intelligence Research, funded by the NextGenerationEU program (Italy); the Latvian Council of Science; the Ministry of Education and Science, project no. 2022/WK/14, and the National Science Center, contracts Opus 2021/41/B/ST2/01369 and 2021/43/B/ST2/01552 (Poland); the Fundação para a Ciência e a Tecnologia, grant CEECIND/01334/2018 (Portugal); the National Priorities Research Program by Qatar National Research Fund; MCIN/AEI/10.13039/501100011033, ERDF “a way of making Europe”, and the Programa Estatal de Fomento de la Investigación Científica y Técnica de Excelencia María de Maeztu, grant MDM-2017-0765 and Programa Severo Ochoa del Principado de Asturias (Spain); the Chulalongkorn Academic into Its 2nd Century Project Advancement Project, and the National Science, Research and Innovation Fund via the Program Management Unit for Human Resources & Institutional Development, Research and Innovation, grant B39G670016 (Thailand); the Kavli Foundation; the Nvidia Corporation; the SuperMicro Corporation; the Welch Foundation, contract C-1845; and the Weston Havens Foundation (USA).

References

- [1] S. Alekhin, A. Djouadi, and S. Moch, “The top quark and Higgs boson masses and the stability of the electroweak vacuum”, *Phys. Lett. B* **716** (2012) 214, doi:[10.1016/j.physletb.2012.08.024](https://doi.org/10.1016/j.physletb.2012.08.024), arXiv:[1207.0980](https://arxiv.org/abs/1207.0980).
- [2] B. A. Dobrescu and C. T. Hill, “Electroweak symmetry breaking via top condensation seesaw”, *Phys. Rev. Lett.* **81** (1998) 2634, doi:[10.1103/PhysRevLett.81.2634](https://doi.org/10.1103/PhysRevLett.81.2634), arXiv:[hep-ph/9712319](https://arxiv.org/abs/hep-ph/9712319).
- [3] R. S. Chivukula, B. A. Dobrescu, H. Georgi, and C. T. Hill, “Top quark seesaw theory of electroweak symmetry breaking”, *Phys. Rev. D* **59** (1999) 075003, doi:[10.1103/PhysRevD.59.075003](https://doi.org/10.1103/PhysRevD.59.075003), arXiv:[hep-ph/9809470](https://arxiv.org/abs/hep-ph/9809470).
- [4] ATLAS Collaboration, “Observation of Higgs boson production in association with a top quark pair at the LHC with the ATLAS detector”, *Phys. Lett. B* **784** (2018) 159, doi:[10.1016/j.physletb.2018.07.035](https://doi.org/10.1016/j.physletb.2018.07.035), arXiv:[1806.00425](https://arxiv.org/abs/1806.00425).
- [5] CMS Collaboration, “Observation of $t\bar{t}H$ production”, *Phys. Rev. Lett.* **120** (2018) 231801, doi:[10.1103/PhysRevLett.120.231801](https://doi.org/10.1103/PhysRevLett.120.231801), arXiv:[1804.02610](https://arxiv.org/abs/1804.02610).
- [6] ATLAS Collaboration, “Measurement of the properties of Higgs boson production at $\sqrt{s} = 13 \text{ TeV}$ in the $H \rightarrow \gamma\gamma$ channel using 139 fb^{-1} of pp collision data with the ATLAS experiment”, *JHEP* **07** (2023) 088, doi:[10.1007/JHEP07\(2023\)088](https://doi.org/10.1007/JHEP07(2023)088), arXiv:[2207.00348](https://arxiv.org/abs/2207.00348).
- [7] ATLAS Collaboration, “ CP properties of Higgs boson interactions with top quarks in the $t\bar{t}H$ and tH processes using $H \rightarrow \gamma\gamma$ with the ATLAS detector”, *Phys. Rev. Lett.* **125** (2020) 061802, doi:[10.1103/PhysRevLett.125.061802](https://doi.org/10.1103/PhysRevLett.125.061802), arXiv:[2004.04545](https://arxiv.org/abs/2004.04545).
- [8] CMS Collaboration, “Measurements of $t\bar{t}H$ production and the CP structure of the Yukawa interaction between the Higgs boson and top quark in the diphoton decay channel”, *Phys. Rev. Lett.* **125** (2020) 061801, doi:[10.1103/PhysRevLett.125.061801](https://doi.org/10.1103/PhysRevLett.125.061801), arXiv:[2003.10866](https://arxiv.org/abs/2003.10866).
- [9] CMS Collaboration, “Measurements of Higgs boson production cross sections and couplings in the diphoton decay channel at $\sqrt{s} = 13 \text{ TeV}$ ”, *JHEP* **07** (2021) 027, doi:[10.1007/JHEP07\(2021\)027](https://doi.org/10.1007/JHEP07(2021)027), arXiv:[2103.06956](https://arxiv.org/abs/2103.06956).

- [10] CMS Collaboration, "Measurement of the Higgs boson production rate in association with top quarks in final states with electrons, muons, and hadronically decaying tau leptons at $\sqrt{s} = 13 \text{ TeV}$ ", *Eur. Phys. J. C* **81** (2021) 378, doi:[10.1140/epjc/s10052-021-09014-x](https://doi.org/10.1140/epjc/s10052-021-09014-x), arXiv:[2011.03652](https://arxiv.org/abs/2011.03652).
- [11] ATLAS Collaboration, "Measurement of Higgs boson decay into b-quarks in associated production with a top-quark pair in pp collisions at $\sqrt{s} = 13 \text{ TeV}$ with the ATLAS detector", *JHEP* **06** (2022) 097, doi:[10.1007/JHEP06\(2022\)097](https://doi.org/10.1007/JHEP06(2022)097), arXiv:[2111.06712](https://arxiv.org/abs/2111.06712).
- [12] CMS Collaboration, "Search for $t\bar{t}H$ production in the $H \rightarrow b\bar{b}$ decay channel with leptonic $t\bar{t}$ decays in proton-proton collisions at $\sqrt{s} = 13 \text{ TeV}$ ", *JHEP* **03** (2019) 026, doi:[10.1007/JHEP03\(2019\)026](https://doi.org/10.1007/JHEP03(2019)026), arXiv:[1804.03682](https://arxiv.org/abs/1804.03682).
- [13] CMS Collaboration, "Search for $t\bar{t}H$ production in the all-jet final state in proton-proton collisions at $\sqrt{s} = 13 \text{ TeV}$ ", *JHEP* **06** (2018) 101, doi:[10.1007/JHEP06\(2018\)101](https://doi.org/10.1007/JHEP06(2018)101), arXiv:[1803.06986](https://arxiv.org/abs/1803.06986).
- [14] F. Maltoni, K. Paul, T. Stelzer, and S. Willenbrock, "Associated production of Higgs and single top at hadron colliders", *Phys. Rev. D* **64** (2001) 094023, doi:[10.1103/PhysRevD.64.094023](https://doi.org/10.1103/PhysRevD.64.094023), arXiv:[hep-ph/0106293](https://arxiv.org/abs/hep-ph/0106293).
- [15] M. Farina et al., "Lifting degeneracies in Higgs couplings using single top production in association with a Higgs boson", *JHEP* **05** (2013) 022, doi:[10.1007/JHEP05\(2013\)022](https://doi.org/10.1007/JHEP05(2013)022), arXiv:[1211.3736](https://arxiv.org/abs/1211.3736).
- [16] P. Agrawal, S. Mitra, and A. Shivaji, "Effect of anomalous couplings on the associated production of a single top quark and a Higgs boson at the LHC", *JHEP* **12** (2013) 077, doi:[10.1007/JHEP12\(2013\)077](https://doi.org/10.1007/JHEP12(2013)077), arXiv:[1211.4362](https://arxiv.org/abs/1211.4362).
- [17] F. Demartin, F. Maltoni, K. Mawatari, and M. Zaro, "Higgs production in association with a single top quark at the LHC", *Eur. Phys. J. C* **75** (2015) 267, doi:[10.1140/epjc/s10052-015-3475-9](https://doi.org/10.1140/epjc/s10052-015-3475-9), arXiv:[1504.00611](https://arxiv.org/abs/1504.00611).
- [18] CMS Collaboration, "Search for associated production of a Higgs boson and a single top quark in proton-proton collisions at $\sqrt{s} = 13 \text{ TeV}$ ", *Phys. Rev. D* **99** (2019) 092005, doi:[10.1103/PhysRevD.99.092005](https://doi.org/10.1103/PhysRevD.99.092005), arXiv:[1811.09696](https://arxiv.org/abs/1811.09696).
- [19] CMS Collaboration, "Constraints on anomalous Higgs boson couplings to vector bosons and fermions in its production and decay using the four-lepton final state", *Phys. Rev. D* **104** (2021) 052004, doi:[10.1103/PhysRevD.104.052004](https://doi.org/10.1103/PhysRevD.104.052004), arXiv:[2104.12152](https://arxiv.org/abs/2104.12152).
- [20] CMS Collaboration, "Search for CP violation in $t\bar{t}H$ and tH production in multilepton channels in proton-proton collisions at $\sqrt{s} = 13 \text{ TeV}$ ", *JHEP* **07** (2023) 092, doi:[10.1007/JHEP07\(2023\)092](https://doi.org/10.1007/JHEP07(2023)092), arXiv:[2208.02686](https://arxiv.org/abs/2208.02686).
- [21] ATLAS Collaboration, "Probing the CP nature of the top-Higgs Yukawa coupling in $t\bar{t}H$ and tH events with $H \rightarrow b\bar{b}$ decays using the ATLAS detector at the LHC", *Phys. Lett. B* **849** (2024) 138469, doi:[10.1016/j.physletb.2024.138469](https://doi.org/10.1016/j.physletb.2024.138469), arXiv:[2303.05974](https://arxiv.org/abs/2303.05974).
- [22] LHC Higgs Cross Section Working Group, "Handbook of LHC Higgs cross sections: 4. deciphering the nature of the Higgs sector", 2017. arXiv:[1610.07922](https://arxiv.org/abs/1610.07922).

- [23] ATLAS Collaboration, "Measurement of the associated production of a top-antitop-quark pair and a Higgs boson decaying into a $b\bar{b}$ pair in pp collisions at $\sqrt{s} = 13$ TeV using the ATLAS detector at the LHC", 2024. arXiv:2407.10904. Submitted to *Eur. Phys. J. C.*
- [24] T. Ježo, J. M. Lindert, N. Moretti, and S. Pozzorini, "New NLOPS predictions for $t\bar{t} + b$ -jet production at the LHC", *Eur. Phys. J. C* **78** (2018) 502, doi:10.1140/epjc/s10052-018-5956-0, arXiv:1802.00426.
- [25] F. Buccioni, S. Kallweit, S. Pozzorini, and M. F. Zoller, "NLO QCD predictions for $t\bar{t}bb$ production in association with a light jet at the LHC", *JHEP* **12** (2019) 015, doi:10.1007/JHEP12(2019)015, arXiv:1907.13624.
- [26] HEPData record for this analysis, 2024. doi:10.17182/hepdata.152799.
- [27] CMS Collaboration, "The CMS experiment at the CERN LHC", *JINST* **3** (2008) S08004, doi:10.1088/1748-0221/3/08/S08004.
- [28] CMS Tracker Group Collaboration, "The CMS phase-1 pixel detector upgrade", *JINST* **16** (2021) P02027, doi:10.1088/1748-0221/16/02/P02027, arXiv:2012.14304.
- [29] CMS Collaboration, "The CMS trigger system", *JINST* **12** (2017) P01020, doi:10.1088/1748-0221/12/01/P01020, arXiv:1609.02366.
- [30] CMS Collaboration, "Performance of the CMS level-1 trigger in proton-proton collisions at $\sqrt{s} = 13$ TeV", *JINST* **15** (2020) P10017, doi:10.1088/1748-0221/15/10/P10017, arXiv:2006.10165.
- [31] CMS Collaboration, "Precision luminosity measurement in proton-proton collisions at $\sqrt{s} = 13$ TeV in 2015 and 2016 at CMS", *Eur. Phys. J. C* **81** (2021) 800, doi:10.1140/epjc/s10052-021-09538-2, arXiv:2104.01927.
- [32] CMS Collaboration, "CMS luminosity measurement for the 2017 data-taking period at $\sqrt{s} = 13$ TeV", CMS Physics Analysis Summary CMS-PAS-LUM-17-004, 2017.
- [33] CMS Collaboration, "CMS luminosity measurement for the 2018 data-taking period at $\sqrt{s} = 13$ TeV", CMS Physics Analysis Summary CMS-PAS-LUM-18-002, 2018.
- [34] CMS Collaboration, "Performance of the CMS muon trigger system in proton-proton collisions at $\sqrt{s} = 13$ TeV", *JINST* **16** (2021) P07001, doi:10.1088/1748-0221/16/07/P07001, arXiv:2102.04790.
- [35] CMS Collaboration, "Electron and photon reconstruction and identification with the CMS experiment at the CERN LHC", *JINST* **16** (2021) P05014, doi:10.1088/1748-0221/16/05/P05014, arXiv:2012.06888.
- [36] GEANT4 Collaboration, "GEANT4—a simulation toolkit", *Nucl. Instrum. Meth. A* **506** (2003) 250, doi:10.1016/S0168-9002(03)01368-8.
- [37] P. Nason, "A new method for combining NLO QCD with shower Monte Carlo algorithms", *JHEP* **11** (2004) 040, doi:10.1088/1126-6708/2004/11/040, arXiv:hep-ph/0409146.
- [38] S. Frixione, P. Nason, and C. Oleari, "Matching NLO QCD computations with parton shower simulations: the POWHEG method", *JHEP* **11** (2007) 070, doi:10.1088/1126-6708/2007/11/070, arXiv:0709.2092.

- [39] S. Alioli, P. Nason, C. Oleari, and E. Re, “A general framework for implementing NLO calculations in shower Monte Carlo programs: the POWHEG BOX”, *JHEP* **06** (2010) 043, doi:[10.1007/JHEP06\(2010\)043](https://doi.org/10.1007/JHEP06(2010)043), arXiv:[1002.2581](https://arxiv.org/abs/1002.2581).
- [40] T. Ježo and P. Nason, “On the treatment of resonances in next-to-leading order calculations matched to a parton shower”, *JHEP* **12** (2015) 065, doi:[10.1007/JHEP12\(2015\)065](https://doi.org/10.1007/JHEP12(2015)065), arXiv:[1509.09071](https://arxiv.org/abs/1509.09071).
- [41] H. B. Hartanto, B. Jager, L. Reina, and D. Wackeroth, “Higgs boson production in association with top quarks in the POWHEG BOX”, *Phys. Rev. D* **91** (2015) 094003, doi:[10.1103/PhysRevD.91.094003](https://doi.org/10.1103/PhysRevD.91.094003), arXiv:[1501.04498](https://arxiv.org/abs/1501.04498).
- [42] J. Alwall et al., “The automated computation of tree-level and next-to-leading order differential cross sections, and their matching to parton shower simulations”, *JHEP* **07** (2014) 079, doi:[10.1007/JHEP07\(2014\)079](https://doi.org/10.1007/JHEP07(2014)079), arXiv:[1405.0301](https://arxiv.org/abs/1405.0301).
- [43] T. Sjöstrand et al., “An introduction to PYTHIA 8.2”, *Comput. Phys. Commun.* **191** (2015) 159, doi:[10.1016/j.cpc.2015.01.024](https://doi.org/10.1016/j.cpc.2015.01.024), arXiv:[1410.3012](https://arxiv.org/abs/1410.3012).
- [44] NNPDF Collaboration, “Parton distributions from high-precision collider data”, *Eur. Phys. J. C* **77** (2017) 663, doi:[10.1140/epjc/s10052-017-5199-5](https://doi.org/10.1140/epjc/s10052-017-5199-5), arXiv:[1706.00428](https://arxiv.org/abs/1706.00428).
- [45] NNPDF Collaboration, “Parton distributions for the LHC Run II”, *JHEP* **04** (2015) 040, doi:[10.1007/JHEP04\(2015\)040](https://doi.org/10.1007/JHEP04(2015)040), arXiv:[1410.8849](https://arxiv.org/abs/1410.8849).
- [46] CMS Collaboration, “Extraction and validation of a new set of CMS PYTHIA 8 tunes from underlying-event measurements”, *Eur. Phys. J. C* **80** (2020) 4, doi:[10.1140/epjc/s10052-019-7499-4](https://doi.org/10.1140/epjc/s10052-019-7499-4), arXiv:[1903.12179](https://arxiv.org/abs/1903.12179).
- [47] CMS Collaboration, “Event generator tunes obtained from underlying event and multiparton scattering measurements”, *Eur. Phys. J. C* **76** (2016) 155, doi:[10.1140/epjc/s10052-016-3988-x](https://doi.org/10.1140/epjc/s10052-016-3988-x), arXiv:[1512.00815](https://arxiv.org/abs/1512.00815).
- [48] F. Maltoni, G. Ridolfi, and M. Ubiali, “ b -initiated processes at the LHC: a reappraisal”, *JHEP* **07** (2012) 022, doi:[10.1007/JHEP07\(2012\)022](https://doi.org/10.1007/JHEP07(2012)022), arXiv:[1203.6393](https://arxiv.org/abs/1203.6393). [Erratum: doi:[10.1007/JHEP04\(2013\)095](https://doi.org/10.1007/JHEP04(2013)095)].
- [49] F. Demartin et al., “ $t\bar{W}H$ associated production at the LHC”, *Eur. Phys. J. C* **77** (2017) 34, doi:[10.1140/epjc/s10052-017-4601-7](https://doi.org/10.1140/epjc/s10052-017-4601-7), arXiv:[1607.05862](https://arxiv.org/abs/1607.05862).
- [50] J. S. Gainer et al., “Exploring theory space with Monte Carlo reweighting”, *JHEP* **10** (2014) 078, doi:[10.1007/JHEP10\(2014\)078](https://doi.org/10.1007/JHEP10(2014)078), arXiv:[1404.7129](https://arxiv.org/abs/1404.7129).
- [51] O. Mattelaer, “On the maximal use of Monte Carlo samples: re-weighting events at NLO accuracy”, *Eur. Phys. J. C* **76** (2016) 674, doi:[10.1140/epjc/s10052-016-4533-7](https://doi.org/10.1140/epjc/s10052-016-4533-7), arXiv:[1607.00763](https://arxiv.org/abs/1607.00763).
- [52] F. Buccioni et al., “OpenLoops 2”, *Eur. Phys. J. C* **79** (2019) 866, doi:[10.1140/epjc/s10052-019-7306-2](https://doi.org/10.1140/epjc/s10052-019-7306-2), arXiv:[1907.13071](https://arxiv.org/abs/1907.13071).
- [53] F. Cascioli et al., “NLO matching for $t\bar{t}bb$ production with massive b -quarks”, *Phys. Lett. B* **734** (2014) 210, doi:[10.1016/j.physletb.2014.05.040](https://doi.org/10.1016/j.physletb.2014.05.040), arXiv:[1309.5912](https://arxiv.org/abs/1309.5912).

- [54] S. Alioli, P. Nason, C. Oleari, and E. Re, “NLO single-top production matched with shower in POWHEG: s - and t -channel contributions”, *JHEP* **09** (2009) 111, doi:10.1088/1126-6708/2009/09/111, arXiv:0907.4076. [Erratum: doi:10.1007/JHEP02(2010)011].
- [55] R. Frederix, E. Re, and P. Torrielli, “Single-top t -channel hadroproduction in the four-flavour scheme with POWHEG and aMC@NLO”, *JHEP* **09** (2012) 130, doi:10.1007/JHEP09(2012)130, arXiv:1207.5391.
- [56] E. Re, “Single-top Wt -channel production matched with parton showers using the POWHEG method”, *Eur. Phys. J. C* **71** (2011) 1547, doi:10.1140/epjc/s10052-011-1547-z, arXiv:1009.2450.
- [57] R. Frederix and S. Frixione, “Merging meets matching in MC@NLO”, *JHEP* **12** (2012) 061, doi:10.1007/JHEP12(2012)061, arXiv:1209.6215.
- [58] J. Alwall et al., “Comparative study of various algorithms for the merging of parton showers and matrix elements in hadronic collisions”, *Eur. Phys. J. C* **53** (2008) 473, doi:10.1140/epjc/s10052-007-0490-5, arXiv:0706.2569.
- [59] CMS Collaboration, “A measurement of the Higgs boson mass in the diphoton decay channel”, *Phys. Lett. B* **805** (2020) 135425, doi:10.1016/j.physletb.2020.135425, arXiv:2002.06398.
- [60] M. Cacciari et al., “Top-pair production at hadron colliders with next-to-next-to-leading logarithmic soft-gluon resummation”, *Phys. Lett. B* **710** (2012) 612, doi:10.1016/j.physletb.2012.03.013, arXiv:1111.5869.
- [61] P. Bärnreuther, M. Czakon, and A. Mitov, “Percent-level-precision physics at the Tevatron: next-to-next-to-leading order QCD corrections to $q\bar{q} \rightarrow t\bar{t}+X$ ”, *Phys. Rev. Lett.* **109** (2012) 132001, doi:10.1103/PhysRevLett.109.132001, arXiv:1204.5201.
- [62] M. Czakon and A. Mitov, “NNLO corrections to top-pair production at hadron colliders: the all-fermionic scattering channels”, *JHEP* **12** (2012) 054, doi:10.1007/JHEP12(2012)054, arXiv:1207.0236.
- [63] M. Czakon and A. Mitov, “NNLO corrections to top pair production at hadron colliders: the quark-gluon reaction”, *JHEP* **01** (2013) 080, doi:10.1007/JHEP01(2013)080, arXiv:1210.6832.
- [64] M. Beneke, P. Falgari, S. Klein, and C. Schwinn, “Hadronic top-quark pair production with NNLL threshold resummation”, *Nucl. Phys. B* **855** (2012) 695, doi:10.1016/j.nuclphysb.2011.10.021, arXiv:1109.1536.
- [65] M. Czakon, P. Fiedler, and A. Mitov, “Total top-quark pair-production cross section at hadron colliders through $\mathcal{O}(\alpha_s^4)$ ”, *Phys. Rev. Lett.* **110** (2013) 252004, doi:10.1103/PhysRevLett.110.252004, arXiv:1303.6254.
- [66] M. Czakon and A. Mitov, “Top++: a program for the calculation of the top-pair cross-section at hadron colliders”, *Comput. Phys. Commun.* **185** (2014) 2930, doi:10.1016/j.cpc.2014.06.021, arXiv:1112.5675.
- [67] N. Kidonakis, “Two-loop soft anomalous dimensions for single top quark associated production with W^- or H^- ”, *Phys. Rev. D* **82** (2010) 054018, doi:10.1103/PhysRevD.82.054018, arXiv:1005.4451.

- [68] M. Aliev et al., “HATHOR: HAdronic Top and Heavy quarks crOss section calculatoR”, *Comput. Phys. Commun.* **182** (2011) 1034, doi:10.1016/j.cpc.2010.12.040, arXiv:1007.1327.
- [69] P. Kant et al., “HatHor for single top-quark production: Updated predictions and uncertainty estimates for single top-quark production in hadronic collisions”, *Comput. Phys. Commun.* **191** (2015) 74, doi:10.1016/j.cpc.2015.02.001, arXiv:1406.4403.
- [70] F. Maltoni, D. Pagani, and I. Tsinikos, “Associated production of a top-quark pair with vector bosons at NLO in QCD: impact on $t\bar{t}H$ searches at the LHC”, *JHEP* **02** (2016) 113, doi:10.1007/JHEP02(2016)113, arXiv:1507.05640.
- [71] J. M. Campbell, R. K. Ellis, and C. Williams, “Vector boson pair production at the LHC”, *JHEP* **07** (2011) 018, doi:10.1007/JHEP07(2011)018, arXiv:1105.0020.
- [72] CMS Collaboration, “Pileup mitigation at CMS in 13 TeV data”, *JINST* **15** (2020) P09018, doi:10.1088/1748-0221/15/09/P09018, arXiv:2003.00503.
- [73] CMS Collaboration, “Particle-flow reconstruction and global event description with the CMS detector”, *JINST* **12** (2017) P10003, doi:10.1088/1748-0221/12/10/P10003, arXiv:1706.04965.
- [74] CMS Collaboration, “Technical proposal for the phase-2 upgrade of the Compact Muon Solenoid”, CMS Technical Proposal CERN-LHCC-2015-010, CMS-TDR-15-02, 2015.
- [75] CMS Collaboration, “Performance of the CMS muon detector and muon reconstruction with proton-proton collisions at $\sqrt{s} = 13$ TeV”, *JINST* **13** (2018) P06015, doi:10.1088/1748-0221/13/06/P06015, arXiv:1804.04528.
- [76] CMS Collaboration, “ECAL 2016 refined calibration and Run2 summary plots”, CMS Detector Performance Summary CMS-DP-2020-021, 2020.
- [77] M. Cacciari, G. P. Salam, and G. Soyez, “The anti- k_T jet clustering algorithm”, *JHEP* **04** (2008) 063, doi:10.1088/1126-6708/2008/04/063, arXiv:0802.1189.
- [78] M. Cacciari, G. P. Salam, and G. Soyez, “FastJet user manual”, *Eur. Phys. J. C* **72** (2012) 1896, doi:10.1140/epjc/s10052-012-1896-2, arXiv:1111.6097.
- [79] M. Cacciari, G. P. Salam, and G. Soyez, “The catchment area of jets”, *JHEP* **04** (2008) 005, doi:10.1088/1126-6708/2008/04/005, arXiv:0802.1188.
- [80] CMS Collaboration, “Jet energy scale and resolution in the CMS experiment in pp collisions at 8 TeV”, *JINST* **12** (2017) P02014, doi:10.1088/1748-0221/12/02/P02014, arXiv:1607.03663.
- [81] CMS Collaboration, “Jet algorithms performance in 13 TeV data”, CMS Physics Analysis Summary CMS-PAS-JME-16-003, 2017.
- [82] CMS Collaboration, “Identification of heavy-flavour jets with the CMS detector in pp collisions at 13 TeV”, *JINST* **13** (2018) P05011, doi:10.1088/1748-0221/13/05/P05011, arXiv:1712.07158.
- [83] E. Bols et al., “Jet flavour classification using DeepJet”, *JINST* **15** (2020) P12012, doi:10.1088/1748-0221/15/12/P12012, arXiv:2008.10519.

- [84] CMS Collaboration, “B-tagging performance of the CMS legacy dataset 2018”, CMS Detector Performance Summary CMS-DP-2021-004, 2021.
- [85] CMS Collaboration, “Performance of missing transverse momentum reconstruction in proton-proton collisions at $\sqrt{s} = 13$ TeV using the CMS detector”, *JINST* **14** (2019) P07004, doi:10.1088/1748-0221/14/07/P07004, arXiv:1903.06078.
- [86] K. Kondo, “Dynamical likelihood method for reconstruction of events with missing momentum. 1: Method and toy models”, *J. Phys. Soc. Jap.* **57** (1988) 4126, doi:10.1143/JPSJ.57.4126.
- [87] CMS Collaboration, “Search for a standard model Higgs boson produced in association with a top-quark pair and decaying to bottom quarks using a matrix element method”, *Eur. Phys. J. C* **75** (2015) 251, doi:10.1140/epjc/s10052-015-3454-1, arXiv:1502.02485.
- [88] CMS Collaboration, “Inclusive and differential cross section measurements of $t\bar{t}bb\bar{b}$ production in the lepton+jets channel at $\sqrt{s} = 13$ TeV”, *JHEP* **05** (2024) 042, doi:10.1007/JHEP05(2024)042, arXiv:2309.14442.
- [89] CMS Collaboration, “Measurement of the cross section for $t\bar{t}$ production with additional jets and b jets in pp collisions at $\sqrt{s} = 13$ TeV”, *JHEP* **07** (2020) 125, doi:10.1007/JHEP07(2020)125, arXiv:2003.06467.
- [90] CMS Collaboration, “Measurement of the $t\bar{t}bb\bar{b}$ production cross section in the all-jet final state in pp collisions at $\sqrt{s} = 13$ TeV”, *Phys. Lett. B* **803** (2020) 135285, doi:10.1016/j.physletb.2020.135285, arXiv:1909.05306.
- [91] CMS Collaboration, “Object definitions for top quark analyses at the particle level”, CMS Note CMS-NOTE-2017-004, 2017.
- [92] CMS Collaboration, “The CMS statistical analysis and combination tool: COMBINE”, *Comput. Softw. Big Sci.* **8** (2024) 19, doi:10.1007/s41781-024-00121-4, arXiv:2404.06614.
- [93] J. S. Conway, “Incorporating nuisance parameters in likelihoods for multisource spectra”, in *PHYSTAT 2011*. 3, 2011. arXiv:1103.0354. doi:10.5170/CERN-2011-006.115.
- [94] F. Chollet et al., “KERAS”. <https://keras.io>, 2015.
- [95] M. Erdmann, J. Glombitza, G. Kasieczka, and U. Klemhardt, “Deep Learning for Physics Research”. WORLD SCIENTIFIC, 2021. doi:10.1142/12294.
- [96] S. Jasper, L. Hugo, and P. A. Ryan, “Practical bayesian optimization of machine learning algorithms”, 2012. arXiv:1206.2944.
- [97] F. Luca, D. Michele, F. Paolo, and P. Massimiliano, “Forward and reverse gradient-based hyperparameter optimization”, in *Proceedings of the 34th International Conference on Machine Learning*, D. Precup and Y. W. Teh, eds., volume 70 of *Proceedings of Machine Learning Research*, p. 1165. PMLR, 2017.
- [98] G. E. Hinton et al., “Improving neural networks by preventing co-adaptation of feature detectors”, 2012. arXiv:1207.0580.

- [99] S. Wunsch, R. Friese, R. Wolf, and G. Quast, “Identifying the relevant dependencies of the neural network response on characteristics of the input space”, *Comput. Softw. Big Sci.* **2** (2018) 5, doi:10.1007/s41781-018-0012-1, arXiv:1803.08782.
- [100] A. Ghorbani and J. Zou, “Data Shapley: Equitable valuation of data for machine learning”, 2019. arXiv:1904.02868.
- [101] J. D. Bjorken and S. J. Brodsky, “Statistical model for electron-positron annihilation into hadrons”, *Phys. Rev. D* **1** (1970) 1416, doi:10.1103/PhysRevD.1.1416.
- [102] G. C. Fox and S. Wolfram, “Event shapes in e^+e^- annihilation”, *Nucl. Phys. B* **157** (1979) 543, doi:10.1016/0550-3213(79)90120-2.
- [103] I. Goodfellow, Y. Bengio, and A. Courville, “Deep Learning”. MIT Press, 2016.
<http://www.deeplearningbook.org>.
- [104] J. K. Lindsey, “Parametric statistical inference”. Clarendon Press, Oxford, England, 1996.
- [105] P. Skands, S. Carrazza, and J. Rojo, “Tuning PYTHIA 8.1: the Monash 2013 Tune”, *Eur. Phys. J. C* **74** (2014) 3024, doi:10.1140/epjc/s10052-014-3024-y, arXiv:1404.5630.
- [106] CMS Collaboration, “Measurement of differential cross sections for the production of top quark pairs and of additional jets in lepton+jets events from pp collisions at $\sqrt{s} = 13 \text{ TeV}$ ”, *Phys. Rev. D* **97** (2018) 112003, doi:10.1103/PhysRevD.97.112003, arXiv:1803.08856.
- [107] I. W. Stewart and F. J. Tackmann, “Theory uncertainties for Higgs and other searches using jet bins”, *Phys. Rev. D* **85** (2012) 034011, doi:10.1103/PhysRevD.85.034011, arXiv:1107.2117.
- [108] ATLAS Collaboration, “Evaluation of QCD uncertainties for Higgs boson production through gluon fusion and in association with two top quarks for simplified template cross-section measurements”, ATLAS PUB Note ATL-PHYS-PUB-2023-031, 2023.
- [109] R. Barlow and C. Beeston, “Fitting using finite Monte Carlo samples”, *Comp. Phys. Commun.* **77** (1993) 219, doi:10.1016/0010-4655(93)90005-W.
- [110] CMS Collaboration, “First measurement of the cross section for top quark pair production with additional charm jets using dileptonic final states in pp collisions at $\sqrt{s} = 13 \text{ TeV}$ ”, *Phys. Lett. B* **820** (2021) 136565, doi:10.1016/j.physletb.2021.136565, arXiv:2012.09225.
- [111] LHC Higgs Cross Section Working Group, “Handbook of LHC Higgs cross sections: 3. Higgs properties”, 2013. arXiv:1307.1347.
- [112] A. V. Gritsan, R. Röntsch, M. Schulze, and M. Xiao, “Constraining anomalous Higgs boson couplings to the heavy flavor fermions using matrix element techniques”, *Phys. Rev. D* **94** (2016) 055023, doi:10.1103/PhysRevD.94.055023, arXiv:1606.03107.
- [113] F. Demartin et al., “Higgs characterisation at NLO in QCD: CP properties of the top-quark Yukawa interaction”, *Eur. Phys. J. C* **74** (2014) 3065, doi:10.1140/epjc/s10052-014-3065-2, arXiv:1407.5089.

A The CMS Collaboration

Yerevan Physics Institute, Yerevan, Armenia

A. Hayrapetyan, A. Tumasyan¹ 

Institut für Hochenergiephysik, Vienna, Austria

W. Adam , J.W. Andrejkovic, T. Bergauer , S. Chatterjee , K. Damanakis , M. Dragicevic , P.S. Hussain , M. Jeitler² , N. Krammer , A. Li , D. Liko , I. Mikulec , J. Schieck² , R. Schöfbeck , D. Schwarz , M. Sonawane , S. Templ , W. Waltenberger , C.-E. Wulz²

Universiteit Antwerpen, Antwerpen, Belgium

M.R. Darwish³ , T. Janssen , P. Van Mechelen 

Vrije Universiteit Brussel, Brussel, Belgium

N. Breugelmans, J. D'Hondt , S. Dansana , A. De Moor , M. Delcourt , F. Heyen, S. Lowette , I. Makarenko , D. Müller , S. Tavernier , M. Tytgat⁴ , G.P. Van Onsem , S. Van Putte , D. Vannerom 

Université Libre de Bruxelles, Bruxelles, Belgium

B. Bilin , B. Clerbaux , A.K. Das, G. De Lentdecker , H. Evard , L. Favart , P. Gianneios , J. Jaramillo , A. Khalilzadeh, F.A. Khan , K. Lee , M. Mahdavikhorrami , A. Malara , S. Paredes , M.A. Shahzad, L. Thomas , M. Vanden Bemden , C. Vander Velde , P. Vanlaer

Ghent University, Ghent, Belgium

M. De Coen , D. Dobur , G. Gokbulut , Y. Hong , J. Knolle , L. Lambrecht , D. Marckx , K. Mota Amarilo , A. Samalan, K. Skovpen , N. Van Den Bossche , J. van der Linden , L. Wezenbeek 

Université Catholique de Louvain, Louvain-la-Neuve, Belgium

A. Benecke , A. Bethani , G. Bruno , C. Caputo , J. De Favereau De Jeneret , C. Delaere , I.S. Donertas , A. Giammanco , A.O. Guzel , Sa. Jain , V. Lemaitre, J. Lidrych , P. Mastrapasqua , T.T. Tran , S. Wertz 

Centro Brasileiro de Pesquisas Fisicas, Rio de Janeiro, Brazil

G.A. Alves , M. Alves Gallo Pereira , E. Coelho , G. Correia Silva , C. Hensel , T. Menezes De Oliveira , A. Moraes , P. Rebello Teles , M. Soeiro, A. Vilela Pereira⁵ 

Universidade do Estado do Rio de Janeiro, Rio de Janeiro, Brazil

W.L. Aldá Júnior , M. Barroso Ferreira Filho , H. Brandao Malbouisson , W. Carvalho , J. Chinellato⁶, E.M. Da Costa , G.G. Da Silveira⁷ , D. De Jesus Damiao , S. Fonseca De Souza , R. Gomes De Souza, M. Macedo , J. Martins⁸ , C. Mora Herrera , L. Mundim , H. Nogima , J.P. Pinheiro , A. Santoro , A. Sznajder , M. Thiel

Universidade Estadual Paulista, Universidade Federal do ABC, São Paulo, Brazil

C.A. Bernardes⁷ , L. Calligaris , T.R. Fernandez Perez Tomei , E.M. Gregores , I. Maietto Silverio , P.G. Mercadante , S.F. Novaes , B. Orzari , Sandra S. Padula 

Institute for Nuclear Research and Nuclear Energy, Bulgarian Academy of Sciences, Sofia, Bulgaria

A. Aleksandrov , G. Antchev , R. Hadjiiska , P. Iaydjiev , M. Misheva , M. Shopova , G. Sultanov 

University of Sofia, Sofia, Bulgaria

A. Dimitrov , L. Litov , B. Pavlov , P. Petkov , A. Petrov , E. Shumka 

Instituto De Alta Investigación, Universidad de Tarapacá, Casilla 7 D, Arica, Chile
S. Keshri , S. Thakur 

Beihang University, Beijing, China

T. Cheng , T. Javaid , L. Yuan 

Department of Physics, Tsinghua University, Beijing, China

Z. Hu , Z. Liang, J. Liu, K. Yi^{9,10} 

Institute of High Energy Physics, Beijing, China

G.M. Chen¹¹ , H.S. Chen¹¹ , M. Chen¹¹ , F. Iemmi , C.H. Jiang, A. Kapoor¹² , H. Liao , Z.-A. Liu¹³ , R. Sharma¹⁴ , J.N. Song¹³, J. Tao , C. Wang¹¹, J. Wang , Z. Wang¹¹, H. Zhang , J. Zhao 

State Key Laboratory of Nuclear Physics and Technology, Peking University, Beijing, China

A. Agapitos , Y. Ban , S. Deng , B. Guo, C. Jiang , A. Levin , C. Li , Q. Li , Y. Mao, S. Qian, S.J. Qian , X. Qin, X. Sun , D. Wang , H. Yang, L. Zhang , Y. Zhao, C. Zhou 

Guangdong Provincial Key Laboratory of Nuclear Science and Guangdong-Hong Kong Joint Laboratory of Quantum Matter, South China Normal University, Guangzhou, China

S. Yang 

Sun Yat-Sen University, Guangzhou, China

Z. You 

University of Science and Technology of China, Hefei, China

K. Jaffel , N. Lu 

Nanjing Normal University, Nanjing, China

G. Bauer¹⁵, B. Li, J. Zhang 

Institute of Modern Physics and Key Laboratory of Nuclear Physics and Ion-beam Application (MOE) - Fudan University, Shanghai, China

X. Gao¹⁶ 

Zhejiang University, Hangzhou, Zhejiang, China

Z. Lin , C. Lu , M. Xiao 

Universidad de Los Andes, Bogota, Colombia

C. Avila , D.A. Barbosa Trujillo, A. Cabrera , C. Florez , J. Fraga , J.A. Reyes Vega

Universidad de Antioquia, Medellin, Colombia

F. Ramirez , C. Rendón , M. Rodriguez , A.A. Ruales Barbosa , J.D. Ruiz Alvarez 

University of Split, Faculty of Electrical Engineering, Mechanical Engineering and Naval Architecture, Split, Croatia

D. Giljanovic , N. Godinovic , D. Lelas , A. Sculac 

University of Split, Faculty of Science, Split, Croatia

M. Kovac , A. Petkovic , T. Sculac 

Institute Rudjer Boskovic, Zagreb, Croatia

P. Bargassa , V. Brigljevic , B.K. Chitroda , D. Ferencek , K. Jakovcic, S. Mishra , A. Starodumov¹⁷ , T. Susa 

University of Cyprus, Nicosia, Cyprus

A. Attikis , K. Christoforou , A. Hadjiagapiou, C. Leonidou , J. Mousa , C. Nicolaou, L. Paizanos, F. Ptochos , P.A. Razis , H. Rykaczewski, H. Saka , A. Stepennov 

Charles University, Prague, Czech Republic

M. Finger , M. Finger Jr. , A. Kveton 

Universidad San Francisco de Quito, Quito, Ecuador

E. Carrera Jarrin 

Academy of Scientific Research and Technology of the Arab Republic of Egypt, Egyptian Network of High Energy Physics, Cairo, Egypt

Y. Assran^{18,19}, B. El-mahdy , S. Elgammal¹⁹

Center for High Energy Physics (CHEP-FU), Fayoum University, El-Fayoum, Egypt

A. Lotfy , M.A. Mahmoud 

National Institute of Chemical Physics and Biophysics, Tallinn, Estonia

K. Ehataht , M. Kadastik, T. Lange , S. Nandan , C. Nielsen , J. Pata , M. Raidal , L. Tani , C. Veelken 

Department of Physics, University of Helsinki, Helsinki, Finland

H. Kirschenmann , K. Osterberg , M. Voutilainen 

Helsinki Institute of Physics, Helsinki, Finland

S. Bharthuar , N. Bin Norjoharuddeen , E. Brückner , F. Garcia , P. Inkaew , K.T.S. Kallonen , T. Lampén , K. Lassila-Perini , S. Lehti , T. Lindén , L. Martikainen , M. Myllymäki , M.m. Rantanen , H. Siikonen , J. Tuominiemi 

Lappeenranta-Lahti University of Technology, Lappeenranta, Finland

P. Luukka , H. Petrow 

IRFU, CEA, Université Paris-Saclay, Gif-sur-Yvette, France

M. Besancon , F. Couderc , M. Dejardin , D. Denegri, J.L. Faure, F. Ferri , S. Ganjour , P. Gras , G. Hamel de Monchenault , M. Kumar , V. Lohezic , J. Malcles , F. Orlandi , L. Portales , A. Rosowsky , M.Ö. Sahin , A. Savoy-Navarro²⁰ , P. Simkina , M. Titov , M. Tornago 

Laboratoire Leprince-Ringuet, CNRS/IN2P3, Ecole Polytechnique, Institut Polytechnique de Paris, Palaiseau, France

F. Beaudette , G. Boldrini , P. Busson , A. Cappati , C. Charlot , M. Chiusi , F. Damas , O. Davignon , A. De Wit , I.T. Ehle , B.A. Fontana Santos Alves , S. Ghosh , A. Gilbert , R. Granier de Cassagnac , A. Hakimi , B. Harikrishnan , L. Kalipoliti , G. Liu , M. Nguyen , C. Ochando , R. Salerno , J.B. Sauvan , Y. Sirois , L. Urda Gómez , E. Vernazza , A. Zabi , A. Zghiche 

Université de Strasbourg, CNRS, IPHC UMR 7178, Strasbourg, France

J.-L. Agram²¹ , J. Andrea , D. Apparu , D. Bloch , J.-M. Brom , E.C. Chabert , C. Collard , S. Falke , U. Goerlach , R. Haeberle , A.-C. Le Bihan , M. Meena , O. Ponctet , G. Saha , M.A. Sessini , P. Van Hove , P. Vaucelle 

Centre de Calcul de l'Institut National de Physique Nucléaire et de Physique des Particules, CNRS/IN2P3, Villeurbanne, France

A. Di Florio 

Institut de Physique des 2 Infinis de Lyon (IP2I), Villeurbanne, France

D. Amram, S. Beauceron , B. Blançon , G. Boudoul , N. Chanon , D. Contardo 

P. Depasse [ID](#), C. Dozen²² [ID](#), H. El Mamouni, J. Fay [ID](#), S. Gascon [ID](#), M. Gouzevitch [ID](#), C. Greenberg [ID](#), G. Grenier [ID](#), B. Ille [ID](#), E. Jourd'huy, I.B. Laktineh, M. Lethuillier [ID](#), L. Mirabito, S. Perries, A. Purohit [ID](#), M. Vander Donckt [ID](#), P. Verdier [ID](#), J. Xiao [ID](#)

Georgian Technical University, Tbilisi, Georgia

I. Lomidze [ID](#), T. Toriashvili²³ [ID](#), Z. Tsamalaidze²⁴ [ID](#)

RWTH Aachen University, I. Physikalisches Institut, Aachen, Germany

V. Botta [ID](#), S. Consuegra Rodriguez [ID](#), L. Feld [ID](#), K. Klein [ID](#), M. Lipinski [ID](#), D. Meuser [ID](#), A. Pauls [ID](#), D. Pérez Adán [ID](#), N. Röwert [ID](#), M. Teroerde [ID](#)

RWTH Aachen University, III. Physikalisches Institut A, Aachen, Germany

S. Diekmann [ID](#), A. Dodonova [ID](#), N. Eich [ID](#), D. Eliseev [ID](#), F. Engelke [ID](#), J. Erdmann [ID](#), M. Erdmann [ID](#), P. Fackeldey [ID](#), B. Fischer [ID](#), T. Hebbeker [ID](#), K. Hoepfner [ID](#), F. Ivone [ID](#), A. Jung [ID](#), M.y. Lee [ID](#), F. Mausolf [ID](#), M. Merschmeyer [ID](#), A. Meyer [ID](#), S. Mukherjee [ID](#), D. Noll [ID](#), F. Nowotny, A. Pozdnyakov [ID](#), Y. Rath, W. Redjeb [ID](#), F. Rehm, H. Reithler [ID](#), V. Sarkisovi [ID](#), A. Schmidt [ID](#), A. Sharma [ID](#), J.L. Spah [ID](#), A. Stein [ID](#), F. Torres Da Silva De Araujo²⁵ [ID](#), S. Wiedenbeck [ID](#), S. Zaleski

RWTH Aachen University, III. Physikalisches Institut B, Aachen, Germany

C. Dziwok [ID](#), G. Flügge [ID](#), T. Kress [ID](#), A. Nowack [ID](#), O. Pooth [ID](#), A. Stahl [ID](#), T. Ziemons [ID](#), A. Zotz [ID](#)

Deutsches Elektronen-Synchrotron, Hamburg, Germany

H. Aarup Petersen [ID](#), M. Aldaya Martin [ID](#), J. Alimena [ID](#), S. Amoroso, Y. An [ID](#), J. Bach [ID](#), S. Baxter [ID](#), M. Bayatmakou [ID](#), H. Becerril Gonzalez [ID](#), O. Behnke [ID](#), A. Belvedere [ID](#), S. Bhattacharya [ID](#), F. Blekman²⁶ [ID](#), K. Borras²⁷ [ID](#), A. Campbell [ID](#), A. Cardini [ID](#), C. Cheng [ID](#), F. Colombina [ID](#), M. De Silva [ID](#), G. Eckerlin, D. Eckstein [ID](#), L.I. Estevez Banos [ID](#), O. Filatov [ID](#), E. Gallo²⁶ [ID](#), A. Geiser [ID](#), A. Giraldi [ID](#), V. Guglielmi [ID](#), M. Guthoff [ID](#), A. Hinzmann [ID](#), L. Jeppe [ID](#), B. Kaech [ID](#), M. Kasemann [ID](#), C. Kleinwort [ID](#), R. Kogler [ID](#), M. Komm [ID](#), D. Krücker [ID](#), W. Lange, D. Leyva Pernia [ID](#), K. Lipka²⁸ [ID](#), W. Lohmann²⁹ [ID](#), F. Lorkowski [ID](#), R. Mankel [ID](#), I.-A. Melzer-Pellmann [ID](#), M. Mendizabal Morentin [ID](#), A.B. Meyer [ID](#), G. Milella [ID](#), K. Moral Figueroa [ID](#), A. Mussgiller [ID](#), L.P. Nair [ID](#), J. Niedziela [ID](#), A. Nürnberg [ID](#), Y. Otarid, J. Park [ID](#), E. Ranken [ID](#), A. Raspereza [ID](#), D. Rastorguev [ID](#), J. Rübenach, L. Rygaard, A. Saggio [ID](#), M. Scham^{30,27} [ID](#), S. Schnake²⁷ [ID](#), P. Schütze [ID](#), C. Schwanenberger²⁶ [ID](#), D. Selivanova [ID](#), K. Sharko [ID](#), M. Shchedrolosiev [ID](#), D. Stafford [ID](#), F. Vazzoler [ID](#), A. Ventura Barroso [ID](#), R. Walsh [ID](#), D. Wang [ID](#), Q. Wang [ID](#), Y. Wen [ID](#), K. Wichmann, L. Wiens²⁷ [ID](#), C. Wissing [ID](#), Y. Yang [ID](#), A. Zimmermann Castro Santos [ID](#)

University of Hamburg, Hamburg, Germany

A. Albrecht [ID](#), S. Albrecht [ID](#), M. Antonello [ID](#), S. Bein [ID](#), L. Benato [ID](#), S. Bollweg, M. Bonanomi [ID](#), P. Connor [ID](#), K. El Morabit [ID](#), Y. Fischer [ID](#), E. Garutti [ID](#), A. Grohsjean [ID](#), J. Haller [ID](#), H.R. Jabusch [ID](#), G. Kasieczka [ID](#), P. Keicher [ID](#), R. Klanner [ID](#), W. Korcari [ID](#), T. Kramer [ID](#), C.c. Kuo, V. Kutzner [ID](#), F. Labe [ID](#), J. Lange [ID](#), A. Lobanov [ID](#), C. Matthies [ID](#), L. Moureaux [ID](#), M. Mrowietz, A. Nigamova [ID](#), Y. Nissan, A. Paasch [ID](#), K.J. Pena Rodriguez [ID](#), T. Quadfasel [ID](#), B. Raciti [ID](#), M. Rieger [ID](#), D. Savoiu [ID](#), J. Schindler [ID](#), P. Schleper [ID](#), M. Schröder [ID](#), J. Schwandt [ID](#), M. Sommerhalder [ID](#), H. Stadie [ID](#), G. Steinbrück [ID](#), A. Tews, M. Wolf [ID](#)

Karlsruher Institut fuer Technologie, Karlsruhe, Germany

S. Brommer [ID](#), M. Burkart, E. Butz [ID](#), T. Chwalek [ID](#), A. Dierlamm [ID](#), A. Droll, N. Faltermann [ID](#), M. Giffels [ID](#), A. Gottmann [ID](#), F. Hartmann³¹ [ID](#), R. Hofsaess [ID](#), M. Horzela [ID](#), U. Husemann [ID](#), J. Kieseler [ID](#), M. Klute [ID](#), R. Koppenhöfer [ID](#), J.M. Lawhorn [ID](#), M. Link,

A. Lintuluoto , B. Maier , S. Maier , S. Mitra , M. Mormile , Th. Müller , M. Neukum, M. Oh , E. Pfeffer , M. Presilla , G. Quast , K. Rabbertz , B. Regnery , N. Shadskiy , I. Shvetsov , H.J. Simonis , L. Sowa, L. Stockmeier, K. Tauqueer, M. Toms , N. Trevisani , R.F. Von Cube , M. Wassmer , S. Wieland , F. Wittig, R. Wolf , X. Zuo

Institute of Nuclear and Particle Physics (INPP), NCSR Demokritos, Aghia Paraskevi, Greece

G. Anagnostou, G. Daskalakis , A. Kyriakis , A. Papadopoulos³¹, A. Stakia 

National and Kapodistrian University of Athens, Athens, Greece

P. Kontaxakis , G. Melachroinos, Z. Painesis , I. Papavergou , I. Paraskevas , N. Saoulidou , K. Theofilatos , E. Tziaferi , K. Vellidis , I. Zisopoulou 

National Technical University of Athens, Athens, Greece

G. Bakas , T. Chatzistavrou, G. Karapostoli , K. Kousouris , I. Papakrivopoulos , E. Siamarkou, G. Tsipolitis , A. Zacharopoulou

University of Ioánnina, Ioánnina, Greece

K. Adamidis, I. Bestintzos, I. Evangelou , C. Foudas, C. Kamtsikis, P. Katsoulis, P. Kokkas , P.G. Kosmoglou Kioseoglou , N. Manthos , I. Papadopoulos , J. Strologas 

HUN-REN Wigner Research Centre for Physics, Budapest, Hungary

C. Hajdu , D. Horvath^{32,33} , K. Márton, A.J. Rádl³⁴ , F. Sikler , V. Veszpremi 

MTA-ELTE Lendület CMS Particle and Nuclear Physics Group, Eötvös Loránd University, Budapest, Hungary

M. Csand , K. Farkas , A. Fehrkuti³⁵ , M.M.A. Gadallah³⁶ , . Kadlecik , P. Major , G. Pasztor , G.I. Veres 

Faculty of Informatics, University of Debrecen, Debrecen, Hungary

B. Ujvari , G. Zilizi 

HUN-REN ATOMKI - Institute of Nuclear Research, Debrecen, Hungary

G. Bencze, S. Czellar, J. Molnar, Z. Szillasi

Karoly Robert Campus, MATE Institute of Technology, Gyongyos, Hungary

F. Nemes³⁵ , T. Novak 

Panjab University, Chandigarh, India

J. Babbar , S. Bansal , S.B. Beri, V. Bhatnagar , G. Chaudhary , S. Chauhan , N. Dhingra³⁷ , A. Kaur , A. Kaur , H. Kaur , M. Kaur , S. Kumar , K. Sandeep , T. Sheokand, J.B. Singh , A. Singla

University of Delhi, Delhi, India

A. Ahmed , A. Bhardwaj , A. Chhetri , B.C. Choudhary , A. Kumar , A. Kumar , M. Naimuddin , K. Ranjan , M.K. Saini, S. Saumya 

Saha Institute of Nuclear Physics, HBNI, Kolkata, India

S. Baradia , S. Barman³⁸ , S. Bhattacharya , S. Das Gupta, S. Dutta , S. Dutta, S. Sarkar

Indian Institute of Technology Madras, Madras, India

M.M. Ameen , P.K. Behera , S.C. Behera , S. Chatterjee , G. Dash , P. Jana , P. Kalbhor , S. Kamble , J.R. Komaragiri³⁹ , D. Kumar³⁹ , P.R. Pujahari , N.R. Saha , A. Sharma , A.K. Sikdar , R.K. Singh , P. Verma , S. Verma , A. Vijay

Tata Institute of Fundamental Research-A, Mumbai, India

S. Dugad, G.B. Mohanty , B. Parida , M. Shelake, P. Suryadevara

Tata Institute of Fundamental Research-B, Mumbai, India

A. Bala , S. Banerjee , R.M. Chatterjee, M. Guchait , Sh. Jain , A. Jaiswal, S. Kumar , G. Majumder , K. Mazumdar , S. Parolia , A. Thachayath 

National Institute of Science Education and Research, An OCC of Homi Bhabha National Institute, Bhubaneswar, Odisha, India

S. Bahinipati⁴⁰ , C. Kar , D. Maity⁴¹ , P. Mal , T. Mishra , V.K. Muraleedharan Nair Bindhu⁴¹ , K. Naskar⁴¹ , A. Nayak⁴¹ , S. Nayak, K. Pal , P. Sadangi, S.K. Swain , S. Varghese⁴¹ , D. Vats⁴¹ 

Indian Institute of Science Education and Research (IISER), Pune, India

S. Acharya⁴² , A. Alpana , S. Dube , B. Gomber⁴² , P. Hazarika , B. Kansal , A. Laha , B. Sahu⁴² , S. Sharma , K.Y. Vaish

Isfahan University of Technology, Isfahan, Iran

H. Bakhshiansohi⁴³ , A. Jafari⁴⁴ , M. Zeinali⁴⁵ 

Institute for Research in Fundamental Sciences (IPM), Tehran, Iran

S. Bashiri, S. Chenarani⁴⁶ , S.M. Etesami , Y. Hosseini , M. Khakzad , E. Khazaie⁴⁷ , M. Mohammadi Najafabadi , S. Tizchang⁴⁸ 

University College Dublin, Dublin, Ireland

M. Felcini , M. Grunewald 

INFN Sezione di Bari^a, Università di Bari^b, Politecnico di Bari^c, Bari, Italy

M. Abbrescia^{a,b} , A. Colaleo^{a,b} , D. Creanza^{a,c} , B. D'Anzi^{a,b} , N. De Filippis^{a,c} , M. De Palma^{a,b} , W. Elmetenawee^{a,b,49} , L. Fiore^a , G. Iaselli^{a,c} , L. Longo^a , M. Louka^{a,b} , G. Maggi^{a,c} , M. Maggi^a , I. Margjeka^a , V. Mastrapasqua^{a,b} , S. My^{a,b} , S. Nuzzo^{a,b} , A. Pellecchia^{a,b} , A. Pompili^{a,b} , G. Pugliese^{a,c} , R. Radogna^{a,b} , D. Ramos^a , A. Ranieri^a , L. Silvestris^a , F.M. Simone^{a,c} , Ü. Sözbilir^a , A. Stamerra^{a,b} , D. Troiano^{a,b} , R. Venditti^{a,b} , P. Verwilligen^a , A. Zaza^{a,b} 

INFN Sezione di Bologna^a, Università di Bologna^b, Bologna, Italy

G. Abbiendi^a , C. Battilana^{a,b} , D. Bonacorsi^{a,b} , P. Capiluppi^{a,b} , A. Castro^{+a,b} , F.R. Cavallo^a , M. Cuffiani^{a,b} , G.M. Dallavalle^a , T. Diotalevi^{a,b} , F. Fabbri^a , A. Fanfani^{a,b} , D. Fasanella^a , P. Giacomelli^a , L. Giommi^{a,b} , C. Grandi^a , L. Guiducci^{a,b} , S. Lo Meo^{a,50} , M. Lorusso^{a,b} , L. Lunerti^a , S. Marcellini^a , G. Masetti^a , F.L. Navarreria^{a,b} , G. Paggi^{a,b} , A. Perrotta^a , F. Primavera^{a,b} , A.M. Rossi^{a,b} , S. Rossi Tisbeni^{a,b} , T. Rovelli^{a,b} , G.P. Siroli^{a,b}

INFN Sezione di Catania^a, Università di Catania^b, Catania, Italy

S. Costa^{a,b,51} , A. Di Mattia^a , A. Lapertosa^a , R. Potenza^{a,b} , A. Tricomi^{a,b,51} , C. Tuve^{a,b} 

INFN Sezione di Firenze^a, Università di Firenze^b, Firenze, Italy

P. Assiouras^a , G. Barbagli^a , G. Bardelli^{a,b} , B. Camaiani^{a,b} , A. Cassese^a , R. Ceccarelli^a , V. Ciulli^{a,b} , C. Civinini^a , R. D'Alessandro^{a,b} , E. Focardi^{a,b} , T. Kello^a , G. Latino^{a,b} , P. Lenzi^{a,b} , M. Lizzo^a , M. Meschini^a , S. Paoletti^a , A. Papanastassiou^{a,b} , G. Sguazzoni^a , L. Viliani^a

INFN Laboratori Nazionali di Frascati, Frascati, Italy

L. Benussi , S. Bianco , S. Meola⁵² , D. Piccolo 

INFN Sezione di Genova^a, Università di Genova^b, Genova, Italy

P. Chatagnon^a , F. Ferro^a , E. Robutti^a , S. Tosi^{a,b} 

INFN Sezione di Milano-Bicocca^a, Università di Milano-Bicocca^b, Milano, Italy

A. Benaglia^a , F. Brivio^a , F. Cetorelli^{a,b} , F. De Guio^{a,b} , M.E. Dinardo^{a,b} , P. Dini^a , S. Gennai^a , R. Gerosa^{a,b} , A. Ghezzi^{a,b} , P. Govoni^{a,b} , L. Guzzi^a , M.T. Lucchini^{a,b} , M. Malberti^a , S. Malvezzi^a , A. Massironi^a , D. Menasce^a , L. Moroni^a , M. Paganoni^{a,b} , S. Palluotto^{a,b} , D. Pedrini^a , A. Perego^{a,b} , B.S. Pinolini^a, G. Pizzati^{a,b} , S. Ragazzi^{a,b} , T. Tabarelli de Fatis^{a,b} 

INFN Sezione di Napoli^a, Università di Napoli 'Federico II'^b, Napoli, Italy; Università della Basilicata^c, Potenza, Italy; Scuola Superiore Meridionale (SSM)^d, Napoli, Italy

S. Buontempo^a , A. Cagnotta^{a,b} , F. Carnevali^{a,b}, N. Cavallo^{a,c} , F. Fabozzi^{a,c} , A.O.M. Iorio^{a,b} , L. Lista^{a,b,53} , P. Paolucci^{a,31} , B. Rossi^a 

INFN Sezione di Padova^a, Università di Padova^b, Padova, Italy; Università di Trento^c, Trento, Italy

R. Ardino^a , P. Azzi^a , N. Bacchetta^{a,54} , P. Bortignon^a , G. Bortolato^{a,b}, A. Bragagnolo^{a,b} , A.C.M. Bulla^a , R. Carlin^{a,b} , T. Dorigo^a , S. Fantinel^a , F. Fanzago^a , F. Gasparini^{a,b} , U. Gasparini^{a,b} , E. Lusiani^a , M. Margoni^{a,b} , A.T. Meneguzzo^{a,b} , M. Migliorini^{a,b} , J. Pazzini^{a,b} , P. Ronchese^{a,b} , R. Rossin^{a,b} , F. Simonetto^{a,b} , M. Tosi^{a,b} , A. Triossi^{a,b} , S. Ventura^a , M. Zanetti^{a,b} , P. Zotto^{a,b} , A. Zucchetta^{a,b} , G. Zumerle^{a,b} 

INFN Sezione di Pavia^a, Università di Pavia^b, Pavia, Italy

C. Aimè^a , A. Braghieri^a , S. Calzaferri^a , D. Fiorina^a , P. Montagna^{a,b} , V. Re^a , C. Riccardi^{a,b} , P. Salvini^a , I. Vai^{a,b} , P. Vitulo^{a,b} 

INFN Sezione di Perugia^a, Università di Perugia^b, Perugia, Italy

S. Ajmal^{a,b} , M.E. Ascoli^{a,b}, G.M. Bilei^a , C. Carrivale^{a,b}, D. Ciangottini^{a,b} , L. Fanò^{a,b} , M. Magherini^{a,b} , V. Mariani^{a,b} , M. Menichelli^a , F. Moscatelli^{a,55} , A. Rossi^{a,b} , A. Santocchia^{a,b} , D. Spiga^a , T. Tedeschi^{a,b} 

INFN Sezione di Pisa^a, Università di Pisa^b, Scuola Normale Superiore di Pisa^c, Pisa, Italy; Università di Siena^d, Siena, Italy

C.A. Alexe^{a,c} , P. Asenov^{a,b} , P. Azzurri^a , G. Bagliesi^a , R. Bhattacharya^a , L. Bianchini^{a,b} , T. Boccali^a , E. Bossini^a , D. Bruschini^{a,c} , R. Castaldi^a , M.A. Ciocci^{a,b} , M. Cipriani^{a,b} , V. D'Amante^{a,d} , R. Dell'Orso^a , S. Donato^a , A. Giassi^a , F. Ligabue^{a,c} , A.C. Marini^a , D. Matos Figueiredo^a , A. Messineo^{a,b} , M. Musich^{a,b} , F. Palla^a , A. Rizzi^{a,b} , G. Rolandi^{a,c} , S. Roy Chowdhury^a , T. Sarkar^a , A. Scribano^a , P. Spagnolo^a , R. Tenchini^a , G. Tonelli^{a,b} , N. Turini^{a,d} , F. Vaselli^{a,c} , A. Venturi^a , P.G. Verdini^a 

INFN Sezione di Roma^a, Sapienza Università di Roma^b, Roma, Italy

C. Baldenegro Barrera^{a,b} , P. Barria^a , C. Basile^{a,b} , M. Campana^{a,b} , F. Cavallari^a , L. Cunqueiro Mendez^{a,b} , D. Del Re^{a,b} , E. Di Marco^{a,b} , M. Diemoz^a , F. Errico^{a,b} , E. Longo^{a,b} , J. Mijuskovic^{a,b} , G. Organtini^{a,b} , F. Pandolfi^a , R. Paramatti^{a,b} , C. Quaranta^{a,b} , S. Rahatlou^{a,b} , C. Rovelli^a , F. Santanastasio^{a,b} , L. Soffi^a 

INFN Sezione di Torino^a, Università di Torino^b, Torino, Italy; Università del Piemonte Orientale^c, Novara, Italy

N. Amapane^{a,b} , R. Arcidiacono^{a,c} , S. Argiro^{a,b} , M. Arneodo^{a,c} , N. Bartosik^a , R. Bellan^{a,b} , A. Bellora^{a,b} , C. Biino^a , C. Borca^{a,b} , N. Cartiglia^a , M. Costa^{a,b} 

R. Covarelli^{a,b} , N. Demaria^a , L. Finco^a , M. Grippo^{a,b} , B. Kiani^{a,b} , F. Legger^a , F. Luongo^{a,b} , C. Mariotti^a , L. Markovic^{a,b} , S. Maselli^a , A. Mecca^{a,b} , L. Menzio^{a,b} , P. Meridiani^a , E. Migliore^{a,b} , M. Monteno^a , R. Mulargia^a , M.M. Obertino^{a,b} , G. Ortona^a , L. Pacher^{a,b} , N. Pastrone^a , M. Pelliccioni^a , M. Ruspa^{a,c} , F. Siviero^{a,b} , V. Sola^{a,b} , A. Solano^{a,b} , A. Staiano^a , C. Tarricone^{a,b} , D. Trocino^a , G. Umoret^{a,b} , R. White^{a,b}

INFN Sezione di Trieste^a, Università di Trieste^b, Trieste, Italy

S. Belforte^a , V. Candeliere^{a,b} , M. Casarsa^a , F. Cossutti^a , K. De Leo^a , G. Della Ricca^{a,b} 

Kyungpook National University, Daegu, Korea

S. Dogra , J. Hong , C. Huh , B. Kim , J. Kim, D. Lee, H. Lee, S.W. Lee , C.S. Moon , Y.D. Oh , M.S. Ryu , S. Sekmen , B. Tae, Y.C. Yang 

Department of Mathematics and Physics - GWNU, Gangneung, Korea

M.S. Kim 

Chonnam National University, Institute for Universe and Elementary Particles, Kwangju, Korea

G. Bak , P. Gwak , H. Kim , D.H. Moon 

Hanyang University, Seoul, Korea

E. Asilar , J. Choi , D. Kim , T.J. Kim , J.A. Merlin, Y. Ryou

Korea University, Seoul, Korea

S. Choi , S. Han, B. Hong , K. Lee, K.S. Lee , S. Lee , J. Yoo 

Kyung Hee University, Department of Physics, Seoul, Korea

J. Goh , S. Yang 

Sejong University, Seoul, Korea

H. S. Kim , Y. Kim, S. Lee

Seoul National University, Seoul, Korea

J. Almond, J.H. Bhyun, J. Choi , J. Choi, W. Jun , J. Kim , S. Ko , H. Kwon , H. Lee , J. Lee , J. Lee , B.H. Oh , S.B. Oh , H. Seo , U.K. Yang, I. Yoon

University of Seoul, Seoul, Korea

W. Jang , D.Y. Kang, Y. Kang , S. Kim , B. Ko, J.S.H. Lee , Y. Lee , I.C. Park , Y. Roh, I.J. Watson 

Yonsei University, Department of Physics, Seoul, Korea

S. Ha , H.D. Yoo 

Sungkyunkwan University, Suwon, Korea

M. Choi , M.R. Kim , H. Lee, Y. Lee , I. Yu 

College of Engineering and Technology, American University of the Middle East (AUM), Dasman, Kuwait

T. Beyrouthy , Y. Gharbia 

Kuwait University - College of Science - Department of Physics, Safat, Kuwait

F. Alazemi 

Riga Technical University, Riga, Latvia

K. Dreimanis , A. Gaile , G. Pikurs, A. Potrebko , M. Seidel , D. Sidiropoulos Kontos 

University of Latvia (LU), Riga, LatviaN.R. Strautnieks **Vilnius University, Vilnius, Lithuania**M. Ambrozas , A. Juodagalvis , A. Rinkevicius , G. Tamulaitis **National Centre for Particle Physics, Universiti Malaya, Kuala Lumpur, Malaysia**I. Yusuff⁵⁶ , Z. Zolkapli**Universidad de Sonora (UNISON), Hermosillo, Mexico**J.F. Benitez , A. Castaneda Hernandez , H.A. Encinas Acosta, L.G. Gallegos Maríñez, M. León Coello , J.A. Murillo Quijada , A. Sehrawat , L. Valencia Palomo **Centro de Investigacion y de Estudios Avanzados del IPN, Mexico City, Mexico**G. Ayala , H. Castilla-Valdez , H. Crotte Ledesma, E. De La Cruz-Burelo , I. Heredia-De La Cruz⁵⁷ , R. Lopez-Fernandez , J. Mejia Guisao , C.A. Mondragon Herrera, A. Sánchez Hernández **Universidad Iberoamericana, Mexico City, Mexico**C. Oropeza Barrera , D.L. Ramirez Guadarrama, M. Ramírez García **Benemerita Universidad Autonoma de Puebla, Puebla, Mexico**I. Bautista , I. Pedraza , H.A. Salazar Ibarguen , C. Uribe Estrada **University of Montenegro, Podgorica, Montenegro**I. Bubanja , N. Raicevic **University of Canterbury, Christchurch, New Zealand**P.H. Butler **National Centre for Physics, Quaid-I-Azam University, Islamabad, Pakistan**A. Ahmad , M.I. Asghar, A. Awais , M.I.M. Awan, H.R. Hoorani , W.A. Khan **AGH University of Krakow, Faculty of Computer Science, Electronics and Telecommunications, Krakow, Poland**L. Grzanka , M. Malawski **National Centre for Nuclear Research, Swierk, Poland**H. Bialkowska , M. Bluj , M. Górski , M. Kazana , M. Szleper , P. Zalewski **Institute of Experimental Physics, Faculty of Physics, University of Warsaw, Warsaw, Poland**K. Bunkowski , K. Doroba , A. Kalinowski , M. Konecki , J. Krolikowski , A. Muhammad **Warsaw University of Technology, Warsaw, Poland**K. Pozniak , W. Zabolotny **Laboratório de Instrumentação e Física Experimental de Partículas, Lisboa, Portugal**M. Araujo , D. Bastos , C. Beirão Da Cruz E Silva , A. Boletti , M. Bozzo , T. Camporesi , G. Da Molin , P. Faccioli , M. Gallinaro , J. Hollar , N. Leonardo , G.B. Marozzo , T. Niknejad , A. Petrilli , M. Pisano , J. Seixas , J. Varela , J.W. Wulff **Faculty of Physics, University of Belgrade, Belgrade, Serbia**P. Adzic , P. Milenovic **VINCA Institute of Nuclear Sciences, University of Belgrade, Belgrade, Serbia**M. Dordevic , J. Milosevic , L. Nadderd , V. Rekovic

Centro de Investigaciones Energéticas Medioambientales y Tecnológicas (CIEMAT), Madrid, Spain

J. Alcaraz Maestre , Cristina F. Bedoya , Oliver M. Carretero , M. Cepeda , M. Cerrada , N. Colino , B. De La Cruz , A. Delgado Peris , A. Escalante Del Valle , D. Fernández Del Val , J.P. Fernández Ramos , J. Flix , M.C. Fouz , O. Gonzalez Lopez , S. Goy Lopez , J.M. Hernandez , M.I. Josa , E. Martin Viscasillas , D. Moran , C. M. Morcillo Perez , Á. Navarro Tobar , C. Perez Dengra , A. Pérez-Calero Yzquierdo , J. Puerta Pelayo , I. Redondo , S. Sánchez Navas , J. Sastre , J. Vazquez Escobar

Universidad Autónoma de Madrid, Madrid, Spain

J.F. de Trocóniz 

Universidad de Oviedo, Instituto Universitario de Ciencias y Tecnologías Espaciales de Asturias (ICTEA), Oviedo, Spain

B. Alvarez Gonzalez , J. Cuevas , J. Fernandez Menendez , S. Folgueras , I. Gonzalez Caballero , J.R. González Fernández , P. Leguina , E. Palencia Cortezon , J. Prado Pico , C. Ramón Álvarez , V. Rodríguez Bouza , A. Soto Rodríguez , A. Trapote , C. Vico Villalba , P. Vischia

Instituto de Física de Cantabria (IFCA), CSIC-Universidad de Cantabria, Santander, Spain

S. Bhowmik , S. Blanco Fernández , J.A. Brochero Cifuentes , I.J. Cabrillo , A. Calderon , J. Duarte Campderros , M. Fernandez , G. Gomez , C. Lasosa García , R. Lopez Ruiz , C. Martinez Rivero , P. Martinez Ruiz del Arbol , F. Matorras , P. Matorras Cuevas , E. Navarrete Ramos , J. Piedra Gomez , L. Scodellaro , I. Vila , J.M. Vizan Garcia

University of Colombo, Colombo, Sri Lanka

B. Kailasapathy⁵⁸ , D.D.C. Wickramarathna 

University of Ruhuna, Department of Physics, Matara, Sri Lanka

W.G.D. Dharmaratna⁵⁹ , K. Liyanage , N. Perera 

CERN, European Organization for Nuclear Research, Geneva, Switzerland

D. Abbaneo , C. Amendola , E. Auffray , G. Auzinger , J. Baechler, D. Barney , A. Bermúdez Martínez , M. Bianco , A.A. Bin Anuar , A. Bocci , L. Borgonovi , C. Botta , E. Brondolin , C. Caillol , G. Cerminara , N. Chernyavskaya , D. d'Enterria , A. Dabrowski , A. David , A. De Roeck , M.M. Defranchis , M. Deile , M. Dobson , G. Franzoni , W. Funk , S. Giani, D. Gigi, K. Gill , F. Glege , J. Hegeman , J.K. Heikkilä , B. Huber , V. Innocente , T. James , P. Janot , O. Kaluzinska , O. Karacheban²⁹ , S. Laurila , P. Lecoq , E. Leutgeb , C. Lourenço , L. Malgeri , M. Mannelli , M. Matthewman, A. Mehta , F. Meijers , S. Mersi , E. Meschi , V. Milosevic , F. Monti , F. Moortgat , M. Mulders , I. Neutelings , S. Orfanelli , F. Pantaleo , G. Petrucciani , A. Pfeiffer , M. Pierini , H. Qu , D. Rabady , B. Ribeiro Lopes , M. Rovere , H. Sakulin , S. Sanchez Cruz , S. Scarfi , C. Schwick, M. Selvaggi , A. Sharma , K. Shchelina , P. Silva , P. Sphicas⁶⁰ , A.G. Stahl Leiton , A. Steen , S. Summers , D. Treille , P. Tropea , D. Walter , J. Wanczyk⁶¹ , J. Wang, S. Wuchterl , P. Zehetner , P. Zejdl , W.D. Zeuner

PSI Center for Neutron and Muon Sciences, Villigen, Switzerland

T. Bevilacqua⁶² , L. Caminada⁶² , A. Ebrahimi , W. Erdmann , R. Horisberger , Q. Ingram , H.C. Kaestli , D. Kotlinski , C. Lange , M. Missiroli⁶² , L. Noehte⁶² , T. Rohe

ETH Zurich - Institute for Particle Physics and Astrophysics (IPA), Zurich, Switzerland
 T.K. Aarrestad , K. Androsov⁶¹ , M. Backhaus , G. Bonomelli , A. Calandri , C. Cazzaniga , K. Datta , P. De Bryas Dexmiers D'archiac⁶¹ , A. De Cosa , G. Dissertori , M. Dittmar, M. Donegà , F. Eble , M. Galli , K. Gedia , F. Glessgen , C. Grab , N. Härringer , T.G. Harte, D. Hits , W. Lustermann , A.-M. Lyon , R.A. Manzoni , M. Marchegiani , L. Marchese , C. Martin Perez , A. Mascellani⁶¹ , F. Nessi-Tedaldi , F. Pauss , V. Perovic , S. Pigazzini , C. Reissel , T. Reitenspiess , B. Ristic , F. Riti , R. Seidita , J. Steggemann⁶¹ , A. Tarabini , D. Valsecchi , R. Wallny

Universität Zürich, Zurich, Switzerland

C. Amsler⁶³ , P. Bärtschi , M.F. Canelli , K. Cormier , M. Huwiler , W. Jin , A. Jofrehei , B. Kilminster , S. Leontsinis , S.P. Liechti , A. Macchiolo , P. Meiring , F. Meng , U. Molinatti , J. Motta , A. Reimers , P. Robmann, K. Schweiger , M. Senger , E. Shokr, F. Stäger , R. Tramontano

National Central University, Chung-Li, Taiwan

C. Adloff⁶⁴, D. Bhowmik, C.M. Kuo, W. Lin, P.K. Rout , P.C. Tiwari³⁹ , S.S. Yu 

National Taiwan University (NTU), Taipei, Taiwan

L. Ceard, K.F. Chen , P.s. Chen, Z.g. Chen, A. De Iorio , W.-S. Hou , T.h. Hsu, Y.w. Kao, S. Karmakar , G. Kole , Y.y. Li , R.-S. Lu , E. Paganis , X.f. Su , J. Thomas-Wilsker , L.s. Tsai, H.y. Wu, E. Yazgan

High Energy Physics Research Unit, Department of Physics, Faculty of Science, Chulalongkorn University, Bangkok, Thailand

C. Asawatangtrakuldee , N. Srimanobhas , V. Wachirapusanand 

Çukurova University, Physics Department, Science and Art Faculty, Adana, Turkey

D. Agyel , F. Boran , F. Dolek , I. Dumanoglu⁶⁵ , E. Eskut , Y. Guler⁶⁶ , E. Gurpinar Guler⁶⁶ , C. Isik , O. Kara, A. Kayis Topaksu , U. Kiminsu , G. Onengut , K. Ozdemir⁶⁷ , A. Polatoz , B. Tali⁶⁸ , U.G. Tok , S. Turkcapar , E. Uslan , I.S. Zorbakir

Middle East Technical University, Physics Department, Ankara, Turkey

G. Sokmen, M. Yalvac⁶⁹ 

Bogazici University, Istanbul, Turkey

B. Akgun , I.O. Atakisi , E. Gülmез , M. Kaya⁷⁰ , O. Kaya⁷¹ , S. Tekten⁷² 

Istanbul Technical University, Istanbul, Turkey

A. Cakir , K. Cankocak^{65,73} , G.G. Dincer⁶⁵ , Y. Komurcu , S. Sen⁷⁴ 

Istanbul University, Istanbul, Turkey

O. Aydilek⁷⁵ , B. Hacisahinoglu , I. Hos⁷⁶ , B. Kaynak , S. Ozkorucuklu , O. Potok , H. Sert , C. Simsek , C. Zorbilmez

Yildiz Technical University, Istanbul, Turkey

S. Cerci⁶⁸ , B. Isildak⁷⁷ , D. Sunar Cerci , T. Yetkin 

Institute for Scintillation Materials of National Academy of Science of Ukraine, Kharkiv, Ukraine

A. Boyaryntsev , B. Grynyov 

National Science Centre, Kharkiv Institute of Physics and Technology, Kharkiv, Ukraine

L. Levchuk 

University of Bristol, Bristol, United Kingdom

D. Anthony [ID](#), J.J. Brooke [ID](#), A. Bundock [ID](#), F. Bury [ID](#), E. Clement [ID](#), D. Cussans [ID](#), H. Flacher [ID](#), M. Glowacki, J. Goldstein [ID](#), H.F. Heath [ID](#), M.-L. Holmberg [ID](#), L. Kreczko [ID](#), S. Paramesvaran [ID](#), L. Robertshaw, S. Seif El Nasr-Storey, V.J. Smith [ID](#), N. Stylianou⁷⁸ [ID](#), K. Walkingshaw Pass

Rutherford Appleton Laboratory, Didcot, United Kingdom

A.H. Ball, K.W. Bell [ID](#), A. Belyaev⁷⁹ [ID](#), C. Brew [ID](#), R.M. Brown [ID](#), D.J.A. Cockerill [ID](#), C. Cooke [ID](#), A. Elliot [ID](#), K.V. Ellis, K. Harder [ID](#), S. Harper [ID](#), J. Linacre [ID](#), K. Manolopoulos, D.M. Newbold [ID](#), E. Olaiya, D. Petyt [ID](#), T. Reis [ID](#), A.R. Sahasransu [ID](#), G. Salvi [ID](#), T. Schuh, C.H. Shepherd-Themistocleous [ID](#), I.R. Tomalin [ID](#), K.C. Whalen [ID](#), T. Williams [ID](#)

Imperial College, London, United Kingdom

I. Andreou [ID](#), R. Bainbridge [ID](#), P. Bloch [ID](#), C.E. Brown [ID](#), O. Buchmuller, V. Cacchio, C.A. Carrillo Montoya [ID](#), G.S. Chahal⁸⁰ [ID](#), D. Colling [ID](#), J.S. Dancu, I. Das [ID](#), P. Dauncey [ID](#), G. Davies [ID](#), J. Davies, M. Della Negra [ID](#), S. Fayer, G. Fedi [ID](#), G. Hall [ID](#), M.H. Hassanshahi [ID](#), A. Howard, G. Iles [ID](#), M. Knight [ID](#), J. Langford [ID](#), J. León Holgado [ID](#), L. Lyons [ID](#), A.-M. Magnan [ID](#), S. Mallios, M. Mieskolainen [ID](#), J. Nash⁸¹ [ID](#), M. Pesaresi [ID](#), P.B. Pradeep, B.C. Radburn-Smith [ID](#), A. Richards, A. Rose [ID](#), K. Savva [ID](#), C. Seez [ID](#), R. Shukla [ID](#), A. Tapper [ID](#), K. Uchida [ID](#), G.P. Uttley [ID](#), L.H. Vage, T. Virdee³¹ [ID](#), M. Vojinovic [ID](#), N. Wardle [ID](#), D. Winterbottom [ID](#)

Brunel University, Uxbridge, United Kingdom

K. Coldham, J.E. Cole [ID](#), A. Khan, P. Kyberd [ID](#), I.D. Reid [ID](#)

Baylor University, Waco, Texas, USA

S. Abdullin [ID](#), A. Brinkerhoff [ID](#), E. Collins [ID](#), J. Dittmann [ID](#), K. Hatakeyama [ID](#), J. Hiltbrand [ID](#), B. McMaster [ID](#), J. Samudio [ID](#), S. Sawant [ID](#), C. Sutantawibul [ID](#), J. Wilson [ID](#)

Catholic University of America, Washington, DC, USA

R. Bartek [ID](#), A. Dominguez [ID](#), C. Huerta Escamilla, A.E. Simsek [ID](#), R. Uniyal [ID](#), A.M. Vargas Hernandez [ID](#)

The University of Alabama, Tuscaloosa, Alabama, USA

B. Bam [ID](#), A. Buchot Perraguin [ID](#), R. Chudasama [ID](#), S.I. Cooper [ID](#), C. Crovella [ID](#), S.V. Gleyzer [ID](#), E. Pearson, C.U. Perez [ID](#), P. Rumerio⁸² [ID](#), E. Usai [ID](#), R. Yi [ID](#)

Boston University, Boston, Massachusetts, USA

A. Akpinar [ID](#), C. Cosby [ID](#), G. De Castro, Z. Demiragli [ID](#), C. Erice [ID](#), C. Fangmeier [ID](#), C. Fernandez Madrazo [ID](#), E. Fontanesi [ID](#), D. Gastler [ID](#), F. Golf [ID](#), S. Jeon [ID](#), J. O'cain, I. Reed [ID](#), J. Rohlf [ID](#), K. Salyer [ID](#), D. Sperka [ID](#), D. Spitzbart [ID](#), I. Suarez [ID](#), A. Tsatsos [ID](#), A.G. Zecchinelli [ID](#)

Brown University, Providence, Rhode Island, USA

G. Benelli [ID](#), D. Cutts [ID](#), L. Gouskos [ID](#), M. Hadley [ID](#), U. Heintz [ID](#), J.M. Hogan⁸³ [ID](#), T. Kwon [ID](#), G. Landsberg [ID](#), K.T. Lau [ID](#), D. Li [ID](#), J. Luo [ID](#), S. Mondal [ID](#), M. Narain⁺ [ID](#), N. Pervan [ID](#), T. Russell, S. Sagir⁸⁴ [ID](#), F. Simpson [ID](#), M. Stamenkovic [ID](#), N. Venkatasubramanian, X. Yan [ID](#)

University of California, Davis, Davis, California, USA

S. Abbott [ID](#), C. Brainerd [ID](#), R. Breedon [ID](#), H. Cai [ID](#), M. Calderon De La Barca Sanchez [ID](#), M. Chertok [ID](#), M. Citron [ID](#), J. Conway [ID](#), P.T. Cox [ID](#), R. Erbacher [ID](#), F. Jensen [ID](#), O. Kukral [ID](#), G. Mocellin [ID](#), M. Mulhearn [ID](#), S. Ostrom [ID](#), W. Wei [ID](#), Y. Yao [ID](#), S. Yoo [ID](#), F. Zhang [ID](#)

University of California, Los Angeles, California, USA

M. Bachtis [id](#), R. Cousins [id](#), A. Datta [id](#), G. Flores Avila [id](#), J. Hauser [id](#), M. Ignatenko [id](#),
M.A. Iqbal [id](#), T. Lam [id](#), E. Manca [id](#), A. Nunez Del Prado, D. Saltzberg [id](#), V. Valuev [id](#)

University of California, Riverside, Riverside, California, USA

R. Clare [id](#), J.W. Gary [id](#), M. Gordon, G. Hanson [id](#), W. Si [id](#)

University of California, San Diego, La Jolla, California, USA

A. Aportela, A. Arora [id](#), J.G. Branson [id](#), S. Cittolin [id](#), S. Cooperstein [id](#), D. Diaz [id](#),
J. Duarte [id](#), L. Giannini [id](#), Y. Gu, J. Guiang [id](#), R. Kansal [id](#), V. Krutelyov [id](#), R. Lee [id](#),
J. Letts [id](#), M. Masciovecchio [id](#), F. Mokhtar [id](#), S. Mukherjee [id](#), M. Pieri [id](#), M. Quinnan [id](#),
B.V. Sathia Narayanan [id](#), V. Sharma [id](#), M. Tadel [id](#), E. Vourliotis [id](#), F. Würthwein [id](#),
Y. Xiang [id](#), A. Yagil [id](#)

University of California, Santa Barbara - Department of Physics, Santa Barbara, California, USA

A. Barzdukas [id](#), L. Brennan [id](#), C. Campagnari [id](#), K. Downham [id](#), C. Grieco [id](#), J. Incandela [id](#),
J. Kim [id](#), A.J. Li [id](#), P. Masterson [id](#), H. Mei [id](#), J. Richman [id](#), S.N. Santpur [id](#), U. Sarica [id](#),
R. Schmitz [id](#), F. Setti [id](#), J. Sheplock [id](#), D. Stuart [id](#), T.Á. Vámi [id](#), S. Wang [id](#), D. Zhang

California Institute of Technology, Pasadena, California, USA

A. Bornheim [id](#), O. Cerri, A. Latorre, J. Mao [id](#), H.B. Newman [id](#), G. Reales Gutiérrez,
M. Spiropulu [id](#), J.R. Vlimant [id](#), C. Wang [id](#), S. Xie [id](#), R.Y. Zhu [id](#)

Carnegie Mellon University, Pittsburgh, Pennsylvania, USA

J. Alison [id](#), S. An [id](#), P. Bryant [id](#), M. Cremonesi, V. Dutta [id](#), T. Ferguson [id](#), T.A. Gómez Espinosa [id](#),
A. Harilal [id](#), A. Kallil Tharayil, C. Liu [id](#), T. Mudholkar [id](#), S. Murthy [id](#), P. Palit [id](#),
K. Park, M. Paulini [id](#), A. Roberts [id](#), A. Sanchez [id](#), W. Terrill [id](#)

University of Colorado Boulder, Boulder, Colorado, USA

J.P. Cumalat [id](#), W.T. Ford [id](#), A. Hart [id](#), A. Hassani [id](#), G. Karathanasis [id](#), N. Manganelli [id](#),
A. Perloff [id](#), C. Savard [id](#), N. Schonbeck [id](#), K. Stenson [id](#), K.A. Ulmer [id](#), S.R. Wagner [id](#),
N. Zipper [id](#), D. Zuolo [id](#)

Cornell University, Ithaca, New York, USA

J. Alexander [id](#), S. Bright-Thonney [id](#), X. Chen [id](#), D.J. Cranshaw [id](#), J. Fan [id](#), X. Fan [id](#),
S. Hogan [id](#), P. Kotamnives, J. Monroy [id](#), M. Oshiro [id](#), J.R. Patterson [id](#), M. Reid [id](#), A. Ryd [id](#),
J. Thom [id](#), P. Wittich [id](#), R. Zou [id](#)

Fermi National Accelerator Laboratory, Batavia, Illinois, USA

M. Albrow [id](#), M. Alyari [id](#), O. Amram [id](#), G. Apollinari [id](#), A. Apresyan [id](#), L.A.T. Bauerick [id](#),
D. Berry [id](#), J. Berryhill [id](#), P.C. Bhat [id](#), K. Burkett [id](#), J.N. Butler [id](#), A. Canepa [id](#), G.B. Cerati [id](#),
H.W.K. Cheung [id](#), F. Chlebana [id](#), G. Cummings [id](#), J. Dickinson [id](#), I. Dutta [id](#), V.D. Elvira [id](#),
Y. Feng [id](#), J. Freeman [id](#), A. Gandrakota [id](#), Z. Gecse [id](#), L. Gray [id](#), D. Green, A. Grummer [id](#),
S. Grünendahl [id](#), D. Guerrero [id](#), O. Gutsche [id](#), R.M. Harris [id](#), R. Heller [id](#), T.C. Herwig [id](#),
J. Hirschauer [id](#), B. Jayatilaka [id](#), S. Jindariani [id](#), M. Johnson [id](#), U. Joshi [id](#), T. Klijnsma [id](#),
B. Klima [id](#), K.H.M. Kwok [id](#), S. Lammel [id](#), D. Lincoln [id](#), R. Lipton [id](#), T. Liu [id](#), C. Madrid [id](#),
K. Maeshima [id](#), C. Mantilla [id](#), D. Mason [id](#), P. McBride [id](#), P. Merkel [id](#), S. Mrenna [id](#),
S. Nahn [id](#), J. Ngadiuba [id](#), D. Noonan [id](#), S. Norberg, V. Papadimitriou [id](#), N. Pastika [id](#),
K. Pedro [id](#), C. Pena⁸⁵ [id](#), F. Ravera [id](#), A. Reinsvold Hall⁸⁶ [id](#), L. Ristori [id](#), M. Safdari [id](#),
E. Sexton-Kennedy [id](#), N. Smith [id](#), A. Soha [id](#), L. Spiegel [id](#), S. Stoynev [id](#), J. Strait [id](#),
L. Taylor [id](#), S. Tkaczyk [id](#), N.V. Tran [id](#), L. Uplegger [id](#), E.W. Vaandering [id](#), I. Zoi [id](#)

University of Florida, Gainesville, Florida, USA

C. Aruta [ID](#), P. Avery [ID](#), D. Bourilkov [ID](#), P. Chang [ID](#), V. Cherepanov [ID](#), R.D. Field, E. Koenig [ID](#), M. Kolosova [ID](#), J. Konigsberg [ID](#), A. Korytov [ID](#), K. Matchev [ID](#), N. Menendez [ID](#), G. Mitselmakher [ID](#), K. Mohrman [ID](#), A. Muthirakalayil Madhu [ID](#), N. Rawal [ID](#), S. Rosenzweig [ID](#), Y. Takahashi [ID](#), J. Wang [ID](#)

Florida State University, Tallahassee, Florida, USA

T. Adams [ID](#), A. Al Kadhim [ID](#), A. Askew [ID](#), S. Bower [ID](#), R. Habibullah [ID](#), V. Hagopian [ID](#), R. Hashmi [ID](#), R.S. Kim [ID](#), S. Kim [ID](#), T. Kolberg [ID](#), G. Martinez, H. Prosper [ID](#), P.R. Prova, M. Wulansatiti [ID](#), R. Yohay [ID](#), J. Zhang

Florida Institute of Technology, Melbourne, Florida, USA

B. Alsufyani [ID](#), M.M. Baarmand [ID](#), S. Butalla [ID](#), S. Das [ID](#), T. Elkafrawy⁸⁷ [ID](#), M. Hohlmann [ID](#), M. Rahmani, E. Yanes

University of Illinois Chicago, Chicago, Illinois, USA

M.R. Adams [ID](#), A. Baty [ID](#), C. Bennett, R. Cavanaugh [ID](#), R. Escobar Franco [ID](#), O. Evdokimov [ID](#), C.E. Gerber [ID](#), M. Hawksworth, A. Hingrajiya, D.J. Hofman [ID](#), J.h. Lee [ID](#), D. S. Lemos [ID](#), A.H. Merrit [ID](#), C. Mills [ID](#), S. Nanda [ID](#), G. Oh [ID](#), B. Ozek [ID](#), D. Pilipovic [ID](#), R. Pradhan [ID](#), E. Prifti, T. Roy [ID](#), S. Rudrabhatla [ID](#), M.B. Tonjes [ID](#), N. Varelas [ID](#), M.A. Wadud [ID](#), Z. Ye [ID](#), J. Yoo [ID](#)

The University of Iowa, Iowa City, Iowa, USA

M. Alhusseini [ID](#), D. Blend, K. Dilsiz⁸⁸ [ID](#), L. Emediato [ID](#), G. Karaman [ID](#), O.K. Köseyan [ID](#), J.-P. Merlo, A. Mestvirishvili⁸⁹ [ID](#), O. Neogi, H. Ogul⁹⁰ [ID](#), Y. Onel [ID](#), A. Penzo [ID](#), C. Snyder, E. Tiras⁹¹ [ID](#)

Johns Hopkins University, Baltimore, Maryland, USA

B. Blumenfeld [ID](#), L. Corcodilos [ID](#), J. Davis [ID](#), A.V. Gritsan [ID](#), L. Kang [ID](#), S. Kyriacou [ID](#), P. Maksimovic [ID](#), M. Roguljic [ID](#), J. Roskes [ID](#), S. Sekhar [ID](#), M. Swartz [ID](#)

The University of Kansas, Lawrence, Kansas, USA

A. Abreu [ID](#), L.F. Alcerro Alcerro [ID](#), J. Anguiano [ID](#), S. Arteaga Escatel [ID](#), P. Baringer [ID](#), A. Bean [ID](#), Z. Flowers [ID](#), D. Grove [ID](#), J. King [ID](#), G. Krintiras [ID](#), M. Lazarovits [ID](#), C. Le Mahieu [ID](#), J. Marquez [ID](#), M. Murray [ID](#), M. Nickel [ID](#), M. Pitt [ID](#), S. Popescu⁹² [ID](#), C. Rogan [ID](#), C. Royon [ID](#), R. Salvatico [ID](#), S. Sanders [ID](#), C. Smith [ID](#), G. Wilson [ID](#)

Kansas State University, Manhattan, Kansas, USA

B. Allmond [ID](#), R. Guju Gurunadha [ID](#), A. Ivanov [ID](#), K. Kaadze [ID](#), Y. Maravin [ID](#), J. Natoli [ID](#), D. Roy [ID](#), G. Sorrentino [ID](#)

University of Maryland, College Park, Maryland, USA

A. Baden [ID](#), A. Belloni [ID](#), J. Bistany-riebman, Y.M. Chen [ID](#), S.C. Eno [ID](#), N.J. Hadley [ID](#), S. Jabeen [ID](#), R.G. Kellogg [ID](#), T. Koeth [ID](#), B. Kronheim, Y. Lai [ID](#), S. Lascio [ID](#), A.C. Mignerey [ID](#), S. Nabili [ID](#), C. Palmer [ID](#), C. Papageorgakis [ID](#), M.M. Paranjpe, L. Wang [ID](#)

Massachusetts Institute of Technology, Cambridge, Massachusetts, USA

J. Bendavid [ID](#), I.A. Cali [ID](#), P.c. Chou [ID](#), M. D'Alfonso [ID](#), J. Eysermans [ID](#), C. Freer [ID](#), G. Gomez-Ceballos [ID](#), M. Goncharov, G. Grossi, P. Harris, D. Hoang, D. Kovalevskyi [ID](#), J. Krupa [ID](#), L. Lavezzo [ID](#), Y.-J. Lee [ID](#), K. Long [ID](#), C. Mcginn [ID](#), A. Novak [ID](#), C. Paus [ID](#), C. Roland [ID](#), G. Roland [ID](#), S. Rothman [ID](#), G.S.F. Stephans [ID](#), Z. Wang [ID](#), B. Wyslouch [ID](#), T. J. Yang [ID](#)

University of Minnesota, Minneapolis, Minnesota, USA

B. Crossman [ID](#), B.M. Joshi [ID](#), C. Kapsiak [ID](#), M. Krohn [ID](#), D. Mahon [ID](#), J. Mans [ID](#),

B. Marzocchi [ID](#), M. Revering [ID](#), R. Rusack [ID](#), R. Saradhy [ID](#), N. Strobbe [ID](#)

University of Nebraska-Lincoln, Lincoln, Nebraska, USA

K. Bloom [ID](#), D.R. Claes [ID](#), G. Haza [ID](#), J. Hossain [ID](#), C. Joo [ID](#), I. Kravchenko [ID](#), J.E. Siado [ID](#), W. Tabb [ID](#), A. Vagnerini [ID](#), A. Wightman [ID](#), F. Yan [ID](#), D. Yu [ID](#)

State University of New York at Buffalo, Buffalo, New York, USA

H. Bandyopadhyay [ID](#), L. Hay [ID](#), H.w. Hsia [ID](#), I. Iashvili [ID](#), A. Kalogeropoulos [ID](#), A. Kharchilava [ID](#), M. Morris [ID](#), D. Nguyen [ID](#), S. Rappoccio [ID](#), H. Rejeb Sfar, A. Williams [ID](#), P. Young [ID](#)

Northeastern University, Boston, Massachusetts, USA

G. Alverson [ID](#), E. Barberis [ID](#), J. Bonilla [ID](#), J. Dervan [ID](#), Y. Haddad [ID](#), Y. Han [ID](#), A. Krishna [ID](#), J. Li [ID](#), M. Lu [ID](#), G. Madigan [ID](#), R. McCarthy [ID](#), D.M. Morse [ID](#), V. Nguyen [ID](#), T. Orimoto [ID](#), A. Parker [ID](#), L. Skinnari [ID](#), D. Wood [ID](#)

Northwestern University, Evanston, Illinois, USA

J. Bueghly, S. Dittmer [ID](#), K.A. Hahn [ID](#), Y. Liu [ID](#), Y. Miao [ID](#), D.G. Monk [ID](#), M.H. Schmitt [ID](#), A. Taliercio [ID](#), M. Velasco

University of Notre Dame, Notre Dame, Indiana, USA

G. Agarwal [ID](#), R. Band [ID](#), R. Bucci, S. Castells [ID](#), A. Das [ID](#), R. Goldouzian [ID](#), M. Hildreth [ID](#), K.W. Ho [ID](#), K. Hurtado Anampa [ID](#), T. Ivanov [ID](#), C. Jessop [ID](#), K. Lannon [ID](#), J. Lawrence [ID](#), N. Loukas [ID](#), L. Lutton [ID](#), J. Mariano, N. Marinelli, I. Mcalister, T. McCauley [ID](#), C. Mcgrady [ID](#), C. Moore [ID](#), Y. Musienko²⁴ [ID](#), H. Nelson [ID](#), M. Osherson [ID](#), A. Piccinelli [ID](#), R. Ruchti [ID](#), A. Townsend [ID](#), Y. Wan, M. Wayne [ID](#), H. Yockey, M. Zarucki [ID](#), L. Zygalas [ID](#)

The Ohio State University, Columbus, Ohio, USA

A. Basnet [ID](#), B. Bylsma, M. Carrigan [ID](#), L.S. Durkin [ID](#), C. Hill [ID](#), M. Joyce [ID](#), M. Nunez Ornelas [ID](#), K. Wei, B.L. Winer [ID](#), B. R. Yates [ID](#)

Princeton University, Princeton, New Jersey, USA

H. Bouchamaoui [ID](#), P. Das [ID](#), G. Dezoort [ID](#), P. Elmer [ID](#), A. Frankenthal [ID](#), B. Greenberg [ID](#), N. Haubrich [ID](#), K. Kennedy, G. Kopp [ID](#), S. Kwan [ID](#), D. Lange [ID](#), A. Loeliger [ID](#), D. Marlow [ID](#), I. Ojalvo [ID](#), J. Olsen [ID](#), A. Shevelev [ID](#), D. Stickland [ID](#), C. Tully [ID](#)

University of Puerto Rico, Mayaguez, Puerto Rico, USA

S. Malik [ID](#)

Purdue University, West Lafayette, Indiana, USA

A.S. Bakshi [ID](#), S. Chandra [ID](#), R. Chawla [ID](#), A. Gu [ID](#), L. Gutay, M. Jones [ID](#), A.W. Jung [ID](#), A.M. Koshy, M. Liu [ID](#), G. Negro [ID](#), N. Neumeister [ID](#), G. Paspalaki [ID](#), S. Piperov [ID](#), V. Scheurer, J.F. Schulte [ID](#), M. Stojanovic [ID](#), J. Thieman [ID](#), A. K. Virdi [ID](#), F. Wang [ID](#), W. Xie [ID](#)

Purdue University Northwest, Hammond, Indiana, USA

J. Dolen [ID](#), N. Parashar [ID](#), A. Pathak [ID](#)

Rice University, Houston, Texas, USA

D. Acosta [ID](#), T. Carnahan [ID](#), K.M. Ecklund [ID](#), P.J. Fernández Manteca [ID](#), S. Freed, P. Gardner, F.J.M. Geurts [ID](#), W. Li [ID](#), J. Lin [ID](#), O. Miguel Colin [ID](#), B.P. Padley [ID](#), R. Redjimi, J. Rotter [ID](#), E. Yigitbasi [ID](#), Y. Zhang [ID](#)

University of Rochester, Rochester, New York, USA

A. Bodek [ID](#), P. de Barbaro [ID](#), R. Demina [ID](#), J.L. Dulemba [ID](#), A. Garcia-Bellido [ID](#), O. Hindrichs [ID](#), A. Khukhunaishvili [ID](#), N. Parmar [ID](#), P. Parygin⁹³ [ID](#), E. Popova⁹³ [ID](#), R. Taus [ID](#)

Rutgers, The State University of New Jersey, Piscataway, New Jersey, USA

B. Chiarito, J.P. Chou , S.V. Clark , D. Gadkari , Y. Gershtein , E. Halkiadakis , M. Heindl , C. Houghton , D. Jaroslawski , S. Konstantinou , I. Laflotte , A. Lath , R. Montalvo, K. Nash, J. Reichert , H. Routray , P. Saha , S. Salur , S. Schnetzer, S. Somalwar , R. Stone , S.A. Thayil , S. Thomas, J. Vora , H. Wang 

University of Tennessee, Knoxville, Tennessee, USA

D. Ally , A.G. Delannoy , S. Fiorendi , S. Higginbotham , T. Holmes , A.R. Kanuganti , N. Karunarathna , L. Lee , E. Nibigira , S. Spanier 

Texas A&M University, College Station, Texas, USA

D. Aebi , M. Ahmad , T. Akhter , O. Bouhali⁹⁴ , R. Eusebi , J. Gilmore , T. Huang , T. Kamon⁹⁵ , H. Kim , S. Luo , R. Mueller , D. Overton , D. Rathjens , A. Safonov

Texas Tech University, Lubbock, Texas, USA

N. Akchurin , J. Damgov , N. Gogate , V. Hegde , A. Hussain , Y. Kazhykarim, K. Lamichhane , S.W. Lee , A. Mankel , T. Peltola , I. Volobouev 

Vanderbilt University, Nashville, Tennessee, USA

E. Appelt , Y. Chen , S. Greene, A. Gurrola , W. Johns , R. Kunawalkam Elayavalli , A. Melo , F. Romeo , P. Sheldon , S. Tuo , J. Velkovska , J. Viinikainen 

University of Virginia, Charlottesville, Virginia, USA

B. Cardwell , B. Cox , J. Hakala , R. Hirosky , A. Ledovskoy , C. Neu 

Wayne State University, Detroit, Michigan, USA

S. Bhattacharya , P.E. Karchin 

University of Wisconsin - Madison, Madison, Wisconsin, USA

A. Aravind , S. Banerjee , K. Black , T. Bose , S. Dasu , I. De Bruyn , P. Everaerts , C. Galloni, H. He , M. Herndon , A. Herve , C.K. Koraka , A. Lanaro, R. Loveless , J. Madhusudanan Sreekala , A. Mallampalli , A. Mohammadi , S. Mondal, G. Parida , L. Pétré , D. Pinna, A. Savin, V. Shang , V. Sharma , W.H. Smith , D. Teague, H.F. Tsoi , W. Vetens , A. Warden

Authors affiliated with an international laboratory covered by a cooperation agreement with CERN

S. Afanasiev , V. Alexakhin , D. Budkouski , I. Golutvin[†] , I. Gorbunov , V. Karjavine , V. Korenkov , A. Lanev , A. Malakhov , V. Matveev⁹⁶ , V. Palichik , V. Perelygin , M. Savina , V. Shalaev , S. Shmatov , S. Shulha , V. Smirnov , O. Teryaev , N. Voytishin , B.S. Yuldashev⁹⁷ , A. Zarubin , I. Zhizhin , Yu. Andreev , A. Dermenev , S. Gninenko , N. Golubev , A. Karneyeu , D. Kirpichnikov , M. Kirsanov , N. Krasnikov , I. Tlisova , A. Toropin

Authors affiliated with an institute formerly covered by a cooperation agreement with CERN

G. Gavrilov , V. Golovtcov , Y. Ivanov , V. Kim⁹⁸ , P. Levchenko⁹⁹ , V. Murzin , V. Oreshkin , D. Sosnov , V. Sulimov , L. Uvarov , A. Vorobyev[†], T. Aushev , V. Gavrilov , N. Lychkovskaya , A. Nikitenko^{100,101} , V. Popov , A. Zhokin , M. Chadeeva⁹⁸ , R. Chistov⁹⁸ , S. Polikarpov⁹⁸ , V. Andreev , M. Azarkin , M. Kirakosyan, A. Terkulov , E. Boos , V. Bunichev , M. Dubinin⁸⁵ , L. Dudko , V. Klyukhin , O. Kodolova¹⁰¹ , S. Obraztsov , M. Perfilov , S. Petrushanko , V. Savrin , P. Volkov , G. Vorotnikov , V. Blinov⁹⁸, T. Dimova⁹⁸ , A. Kozyrev⁹⁸ , O. Radchenko⁹⁸ , Y. Skovpen⁹⁸ , V. Kachanov , D. Konstantinov , S. Slabospitskii , A. Uzunian , A. Babaev , V. Borshch , D. Druzhkin¹⁰² , V. Chekhovsky, V. Makarenko

†: Deceased

¹Also at Yerevan State University, Yerevan, Armenia

²Also at TU Wien, Vienna, Austria

³Also at Institute of Basic and Applied Sciences, Faculty of Engineering, Arab Academy for Science, Technology and Maritime Transport, Alexandria, Egypt

⁴Also at Ghent University, Ghent, Belgium

⁵Also at Universidade do Estado do Rio de Janeiro, Rio de Janeiro, Brazil

⁶Also at Universidade Estadual de Campinas, Campinas, Brazil

⁷Also at Federal University of Rio Grande do Sul, Porto Alegre, Brazil

⁸Also at UFMS, Nova Andradina, Brazil

⁹Also at Nanjing Normal University, Nanjing, China

¹⁰Now at The University of Iowa, Iowa City, Iowa, USA

¹¹Also at University of Chinese Academy of Sciences, Beijing, China

¹²Also at China Center of Advanced Science and Technology, Beijing, China

¹³Also at University of Chinese Academy of Sciences, Beijing, China

¹⁴Also at China Spallation Neutron Source, Guangdong, China

¹⁵Now at Henan Normal University, Xinxiang, China

¹⁶Also at Université Libre de Bruxelles, Bruxelles, Belgium

¹⁷Also at an institute formerly covered by a cooperation agreement with CERN

¹⁸Also at Suez University, Suez, Egypt

¹⁹Now at British University in Egypt, Cairo, Egypt

²⁰Also at Purdue University, West Lafayette, Indiana, USA

²¹Also at Université de Haute Alsace, Mulhouse, France

²²Also at İstinye University, Istanbul, Turkey

²³Also at Tbilisi State University, Tbilisi, Georgia

²⁴Also at an international laboratory covered by a cooperation agreement with CERN

²⁵Also at The University of the State of Amazonas, Manaus, Brazil

²⁶Also at University of Hamburg, Hamburg, Germany

²⁷Also at RWTH Aachen University, III. Physikalisches Institut A, Aachen, Germany

²⁸Also at Bergische University Wuppertal (BUW), Wuppertal, Germany

²⁹Also at Brandenburg University of Technology, Cottbus, Germany

³⁰Also at Forschungszentrum Jülich, Juelich, Germany

³¹Also at CERN, European Organization for Nuclear Research, Geneva, Switzerland

³²Also at HUN-REN ATOMKI - Institute of Nuclear Research, Debrecen, Hungary

³³Now at Universitatea Babes-Bolyai - Facultatea de Fizica, Cluj-Napoca, Romania

³⁴Also at MTA-ELTE Lendület CMS Particle and Nuclear Physics Group, Eötvös Loránd University, Budapest, Hungary

³⁵Also at HUN-REN Wigner Research Centre for Physics, Budapest, Hungary

³⁶Also at Physics Department, Faculty of Science, Assiut University, Assiut, Egypt

³⁷Also at Punjab Agricultural University, Ludhiana, India

³⁸Also at University of Visva-Bharati, Santiniketan, India

³⁹Also at Indian Institute of Science (IISc), Bangalore, India

⁴⁰Also at IIT Bhubaneswar, Bhubaneswar, India

⁴¹Also at Institute of Physics, Bhubaneswar, India

⁴²Also at University of Hyderabad, Hyderabad, India

⁴³Also at Deutsches Elektronen-Synchrotron, Hamburg, Germany

⁴⁴Also at Isfahan University of Technology, Isfahan, Iran

⁴⁵Also at Sharif University of Technology, Tehran, Iran

⁴⁶Also at Department of Physics, University of Science and Technology of Mazandaran,

Behshahr, Iran

⁴⁷Also at Department of Physics, Isfahan University of Technology, Isfahan, Iran

⁴⁸Also at Department of Physics, Faculty of Science, Arak University, ARAK, Iran

⁴⁹Also at Helwan University, Cairo, Egypt

⁵⁰Also at Italian National Agency for New Technologies, Energy and Sustainable Economic Development, Bologna, Italy

⁵¹Also at Centro Siciliano di Fisica Nucleare e di Struttura Della Materia, Catania, Italy

⁵²Also at Università degli Studi Guglielmo Marconi, Roma, Italy

⁵³Also at Scuola Superiore Meridionale, Università di Napoli 'Federico II', Napoli, Italy

⁵⁴Also at Fermi National Accelerator Laboratory, Batavia, Illinois, USA

⁵⁵Also at Consiglio Nazionale delle Ricerche - Istituto Officina dei Materiali, Perugia, Italy

⁵⁶Also at Department of Applied Physics, Faculty of Science and Technology, Universiti Kebangsaan Malaysia, Bangi, Malaysia

⁵⁷Also at Consejo Nacional de Ciencia y Tecnología, Mexico City, Mexico

⁵⁸Also at Trincomalee Campus, Eastern University, Sri Lanka, Nilaveli, Sri Lanka

⁵⁹Also at Saegis Campus, Nugegoda, Sri Lanka

⁶⁰Also at National and Kapodistrian University of Athens, Athens, Greece

⁶¹Also at Ecole Polytechnique Fédérale Lausanne, Lausanne, Switzerland

⁶²Also at Universität Zürich, Zurich, Switzerland

⁶³Also at Stefan Meyer Institute for Subatomic Physics, Vienna, Austria

⁶⁴Also at Laboratoire d'Annecy-le-Vieux de Physique des Particules, IN2P3-CNRS, Annecy-le-Vieux, France

⁶⁵Also at Near East University, Research Center of Experimental Health Science, Mersin, Turkey

⁶⁶Also at Konya Technical University, Konya, Turkey

⁶⁷Also at Izmir Bakircay University, Izmir, Turkey

⁶⁸Also at Adiyaman University, Adiyaman, Turkey

⁶⁹Also at Bozok Universitetesi Rektörlüğü, Yozgat, Turkey

⁷⁰Also at Marmara University, Istanbul, Turkey

⁷¹Also at Milli Savunma University, Istanbul, Turkey

⁷²Also at Kafkas University, Kars, Turkey

⁷³Now at Istanbul Okan University, Istanbul, Turkey

⁷⁴Also at Hacettepe University, Ankara, Turkey

⁷⁵Also at Erzincan Binali Yıldırım University, Erzincan, Turkey

⁷⁶Also at Istanbul University - Cerrahpasa, Faculty of Engineering, Istanbul, Turkey

⁷⁷Also at Yildiz Technical University, Istanbul, Turkey

⁷⁸Also at Vrije Universiteit Brussel, Brussel, Belgium

⁷⁹Also at School of Physics and Astronomy, University of Southampton, Southampton, United Kingdom

⁸⁰Also at IPPP Durham University, Durham, United Kingdom

⁸¹Also at Monash University, Faculty of Science, Clayton, Australia

⁸²Also at Università di Torino, Torino, Italy

⁸³Also at Bethel University, St. Paul, Minnesota, USA

⁸⁴Also at Karamanoğlu Mehmetbey University, Karaman, Turkey

⁸⁵Also at California Institute of Technology, Pasadena, California, USA

⁸⁶Also at United States Naval Academy, Annapolis, Maryland, USA

⁸⁷Also at Ain Shams University, Cairo, Egypt

⁸⁸Also at Bingol University, Bingol, Turkey

⁸⁹Also at Georgian Technical University, Tbilisi, Georgia

⁹⁰Also at Sinop University, Sinop, Turkey

⁹¹Also at Erciyes University, Kayseri, Turkey

⁹²Also at Horia Hulubei National Institute of Physics and Nuclear Engineering (IFIN-HH), Bucharest, Romania

⁹³Now at another institute formerly covered by a cooperation agreement with CERN

⁹⁴Also at Texas A&M University at Qatar, Doha, Qatar

⁹⁵Also at Kyungpook National University, Daegu, Korea

⁹⁶Also at another international laboratory covered by a cooperation agreement with CERN

⁹⁷Also at Institute of Nuclear Physics of the Uzbekistan Academy of Sciences, Tashkent, Uzbekistan

⁹⁸Also at another institute formerly covered by a cooperation agreement with CERN

⁹⁹Also at Northeastern University, Boston, Massachusetts, USA

¹⁰⁰Also at Imperial College, London, United Kingdom

¹⁰¹Now at Yerevan Physics Institute, Yerevan, Armenia

¹⁰²Also at Universiteit Antwerpen, Antwerpen, Belgium